INVESTIGATION OF DIRECT TORQUE CONTROL AND PREDICTIVE TORQUE CONTROL STRATEGIES TO AN OPEN-END WINDING INDUCTION MOTOR DRIVE

Submitted in partial fulfilment of the requirements

for the award of the degree of

DOCTOR OF PHILOSOPHY

By

Kunisetti V Praveen Kumar

(Roll No. 715021)

Supervisor:

Dr. T. Vinay Kumar

Assistant Professor

DEPARTMENT OF ELECTRICAL ENGINEERING

NATIONAL INSTITUTE OF TECHNOLOGY

WARANGAL – 506004, TELANGANA STATE, INDIA

APRIL-2019

APPROVAL SHEET

This Thesis entitled "**Investigation of Direct Torque Control and Predictive Torque Control Strategies to an Open-end Winding Induction Motor Drive**" by **Kunisetti V Praveen Kumar** is approved for the degree of Doctor of Philosophy

Examiners

_____

_____

_____

Supervisor
Dr. T. Vinay Kumar
Assistant Professor
EED, NIT Warangal

Chairman
Dr. S. Srinivasa Rao
Professor& Head,
EED, NIT Warangal

Date: _____

DEPARTMENT OF ELECTRICAL ENGINEERING
NATIONAL INSTITUTE OF TECHNOLOGY
WARANGAL – 506 004

DEPARTMENT OF ELECTRICAL ENGINEERING

NATIONAL INSTITUTE OF TECHNOLOGY WARANGAL

CERTIFICATE

This is to certify that the thesis entitled **"Investigation of Direct Torque Control and Predictive Torque Control Strategies to an Open-end Winding Induction Motor Drive"**, which is being submitted by **Mr. Kunisetti V Praveen Kumar** (Roll No. 715021), is a bonafide work submitted to National Institute of Technology, Warangal in partial fulfilment of the requirement for the award of the degree of **Doctor of Philosophy** in Department of Electrical Engineering. To the best of my knowledge, the work incorporated in this thesis has not been submitted elsewhere for the award of any degree.

Dr. T. Vinay Kumar
(Supervisor)
Assistant Professor
Department of Electrical Engineering
National Institute of Technology
Warangal – 506004

Date:

Place: Warangal

DECLARATION

This is to certify that the work presented in the thesis entitled "**Investigation of Direct Torque Control and Predictive Torque Control Strategies to an Open-end Winding Induction Motor Drive"** is a bonafide work done by me under the supervision of **Dr. T. Vinay Kumar**, Department of Electrical Engineering, National Institute of Technology, Warangal, India and was not submitted elsewhere for the award of any degree.

I declare that this written submission represents my ideas in my own words and where others ideas or words have been included; I have adequately cited and referenced the original sources. I also declare that I have adhered to all principles of academic honesty and integrity and have not misrepresented or fabricated or falsified any idea/date/fact/source in my submission. I understand that any violation of the above will be a cause for disciplinary action by the institute and can also evoke penal action from the sources which have thus not been properly cited or from whom proper permission has not been taken when needed.

Kunisetti V Praveen Kumar
(Roll. No: 715021)

Date:
Place: Warangal

ACKNOWLEDGEMENTS

It gives me immense pleasure to express my deep sense of gratitude and thanks to my supervisor **Dr. T. Vinay Kumar,** Assistant Professor, Department of Electrical Engineering, National Institute of Technology Warangal, for his invaluable guidance, support, and suggestions. His knowledge, suggestions, and discussions helped me to become a capable researcher. He has shown me the interesting side of this wonderful and potential research area. His encouragement helped me to overcome the difficulties encountered in my research as well in my life.

I am very much thankful to **Prof. S. Srinivasa Rao**, Head, Department of Electrical Engineering for his constant encouragement, support and cooperation.

I take this privilege to thank all my Doctoral Scrutiny Committee members, **Dr. D. M. Vinod Kumar**, Professor, Department of Electrical Engineering, **Dr. G. Siva Kumar,** Assistant Professor, Department of Electrical Engineering and **Dr. D. Dinakar,** Professor, Department of Physics for their detailed review, constructive suggestions and excellent advice during the progress of this research work.

I also appreciate the encouragement from teaching, non-teaching members, and fraternity of Department of Electrical Engineering of NIT Warangal. They have always been encouraging and supportive.

I wish to express my sincere thanks to **Prof. N.V. Ramana Rao**, Director, NIT Warangal for his official support and encouragement.

I convey my special thanks to contemporary Research Scholars Mr. L. Suresh, Mr. T. Abhilash, Mr. M. Santhosh, Mr. K M Ravi Eswar, Mr. K Eshwar, Mr. S Venu, Mr. Sachidanda Prasad, Mr. M. Hareesh, Mr. A. Pranay Kumar, Mr. T. Ratna Rahul, Mr. S Ram Kumar, Mr. J R Rahul, Mr. B. Kiran Babu and Mr. M. Srikanth (chemistry).

I acknowledge my gratitude to all my teachers and colleagues at various places for supporting and co-operating me to complete the work.

I express my deep sense of gratitude and reverence to my beloved Mother Smt. **Kunisetti V V Lakshmi**, Brother **Kunisetti V Muthyala Rao**, Sister in law **K. L. Vasanthi**, and my grandmother **M. Sambrajyam**, for their sincere prayers, blessings, constant encouragement, shouldering the responsibilities and moral support rendered to me throughout my life, without which my research work would not have been possible. I would like to express my greatest admiration to all my family members for their positive encouragement that they showered on me throughout this research work. Without my family's sacrifice and support, this research work would not have been possible. It is a great pleasure for me to acknowledge and express my appreciation to all my well-wishers for their understanding, relentless supports and encouragement during my research work. Last but not the least, I wish to express my sincere thanks to all those who helped me directly or indirectly at various stages of this work.

This section would remain incomplete without remembering my father **Nageswara Rao** and Grandfather **M. Sambaiah,** who left their souls. I would like to express my love and respect for their everlasting affection and support.

Above all, I express my deepest regards and gratitude to "**ALMIGHTY**" whose divine light and warmth showered upon me the perseverance, inspiration, faith and enough strength to keep the momentum of work high even at tough moments of research work.

Kunisetti V Praveen Kumar

ABSTRACT

Now-a-days, multi-level inverter (MLI) fed induction motor drives have turned as an interesting area for researchers. This thesis focuses on direct torque control (DTC) and predictive torque control (PTC) strategies for the OEWIM drive to curtail ripples in torque, flux, switching frequency and common-mode voltage (CMV). The scheme of DTC offers high dynamic performance and control algorithm in stationary reference frame. In practice DTC also has several limitations. In this thesis, an attempt is made to address some of the limitations and also to provide improved versions of DTC algorithm. If the two inverters of OEWIM are fed with equal DC-link voltages then it provides two-level and three-level inversion. By operating OEWIM drive with unequal DC-link voltages (2:1 ratio); then it gives four-level inversion. To implement three-level and four-level inversion fed DTC algorithms, a three-level torque hysteresis controller and two-level flux hysteresis controllers are used. The voltage vectors are categorized into various groups for three-level and four-level inversion. Proposed MLI fed DTC algorithms can reduce torque and flux ripples, whereas its implementation is cumbersome. In order to address these problems, fast and accurate torque control methods are needed. Fast and accurate torque control can be obtained by employing model predictive control (MPC).

The combined features of MPC and DTC give an effective control strategy for OEWIM drives known as finite control set predictive torque control (FCS-PTC) or simply predictive torque control (PTC). In this thesis a modified cost function based PTC has been introduced to reduce CMV of OEWIM drive fed with two, three and four-level inversion. The limitation of this algorithm is that the cost function comprises of dissimilar quantities, the selection and tuning of weighting factors is unavoidable. To simplify the selection and tuning of weighting factors; normalized weighted sum model (NWSM) based PTC and weighting factor eliminated (WFE) PTC schemes are proposed for the OEWIM drive. The average switching frequency of OEWIM drive can be reduced by NWSM PTC or WFE PTC.

The proposed DTC and PTC strategies are developed in MATLAB/SIMULINK. To verify the effectiveness of the proposed DTC and PTC strategies, these are tested experimentally. The experimental and simulation results are compared with classical DTC and PTC strategies.

Table of Contents

List of Figures

List of Tables

Abbreviations

AC	Alternating current
ADC	Analog to Digital Converter
AI	Artificial Intelligence
ASDs	Adjustable Speed Drives
BNC	Bayonet Neill–Concelman
CCSMPC	Continuous Control Set Model Predictive Control
CHB	Cascaded H-Bridge
CMV	Common-Mode Voltage
DC	Direct Current
DCC	Duty Cycle Control
DSP	Digital Signal Processor
dSPACE	Digital Signal Processing and Control Engineering
DTC	Direct Torque Control
EKF	Extended Kalman Filter
EMF	Electro Magnetic Field
EMI	Electro Magnetic Interference
EV	Electric Vehicle
FBLC	Feedback Linearization Control
FCSMPC	Finite Control Set Model Predictive Control
FCSPTC	Finite Control Set Predictive Torque Control
FOC	Field Oriented Control
GPTC	Generalized Predictive Torque Control
HEV	Hybrid Electric Vehicle
IGBT	Insulated Gate Bipolar Transistor
IM	Induction Motor
MATLAB	MATrix LABoratory
MCDM	Multi-Criterion Decision Making
MLI	Multi-Level Inverter
MPC	Model Predictive Control

MPTC	Model Predictive Torque Control
NPC	Neutral Point Clamped
NWSM	Normalized Weighted Sum Model
OEWIM	Open-end Winding Induction Motor
PI	Proportional Integral
PMSM	Permanent Magnet Synchronous Motor
PTC	Predictive Torque Control
PWM	Pulse Width Modulation
RMF	Rotating Magnetic Field
RMS	Root Mean Square
SCIM	Squirrel Cage Induction Motor
SM	Synchronous Motor
SRIM	Slip Ring Induction Motor
SVM	Space Vector Modulation
THD	Total Harmonic Distortion
VSI	Voltage Source Inverter
WFE	Weighting Factor Elimination
WSM	Weighted Sum Model

List of symbols

T_e	Electromagnetic torque
v_{s1}	Voltage space vector of Inverter-1
v_{s2}	Voltage space vector of Inverter-2
v_s	Resultant voltage space vector
v_α , v_β	Real and imaginary parts of resultant voltage space vector
k,k_1, k_2	Constants
i_f	Field current
i_a	Armature current
ψ_f	Field flux
V_{dc}	Net DC link Voltage (or) DC-link Voltage
x	Constant (2/3)
y	Constant (1/3)
S_r, S_y *and* S_b	Switching pulses applied to top switches of Inverter-1
S_r', S_y' *and* S_b'	Switching pulses applied to top switches of Inverter-2
f_{sw}	Switching frequency
R_s	Stator Resistance
L_s	Stator Inductance
L_r	Rotor Inductance
L_m	Mutual Inductance
i_s	Stator current (or) stator current space vector
$v_{s\alpha}$,$v_{s\beta}$	Stator voltage space vector in stationary reference frame
$i_{s\alpha}$,$i_{s\beta}$	Stator current space vector in stationary reference frame
$\psi_{s\alpha}$, $\psi_{s\beta}$	Stator flux space vector in stationary reference frame
$\lvert\psi_s\rvert$	Magnitude of stator flux space vector
$\psi_{r\alpha}$, $\psi_{r\beta}$	Rotor flux space vector in stationary reference frame
$i_{r\alpha}$, $i_{r\beta}$	Rotor current space vector in stationary reference frame
p	Differential operator (d/dt)
P	Number of Poles

ψ_s	Stator flux space vector
J	Moment of inertia
B	Friction co-efficient
T_l	Load Torque
ω_m	Rotor Speed in rad/s (Mechanical Systems)
ω_r or ω_e	Rotor Speed in rad/s (Electrical Systems)
T_{ref}	Reference Electromagnetic Torque
ψ_{ref}	Flux Reference
i_r, i_y and i_b	Phase currents of OEWIM drive
ryb-αβ	Clarke Transformation
α	Angle between stator current and stator flux
m	Number of voltage space vectors (1, 2, 3….)
$v(t)$	Terminal Voltage
e or e_0	Back EMF
V_{ro}, V_{yo}, *and* V_{bo}	Pole Voltages of Inverter-1
$V_{r'o'}$, $V_{y'o'}$, *and* $V_{b'o'}$	Pole Voltages of Inverter-2
$\Delta V_{rr'}$, $\Delta V_{yy'}$ *and* $\Delta V_{bb'}$	Difference of Pole Voltages of Inverter-1 and 2
V_c or V_o	Common-mode Voltage
$\psi_{s\alpha}(k)$, $\psi_{s\beta}(k)$	Stator flux space vector at k^{th} instant in stationary reference frame
$i_s(k)$	Stator current at k^{th} instant
$v_{s\alpha}(k)$,$v_{s\beta}(k)$	Stator voltage space vector at k^{th} instant
$i_{s\alpha}(k)$,$i_{s\beta}(k)$	Stator current at k^{th} instant in stationary reference frame
$\|\psi_s(k)\|$	Magnitude of flux space vector at k^{th} instant
$\psi_{r\alpha}(k)$, $\psi_{r\beta}(k)$	Rotor flux space vector at k^{th} instant in stationary reference frame
$i_{r\alpha}(k)$, $i_{r\beta}(k)$	Rotor current at k^{th} instant in stationary reference frame
$\psi_s(k+1)$	Flux space vector at $(k+1)$ instant
$\|\psi_s(k+1)\|$	Magnitude of flux space vector at $(k+1)$ instant
$\psi_{s\alpha}(k+1)$, $\psi_{s\beta}(k+1)$	Real and imaginary parts of stator flux at $(k+1)$ instant
$i_{s\alpha}(k+1)$, $i_{s\beta}(k+1)$	Real and imaginary parts of stator current at $(k+1)$ instant
$T_e(k+1)$	Electromagnetic Torque at $(k+1)$ instant

T_s	Sampling Time
σ_T	Torque weighting factor
σ_ψ	Flux weighting factor
σ_n	CMV weighting factor
W	Weighting factor of flux error
g	Cost function
D	Decision Matrix

Chapter 1

Introduction

Chapter 1

Introduction

1.1 Background

Electric motor is an energy conversion device that converts electrical energy into mechanical energy. The mechanical energy produced is due to the electromagnetic interaction that takes place inside the motor. The electromagnetic interaction of stator and rotor magnetic field causes mechanical rotation. The mechanical rotation of the motor can be controlled efficiently by adjusting the force acting on the shaft of the motor. An electric motor with proper control scheme is called as adjustable speed drive (ASD) [1]. ASDs are most familiar in automated industries like paper mills, metal rolling, plastic, steel, textile, railway traction and robotics. Many of the modern industrial works are in progress with electric motors. Electric motors find several applications such as in domestic appliances, elevators, disc drives, compressors, draught fans and other machine tools. In recent times, the electric motors are also preferred in electric vehicles, ship propulsion, which are becoming popular and promising applications of electric motors [2].

1.2 DC and AC Motors

Electric motors are categorized into two types: direct current (DC) motors and alternating current (AC) motors [1]. DC motor comprises an armature (rotor) and field (stator). In a separately excited DC motor, field and armature are excited separately with individual DC sources, to achieve decoupled control of torque and flux. The independent control of torque and flux makes DC motor control easy and simple. However, the current in the armature of DC motor is time varying even if it is excited from DC terminals. The commutators and brushes used in DC motor convert DC into AC and make the current flowing in the armature winding time varying. The interaction of magnetic field developed by armature current and magnetic field of field circuit develops a mechanical force that accelerates the armature of DC motor. The electromagnetic torque of DC motor depends on two magnetic fields and these two magnetic fields are independent of each other, so the control design of DC motor is simple and

easy. The torque of DC motor is given by (1.1), torque is proportional to field current (flux producing current) and armature current (torque producing current).

$$T_e = k i_f i_a = k_1 \psi_f i_a \tag{1.1}$$

In (1.1), k and k_1 are constants, i_f is field current, i_a is armature current and ψ_f is magnetic flux produced by field winding of DC motor.

The field flux of DC motor is stationary and it is generated by permanent magnets or electromagnets. Fast torque control of DC motor is obtained by varying i_a at a faster rate and keeping the field current as constant. However, the presence of commutator and brushes in DC motor makes it: (i) Bulky, (ii) Expensive, (iii) Prone to frequent maintenance and (iv) Difficult to operate in all environmental conditions. In contrast, AC motors do not use commutators and these are excited from AC source [3]. The cost of AC motors is very low in comparison with DC motors. In early 1970s DC motors were used as ASDs and AC motors were used for constant speed applications, whereas in the past three or four decades, DC motors have been replaced by AC motors with the advent of power semiconductor devices, especially insulated gate bipolar transistors (IGBT) and digital signal processors (DSP) technologies. The best cost-effective procedures to control speed of AC motors are ASDs. Numerous methods of converter topologies and various pulse width modulation (PWM) techniques replace AC motors to function as ASDs by supplying variable frequency and voltage from a fixed AC voltage source.

AC motors are basically classified into two categories based on their speed of rotation, these are: synchronous and asynchronous motors. The motors which rotate with constant speed (same as supply frequency) are termed as synchronous motors (SM); on the other hand motors which rotate at less than synchronous speeds are termed as asynchronous motors. Induction motors fall into the category of asynchronous motors. Now-a-days, induction motors are the workhorse of industries. Induction motors are classified into two categories depending on the type of rotor: squirrel cage induction motor (SCIM) and slip ring induction motor/ wound rotor (SRIM). In SCIM, the rotor winding is shorted whereas in the case of SRIM the rotor terminals are available external to the motor. SCIMs with voltage source inverter (VSI) are used as ASDs and these are accepted universally for all ASDs. Unlike DC motors, the stator and rotor variables of AC motors are dependent, since the AC supply is given to stator of motor terminals and creates rotational magnetic field (RMF) in stator core. The interaction of RMF with rotor

creates an electro-motive force (EMF) through the process of induction. The EMF induced in the rotor circulates a current in the rotor and the rotor develops magnetic field (since the rotor terminals are shorted). The magnitude of induced voltage at rotor terminals is dependent on the relative motion (slip) between stator flux and rotor flux. Electromagnetic interaction between stator RMF and rotor magnetic field develops a mechanical force (torque) that accelerates or decelerates the motor. In SCIMs, the stator and rotor variables are dependent on each other, hence the design of speed controller for induction motors is quite complex as compared to DC motors. The controller complexity increases, if the induction motors are employed for high dynamic performance applications. To make the design of controller easy, it is necessary to make stator and rotor fields of induction motor to be controlled independently. By controlling the stator and rotor magnetic fields independently, it is easy to achieve decoupled control of torque and flux. Therefore the decoupled control of torque and flux makes speed control of induction motors is same as that of separately excited DC motors [4].

1.2.1 Classical Control Methods of Induction Motor

The SCIMs are simple, rugged and it is one of cheapest machines for all power ratings when compared with SRIM. Owing to their high dynamic performance and excellent control capabilities, many ASDs are employed with induction motors. In spite of these features, the speed control of induction motors is difficult. The speed control methods of induction motors are of two types: (i) Scalar control and (ii) Vector control. Various speed control methods of induction motor drives are shown in Figure 1.1.

Scalar control is simple and easy to implement [1]. It is most popularly used in industries. It operates on the principle of controlling voltage and frequency of induction motor drive (V/f control). The limitation of scalar control is that it does not provide high dynamic performance. To obtain high dynamic performance, it is preferable to use vector control techniques [4].

Vector control techniques are broadly classified into three categories. These are: (i) Field oriented control (FOC) [5], [6], (ii) Feedback linearization control (FBLC), [7] and (iii) Direct torque control (DTC) [8]. The vector control techniques not only control the magnitude

of voltage, frequency but also control the position of stator flux, magnitude of stator flux and stator current. The vector control offers high dynamic performance.

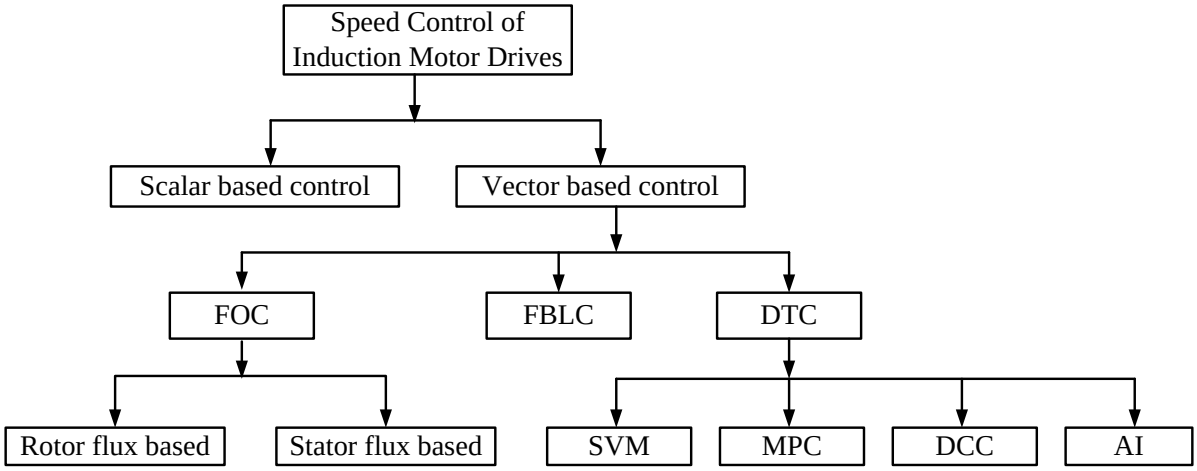

Figure 1.1 Various speed control strategies of induction motor drives

Induction motor has high non-linear structure and also there exists coupling between flux and electromagnetic torque. There are various algorithms available in literature to obtain decoupled control of torque and flux. Therefore several methods are developed with different ideas and analytics by various researchers to implement decoupled control of torque and flux. In the late 1970s, Hasse and Blasche introduced a popular speed control technique for induction motor drives known as FOC [5]. The introduction of FOC made a revolution in ASDs and it is used in many industries. FOC of induction motor is analogy to speed control of separately excited DC motor. The implementation of FOC uses co-ordinate transformation. All motor equations are transmuted into the co-ordinate system that revolves in synchronism with rotor flux. FOC offers high dynamic performance and operates with constant switching frequency. The limitations of FOC are: (i) It does not guarantee exact decoupling of motor torque and flux in dynamic and steady-state operations, since induction motor equations are non-linear and these are fully decoupled for constant flux operation, (ii) The relation between the regulated and control variables is linear only for constant flux operation, (iii) It needs exact information about state variables and electromagnetic torque, (iv) It needs current controllers, (v) Co-ordination transformation is required and (vi) It requires a modulator [6].

FBLC uses non-linear transformation of induction motor state variables, so that in the new co-ordinate system, the speed and rotor flux amplitudes are decoupled by feedback. It guarantees decoupling of torque and flux of induction motor in steady-state and dynamic conditions. This method requires implementation in state variable form and needs complex control algorithm. It needs complete information about motor state variables and torque. It needs a modulator so that constant switching frequency is guaranteed [7].

To overcome the limitations of FOC and FBLC; DTC of induction motor drives was implemented in late 1980's [8]. The control algorithm in DTC uses stationary reference frames, does not need modulator and co-ordinate transformation. In DTC, torque and flux are decoupled by hysteresis controllers. DTC offers a simple control structure and high dynamic performance. The scheme of DTC also has some limitations, these being: (i) The presence of hysteresis controllers which causes variable switching frequency, (ii) Necessity of sampling times, when it is implemented in digital platform, (iii) Poor torque and flux regulation (higher ripples in torque and flux), (iv) Higher common-mode voltage (CMV) and (v) More current distortions. Many of the researchers are working in the area of DTC to overcome the limitations of classical DTC. In order to abate the limitations multi-level inverter (MLI) fed DTC of induction motor drives has been introduced to reduce torque, flux ripples and switching frequency [8]-[10]. This thesis focuses on the implementation of DTC of open-end winding induction motor (OEWIM) drives and another promising control strategy known as predictive torque control (PTC) strategy for OEWIM drive to reduce torque, flux ripple CMV and switching frequency.

1.2.2 Advantages and Applications of OEWIM drive

Classical induction motor drives use a two-level voltage source inverter (VSI); hence they can provide two-level output voltage. Dual inverter fed OEWIM drive can provide multi-level inversion even if it is operated with two-level voltage source inverters [11]. The configuration of OEWIM uses two two-level VSIs operating in dual mode and is shown in Figure 1.2.

Dual inverter fed OEWIM drive is considered one of the best alternative approaches to multi-level inversion. OEWIM drive has several advantages when compared with other MLI

configuration topologies [12]: (i) It uses two two-level VSIs to obtain Multi-level inversion, (ii) Neutral voltage fluctuations and clamping diodes are absent when compared with Neutral Point Clamped (NPC) inverter topology, (iii) It is rich in redundancy of switching states as it gives more common space vector combinations, (iv) It uses simple control and fewer capacitors as compared to Flying capacitor MLIs, (v) Fewer DC-sources as compared to Cascaded H-Bridge (CHB) MLIs, (vi) Capable of operating even during faulty conditions and (vii) Uses fewer number of switches for four-level inversion as compared to NPC, flying capacitor and CHB-MLIs.

OEWIM drives find interesting possibilities in various applications such as electric vehicles [13], ship propulsion [14], rolling mills [15], renewable energy interfacing [16] and hybrid electric vehicles [17]. These interesting possibilities of OEWIM drives in various applications made the researcher embark on the investigation of this intellectually challenging area of research.

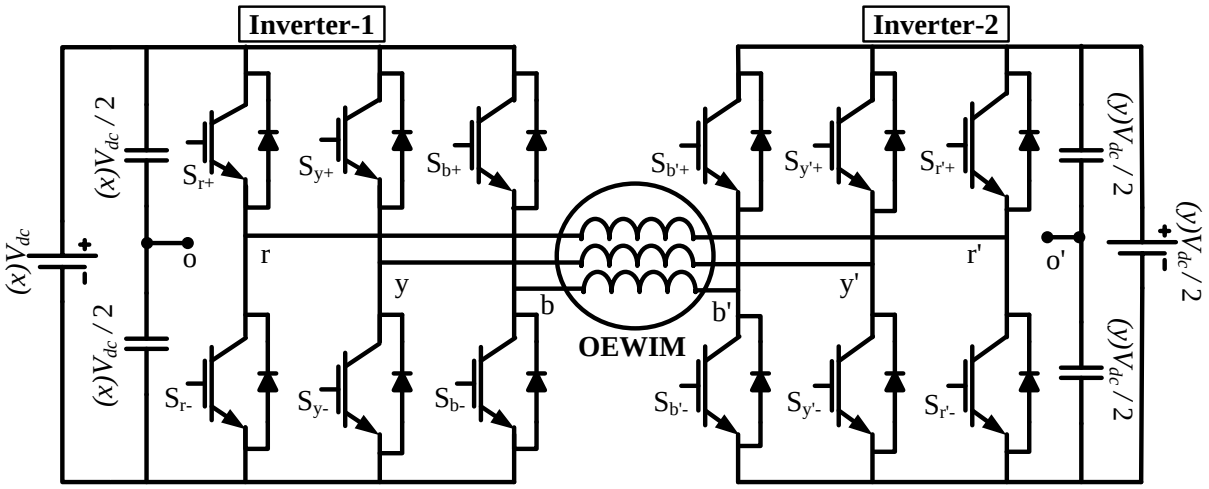

Figure 1.2 Power circuit configuration of OEWIM drive

1.3 Literature Review

This thesis focuses on DTC and PTC strategies for an OEWIM drive to reduce torque, flux ripple and CMV. The literature review contains state of art of DTC and PTC methods for induction motor drives and also to OEWIM drives. To differentiate the state of the art of DTC from PTC strategies, section 1.3.1 describes literature review of DTC strategies and section 1.3.2 presents state of art of PTC strategies.

1.3.1 DTC of Induction Motor Drives fed with Two-level and Multi-level Inversion

In the late 1980, the concept of DTC was introduced by I. Takahasi and T. Nogouchi [8]. In those days, DTC was a novel concept to circumvent many of the problems involved in the implementation of popular vector control method FOC [18]. The implementation of FOC took almost 20 years; in contrast DTC has taken fewer than 10 years for industrial implementation. The DTC strategy has been taken on-board for industrial applications in the second half of 1990s and it is manufactured by ABB [18]-[20]. The concept of FOC predominantly relies on the dynamic model of induction motor, whereas DTC uses physical relations that occur within integrated system of machine and its supply [18], [19]. DTC uses simple signal processing techniques and it completely depends on non-linear nature of voltage source inverter (VSI) that is used to provide input to induction motor [20]. The on-off control of VSI switches are used for the decoupled control of induction motor. It is possible by using power semiconductor devices based VSIs with digital signal processors (DSP). The VSIs with DSP arrangement give variable output voltage and variable frequency by using proper voltage vector selection and the corresponding switching states. In essence, DTC directly controls electromagnetic torque and flux directly by using proper voltage vector selection in contrary while it indirectly controls stator voltage and stator current [20].

The concept of DTC eliminates the presence of inner current loops but it requires outer speed control loop. The control of DTC drive uses two hysteresis controllers and these are operated by errors in torque and flux. In DTC, the reference values of torque and flux are compared with actual torque and flux of induction motor. The torque and flux are estimated by using closed-loop estimators [21]. The output of torque and flux hysteresis controllers is used to determine the voltage vector to be applied for induction machine so that the torque and flux errors are within hysteresis bounds [10]. The features of DTC strategy are listed below [4]:

(i) Direct control of torque and flux.
(ii) Indirect control of stator current and voltage.
(iii) It does not require co-ordinate transformations as used in FOC.
(iv) Modulator is not required.

(v) It needs information about sector of stator flux and it does not need exact position of stator flux space phasor.

(vi) There is no internal current control loop.

(vii) It is sensitive to stator resistance variations only.

DTC offers certain advantages and it also possesses some limitations; these are as follows [4], [19]:

(i) Variable switching frequency due to bang-bang controllers.

(ii) By using optimum voltage vectors there is possibility of excursion of torque and flux outside of the hysteretic bands, hence it causes higher ripples in torque and flux.

(iii) Life span of induction motor decreases due to insulation failure of stator winding. The insulation failures are due to high rate of change of applied voltage, CMV etc.

(iv) Current control is not a direct task; hence there exist higher distortions in stator voltage and current.

(v) Stator flux is estimated through integration, it causes problems of drift and offset at low speeds of operation.

To bring down the limitations of classical DTC, various DTC algorithms are implemented. Figure 1.3 represents various DTC strategies for induction motor drives. In order to maintain fewer ripples in torque and flux modified hysteresis controller based DTC strategies [22]-[26], constant switching frequency based DTC strategies such as dithering [27], [28], space vector modulation (SVM) [29]-[36], MLI-fed DTC strategies [37], [38], DTC of OEWIM drives [39]-[43] and DTC with fuzzy control, adaptive control [44]-[48] are implemented.

Modified hysteresis controller based DTC strategies work on online hysteresis bands variation [22] or off-line hysteresis bands adjustments [23]-[26]. In [23], a novel technique is developed to reduce torque ripple by using modified hysteresis controllers. This uses application of voltage vector for a certain time interval instead of complete control cycle. The voltage vectors are applied in such a way that torque and flux controllers reach upper or lower bands for certain time intervals and the application of voltage vectors are independent of sampling time. This is implemented only for two-level inverter fed induction motor drive. In classical DTC, higher ripple in torque and flux is due to variable switching frequency caused by

hysteresis boundaries. In [23], the DTC of induction motor drive is introduced with modified hysteresis boundaries and [26] introduces a low switching frequency based DTC strategy to maintain fewer ripples in torque and flux.

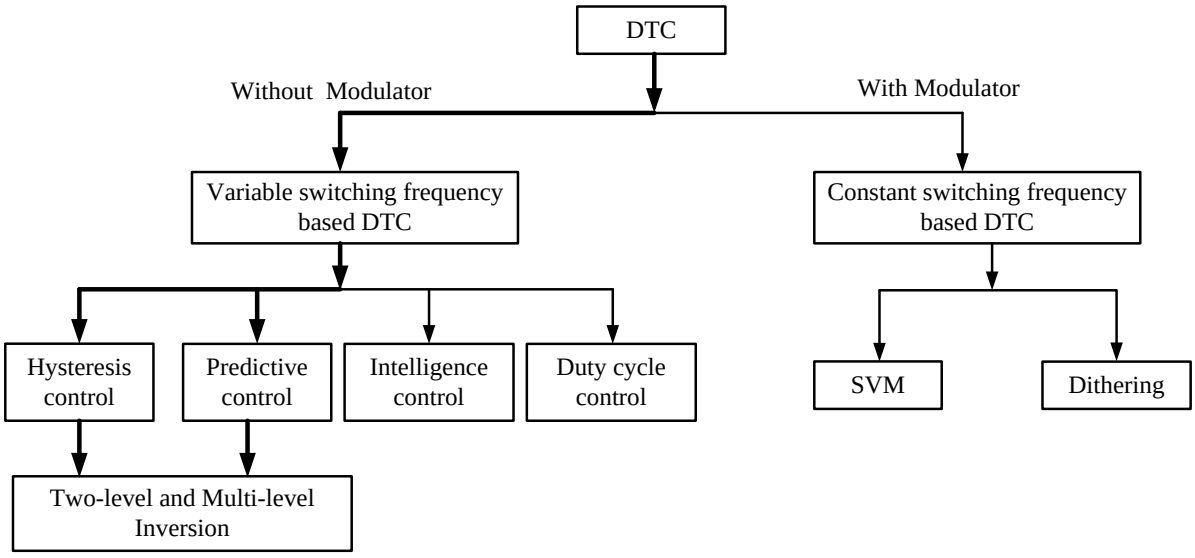

Figure 1.3 Various DTC strategies of induction motor drives

Nevertheless, in [27] and [28], a simple DTC strategy is introduced to maintain constant switching frequency by using dithering. It gives silent operation of induction motor by enlarging switching frequency. The enlargement in switching frequency is done by superimposing the high frequency tri-angular wave onto torque and flux errors. To circumvent the problem of variable switching frequency, SVM based DTC strategies are introduced. DTC with SVM maintains constant switching frequency [29]. It involves computation of reference voltage space vector from the PI controllers of torque and flux errors. However there is extensive research developed on DTC-SVM to make the algorithm simple and dead-beat controllers are introduced [30]-[32]. In [30], [31] a new DTC-SVM algorithm is developed by calculating the reference voltage space vector with the help of RMS torque ripple. In [33], [34] a novel direct torque control algorithm is introduced; the required amount of reference stator flux is obtained by utilizing the sum of change in load angle and rotor flux angle. This method is simpler and requires lower computational efforts. It needs load angle estimator in addition to classical DTC. From [29]-[36], it is observed that the calculation reference voltage space vector and the tuning of PI controllers are quite cumbersome. The DTC-SVM is simplified by

considering fuzzy PI controllers and by using one PI controller instead of two PI controllers [37].

However several MLI fed DTC strategies have been introduced to maintain lower ripple in torque and flux [37], [38]. From [39]-[43], DTC of OEWIM drives has been introduced since the configuration of OEWIM drive found to be an effective alternative to MLI-fed DTC strategies of induction motor drive. In [40], DTC of OEWIM drive is introduced with SVM technique and the concept of imaginary switching times based SVM technique developed for marine propulsion [41], [42]. In addition there are various DTC algorithms where [44] introduces model based and search based non-linear control strategy. In [45] and [46], self-tuned neuro fuzzy controller based DTC algorithms are introduced to minimize the square of error between actual and reference acceleration or deceleration of induction motor drive. In [36] and [46], a comparative study of DTC-SVM with controllers and DTC-SVM with sliding mode controllers is performed and it focuses on maintaining constant switching frequency and torque ripple reduction through an adaptive model. In [47], a low cost DTC strategy is introduced to eliminate AC current sensors. It uses DC current to reconstruct phase currents. In [48], DTC of induction motor drive has been introduced to reduce CMV by eliminating the null-vector for its operation.

From the literature, it is observed that the torque and flux ripples can be reduced by using different methods. It is interesting that in the case of MLIs the torque and flux ripples can be easily decreased noticed from [38].This was the key factor to embark on this research further and it was evident that there is wide scope to reduce torque, flux ripples, switching frequency and CMV. In order to implement MLI fed DTC algorithm a dual inverter fed OEWIM is an effective alternative. The dual inverter fed OEWIM offers several features when compared with other MLI topologies; as described earlier. In [24], [25], DTC of induction motor drives with three-level NPC inverters has been developed with multi-level torque and flux hysteresis controllers. In contrast to DTC-SVM, [26] introduces a modified hysteresis based DTC strategy for the OEWIM, It utilizes five-level torque hysteresis controller and a three-level flux hysteresis controller. For a three-level inversion configuration five-level torque hysteresis controller and a three-level flux hysteresis controllers are required, whereas in four/five-level inverter configurations the implementation of hysteresis controllers and their boundaries

become quite cumbersome. The implementation of look-up tables and defining the hysteresis boundaries is not so easy for multi-level inversion fed DTC strategies.

This thesis focuses on the implementation of DTC strategies for the OEWIM drive, without losing the benefits of classical DTC and also the proposed DTC strategies introduced in such a way that these strategies do not involve complex look-up tables and multi-level hysteresis controllers. From the literature it is obvious that fewer ripples in torque and flux are obtained by introducing MLI fed DTC strategies to induction motor drives. This thesis introduces two, three and four-level inversion schemes for the OEWIM drive. Many research articles contributed to the implementation of DTC of OEWIM drive by considering equal DC-link voltage [26], [39]-[43]. By operating dual inverter fed OEWIM drive with equal DC-link voltage, three-level inversion can be obtained; similarly if the dual inverter configuration is operated with asymmetrical (unequal) DC-link voltage it is possible to obtain four-level inversion [11]. This thesis introduces effective voltage switching state algorithms for an OEWIM drive to reduce torque and flux ripples with three and four-level inversion schemes. The switching state algorithms are developed by considering the operating speed of OEWIM drive. The proposed DTC algorithms utilize three-level and two-level hysteresis controllers for torque and flux respectively; therefore the proposed algorithms do not increase complexity involved in [24]-[26]. The proposed DTC strategies are simple and reduce torque ripple, flux ripple and CMV. The effectiveness and feasibility of the proposed DTC strategies verified experimentally by using dSPACE DS-1104 controller board.

1.3.2 PTC of Induction Motor Drives fed with Two-level and Multi-level inversion

PTC is a combination of model predictive control (MPC) and DTC [49]-[85]. The ideas of MPC were applied for chemical process applications in 1960s. In 1980s MPC was considered for high power systems with low switching frequency. In those days the use of high switching frequencies was not possible. With the advent of DSPs, the concept of MPC was applied to power electronics. MPC for electric drives has drawn attention from the last decade due to its intuitive nature, simplicity, ease of implementation, easy inclusion of constraints, inclusion of modifications and extensions depending on the specific applications [49]. The

basic ideas of MPC are: (i) It uses a model to predict future behaviour over a specified horizon, (ii) A cost function that represents required behaviour of the system and (iii) Minimization of cost function [49]. In addition, MPC meets the necessities of modern control systems. MPC utilizes discrete models of plant and allows us consideration of constraints [49]-[52]. MPC strategies are of two types [53]: continuous control set MPC (CCS-MPC) and finite control set MPC (FCS-MPC). CCS-MPC uses a modulator to generate switching pulses for inverter, whereas FCS-MPC does not require a modulator. In CCS-MPC, controller delivers output for modulator and the modulator gives gating signals to inverter. The presence of modulator in CCS-MPC gives constant switching frequency whereas FCS-MPC operates with variable switching frequency [54]. In FCS-MPC, the switching pulses are obtained by optimizing the cost function. The cost function is evaluated for all possible switching states of inverter; hence the name finite control set MPC. In FCS-MPC, the controller delivers discrete signals and these are used to drive the inverter [54]. The combination of FCS-MPC and DTC yield finite control set predictive torque control (FCS-PTC). The working principle of FCS-PTC is the same as that of classical DTC, whereas FCS-PTC do not use hysteresis controllers, sector identifier, trigonometric calculations to find stator flux angle and look-up table to select voltage vector. In FCS-PTC, torque and flux are evaluated for all possible switching combinations of VSI. The switching combination that gives lower ripple in torque and flux is taken as optimal voltage vector and is applied to inverter in the next control cycle. PTC does not use inner current control loop as involved in FOC [55], but it needs speed control loop and the speed can be controlled directly by introducing the speed error term into the cost function [56]. However, PTC structure is simpler when compared with FOC and DTC [57]. From [49], [57] PTC gives similar or even better performance with respect to FOC or DTC. Table 1.1 shows comparison among FOC, DTC and FCS-PTC. From Table 1.1 it is evident that PTC can be an effective alternate to FOC and DTC strategies. Nevertheless, PTC has several limitations: high computational burden, variable switching frequency, tuning of weighting factors and distortion in current. Several researchers are working on classical PTC to circumvent its limitations. This thesis focuses on the implementation of PTC strategies for the OEWIM drive to reduce torque, flux ripples and the effects of CMV.

Table 1.1 Comparison among various vector control strategies of induction motor drives [49], [57]

Parameter	FOC	DTC	PTC
Complexity	High	Low	Low
Modulator	Required	Not required	Not required
Axis Transformation	Required	Not required	Not required
Parameter Sensitivity	High	Low	High
Exact Position of Flux	Required	Not Required	Not Required
Computational Burden	Low	Low	High
Parameter Sensitivity	High	Low	High
Inclusion of constraints	Difficult	Difficult	Easy
Torque and Flux Ripple	Low	High	Low
Weighting Factor	No	No	Yes

Extensive research has been carried out during the past decade on PTC to reduce torque and flux ripples. Correa. et. al [58] used PI controller and predictive controller together to obtain high dynamic response with the help of multi-level space phasor modulation. It uses a dead-beat controller to calculate slip-angle of rotor. This offers an adorable small-signal operation for MLI fed induction machines. A new PTC algorithm for induction motors was implemented in [59] based on immediate flux control. It doesn't account for the ripples in torque and flux but it reduces switching frequency.

In [60], Discrete-time model of induction motor was developed in terms of state-space equations for prediction of stator flux, torque and provides solution to prevent time delays for prediction algorithm. In [61] and [62] concept, evaluation, implementation and analysis of model predictive torque control (MPTC) of induction motors was developed using extrapolation. PTC offers lower ripple in torque and flux when compared to DTC. In DTC the hysteresis bounds are responsible to generate switching vector, the selection of voltage vector is indirect process, whereas in PTC the selection of voltage vector is direct and obtained from the optimization of cost function. A simple prediction model is implemented for DTC to compensate for delay time [63].

According to recent trends, the branches of PTC aim at reducing torque and flux ripples. Variable switching time point PTC algorithm was introduced in [64], because PTC introduces high current and torque ripples due to switching frequency being less than half of sampling frequency compared to modulator based approaches. To solve real time problems, Variable switching time point was introduced to PTC. The concept of duty-ratio control was added to PTC to reduce torque ripple but it requires high sampling frequencies. In [65]-[69], an

improved MPTC with duty cycle control is implemented to reduce torque and flux ripples by optimizing active voltage vectors as well as the duration. In [70], generalized predictive torque control (GPTC) of induction motor drive is implemented to overcome the difficulties of duty-ratio controlled MPTC by using two-voltage vectors. GPTC reduces the torque ripple but the computational burden is accountable. Computational burden involved in finite control set PTC is expensive and utilizes all voltage vectors for prediction of torque and flux. The computational burden involved in PTC is high compared to DTC; to conquer this novel DTC is developed [71] to reduce switching frequency based on look-up table. The predictions of voltage vectors always depend on two adjacent active vectors and a null vector.

In [72], a novel algorithm has been designed to control the torque of induction motor using the angle between rotor flux and stator current by developing the necessary equations for the prediction of torque. The equations of current and torque predictions are independent of voltage. In PTC the optimization of cost function is dependent on torque and flux weighting factors. Tuning of weighting factor and selection of weighting factor is tedious [73]. To circumvent this, PTC of induction motor is modified as model predictive flux control (MPFC) rather than MPTC and it uses a control variable stator flux to eliminate complex predictions. In [74], MPTC was developed by converting torque and flux in terms of equivalent voltage vectors to eliminate the effects of weighting factors on current and torque ripples. Branch and bound algorithm was used to find the weighting factor [53]-[57], [60]-[64]. Formulation of flux weighting factor is described in [75] and formulation of weighting factor for CMV is reported [76].

The prediction algorithm of PTC involves measurement of speed and currents. In [77], two sensor-less PTC methods are introduced, these being voltage model observer and sliding mode observer. Direct estimation of speed from current is possible but it degrades the steady-state performance. To circumvent this, Extended Kalman Filter (EKF) is introduced and it estimates the speed by using flux and stator currents [78]. In [78], Sensor-less PTC of induction motor was developed by estimating the rotor speed and rotor flux with the help of EKF. There are various methods reported in literature to simplify or to eliminate weighting factors and several heuristic methods are reported [79]-[85].

From the literature it is apparent that PTC also suffers from variable switching frequency as well as higher ripples in torque and flux. To curtail torque and flux ripples it is better to use duty-cycle control or MLI fed induction motor drives. At present, most of the industrial drives are utilizing two-level inverters. For medium and high power applications, it is unavoidable to use MLIs. However, in MLIs the number of voltage vectors is high when compared with two-level VSIs. The cost function is evaluated for all permissible switching combinations of inverter; therefore the computational complexity of control algorithm increases. The computational burden on controller increases and leads to lower sampling frequencies. The multi-level inversion has many advantages when compared with two-level VSIs, such as reduced d*v*/dt stress, lower distortions in current and lower ripples. However, MPC algorithm has been applied for MLIs [50]-[55], [80], [83]. These applications are meant for power and current control where the cost function does not use relatively complex terms. Motor drive control is more complex since these applications require complex control algorithm and the formulation of cost function is cumbersome. Many researchers are working on PTC of induction motor drives with multi-level inversion. In [61]-[63], [78], [79], PTC of three-level inverter has been reported; in these articles, however, the effect of switching frequency was not investigated. In [86], comparison between predictive current control and PTC of single DC-source fed OEWIM drive has been introduced to suppress zero-sequence currents.

This thesis describes the implementation of PTC for OEWIM drive. The rationale behind developing PTC to OEWIM drives are: implementation of discrete model of OEWIM drive, mathematical model of inverter, formulating switching states and their classification. In this thesis OEWIM drive is programmed to operate with two-level and multi-level inversion scheme by classifying the voltage vectors according to operating speed. The computational burden involved can be reduced by classifying the voltage vectors. The voltage vectors used in proposed PTC strategy provides minimum CMV; therefore the proposed PTC strategies maintain minimum CMV when compared with classical predictive torque controlled induction motor drives and PTC of OEWIM drive with two-level inversion. A comparative study has been carried out on torque ripple for different inversion schemes.

Another limitation of classical PTC is variable switching frequency. In this thesis, an attempt is made to reduce switching frequency, torque and flux ripples by using multi-level inversion fed OEWIM configuration. Four-level configuration of OEWIM was obtained by operating two VSI's with unequal DC voltages [11]. To simplify the tuning of weighting factors normalized weighted sum model (WSM) is introduced to optimize the cost function. WSM is a multi-criteria decision making algorithm and it is easy to implement [87], [88]. The reasons for normalized WSM are: enhanced selection of weighting factors, formulation of cost function to reduce ripples (torque and flux) and reduction of switching frequency. The effectiveness of the proposed normalized WSM based PTC algorithm was verified by comparing the obtained simulation and experimental results with classical PTC of OEWIM drive with four-level inversion. By using normalized WSM, selection of weighting factors is simplified but it can't eliminate weighting factors. To eliminate weighting factors, a novel simplified weighting factor eliminated PTC strategy has been introduced. The weighting factor elimination strategy uses splitting of cost function into flux control objective (cost function-I) and torque control objective (cost function-II). The voltage vectors which maintain minimum flux ripple obtained in cost function-I are used in cost function-II to maintain minimum torque ripple. Finally, a voltage vector is chosen in such a way that it maintains minimum torque ripple. To validate the effectiveness of the proposed PTC strategies, experimentation was carried by implementing them with dSPACE DS-1104 controller.

1.4 Thesis Contributions

The contributions of this thesis are as follows:

1) This thesis introduces implementation of DTC and PTC strategies for the OEWIM drive with two, three and four-level inversion.
2) Proposed an effective voltage switching state algorithms to a direct torque controlled OEWIM drive to reduce torque and flux ripples by operating it with equal and unequal DC link voltages.
3) Proposed PTC strategy for the OEWIM drive by classifying the voltage vectors into several categories based on rotor speed to reduce the computational burden, ripples in torque and flux.

4) To reduce switching frequency, normalized WSM based PTC and weighting factor eliminated PTC strategies are proposed for the OEWIM drive.
5) The voltage vectors used in proposed DTC and PTC strategies maintains minimum CMV, hence the effects of CMV are reduced.

1.5 Organization of the Thesis

The thesis work is organized into six chapters and is presented as follows;

Chapter 1 introduces the study and discusses speed control methods of induction motors. Brief introduction and the need for OEWIM drives have been presented. The scope of the work has been highlighted and objectives of the thesis have been summarized.

Chapter 2 presents modelling and analysis of dual inverter fed OEWIM drive with equal DC link voltage. The dynamic model of OEWIM drive in stationary reference frame is exhibited. The principle and voltage space vector locations of dual inverter fed OEWIM drive are illustrated. The DTC of OEWIM drive with three-level inversion is proposed.

Chapter 3 presents principle and voltage space vector locations of OEWIM drive with unequal DC link voltage. This chapter presents classification of active voltage vectors based on operating speed of OEWIM drive. An effective voltage switching state algorithm for direct torque controlled OEWIM drive with four-level inversion has been proposed and the results are compared with classical two-level inversion.

Chapter 4 presents discrete model of power converter and OEWIM drive to predict the control variables. This chapter proposes integration of PTC for dual inverter fed OEWIM drive with multi-level inversion. The proposed PTC strategy is discussed step by step. This chapter also presents how the proposed PTC strategy reduces computational burden on the controller. It illustrates comparative study among two, three and four-level inversion fed OEWIM drive.

Chapter 5 gives a simplified weighting factor selection based PTC and weighting factor eliminated PTC strategies for the OEWIM drive with four-level inversion. A multi-criterion decision making algorithm is introduced to simplify the selection of weighting factors. Normalized WSM is proposed to simplify the tuning process of weighting factors. A modified

cost function based PTC strategy is introduced to reduce the switching frequency of OEWIM drive. Weighting factor eliminated PTC strategy is proposed for the OEWIM drive by splitting the cost function. The proposed PTC strategies are verified experimentally by implementing them in real time for experimental studies. The experimental results are compared with simulation studies and classical four-level PTC algorithm.

Finally, **Chapter 6** gives a summary of key achievements illustrated in this thesis and also gives future scope of the proposed DTC and PTC strategies.

Chapter 2

An Enhanced Three-level Voltage Switching State Scheme for Direct Torque Controlled Open-end Winding Induction Motor

Chapter 2

An Enhanced Three-level Voltage Switching State Scheme for Direct Torque Controlled Open-end Winding Induction Motor

2.1 Introduction

Classical DTC gives higher ripple in torque and flux when compared with FOC. In analog implementation the torque and flux ripples are exactly within the hysteresis bounds, whereas the problem arises due to discrete implementation. In discrete implementation the torque and flux ripples are not in the hysteresis boundaries and causes high ripples in torque and flux [10]. To abate the problems of classical DTC, MLI fed induction motor drives are unavoidable. This chapter introduces DTC of dual inverter fed OEWIM drive with two and three-level inversion. In order to maintain lower ripple in torque and flux, DTC with multi-level inversion is an effective alternative. An improved voltage switching state algorithm is introduced for three-level inversion fed OEWIM drive to reduce torque and flux ripples. The formulation of voltage space vectors and their locations used for two-level and three-level inversion is introduced in this chapter. The proposed DTC algorithm does not use complex look-up tables and hysteresis controllers as used in MLI fed DTC strategies [24]-[26]. This chapter presents dynamic modelling of OEWIM drive, VSIs and also gives the effect of voltage vectors on the performance of OEWIM drive. The location of active voltage vectors is chosen in such a way that the switching transitions and CMV involved with these space vectors are low. The three-level inversion is obtained by operating VSIs with equal DC-link voltages and it produces 18 active voltage vectors. These ‘18’ active voltage vectors are divided into low, medium and high frequencies of operation based on rotor speed.

2.2 Configuration of OEWIM Drive for Two and Three-level Inversion

The power circuit configuration of OEWIM drive is as shown in Figure 2.1. In the power circuit configuration two inverters are operated with isolated DC power supplies and equal DC link voltages. By operating OEWIM drive with equal DC link voltage two and three-

level inversions are obtained. The voltage space vector combinations of Inverter-1 and Inverter-2 are shown in Figure 2.2.

The pole voltages of Inverter-1 are named as V_{ro}, V_{yo} and V_{bo}. The pole voltages of Inverter-2 are named as $V_{r'o'}$, $V_{y'o'}$ and $V_{b'o'}$ and the pole voltages are measured with respect to points o and o'. The pole voltage of Inverter-1 'V_{ro}' assumes $V_{dc}/4$ or $-V_{dc}/4$, similarly the pole voltage of Inverter-2 '$V_{r'o'}$' is $V_{dc}/4$ or $-V_{dc}/4$ [12]. The phase voltages at the terminals of OEWIM are obtained by taking difference of resultant pole voltage and CMV.

$$\begin{bmatrix} V_{ro} \\ V_{yo} \\ V_{bo} \end{bmatrix} = \begin{cases} \dfrac{V_{dc}}{4} \text{ when } S_r = S_y = S_b = 1 \\ -\dfrac{V_{dc}}{4} \text{ when } S_r = S_y = S_b = 0 \end{cases} \tag{2.1}$$

$$\begin{bmatrix} V_{r'o'} \\ V_{y'o'} \\ V_{b'o'} \end{bmatrix} = \begin{cases} \dfrac{V_{dc}}{4} \text{ when } S_{r'} = S_{y'} = S_{b'} = 1 \\ -\dfrac{V_{dc}}{4} \text{ when } S_{r'} = S_{y'} = S_{b'} = 0 \end{cases} \tag{2.2}$$

The resultant pole voltage of dual inverter is given by (2.3). Pole voltages of Inverter-1 are given by (2.1) and pole voltages of Inverter-2 are given by (2.2). In (2.1) and (2.2), if S_r to $S_{b'}$ =1 then the top switch of the respective leg is ON; similarly when S_r to $S_{b'}$ =0 the bottom switch of respective leg is ON.

$$\begin{bmatrix} \Delta V_{rr'} \\ \Delta V_{yy'} \\ \Delta V_{bb'} \end{bmatrix} = \begin{bmatrix} V_{ro} - V_{r'o'} \\ V_{yo} - V_{y'o'} \\ V_{bo} - V_{b'o'} \end{bmatrix} \tag{2.3}$$

CMV of OEWIM is given by (2.4) and it is obtained from resultant pole voltages.

$$V_{oo'} = V_o = \frac{\left(\Delta V_{rr'} + \Delta V_{yy'} + \Delta V_{bb'}\right)}{3} \tag{2.4}$$

The phase voltages of OEWIM are given by (2.5)

$$\begin{bmatrix} V_{rr'} \\ V_{yy'} \\ V_{bb'} \end{bmatrix} = \begin{bmatrix} \Delta V_{rr'} \\ \Delta V_{yy'} \\ \Delta V_{bb'} \end{bmatrix} - \begin{bmatrix} V_o \\ V_o \\ V_o \end{bmatrix} \tag{2.5}$$

From (2.5), the simplified dual inverter model in terms of pole voltages of Inverter-1 and Inverter-2 can be written as (2.6)

$$\begin{bmatrix} V_{rr'} \\ V_{yy'} \\ V_{bb'} \end{bmatrix} = \frac{1}{3}\begin{bmatrix} 2 & -1 & -1 \\ -1 & 2 & -1 \\ -1 & -1 & 2 \end{bmatrix}\begin{bmatrix} \Delta V_{rr'} \\ \Delta V_{yy'} \\ \Delta V_{bb'} \end{bmatrix} \tag{2.6}$$

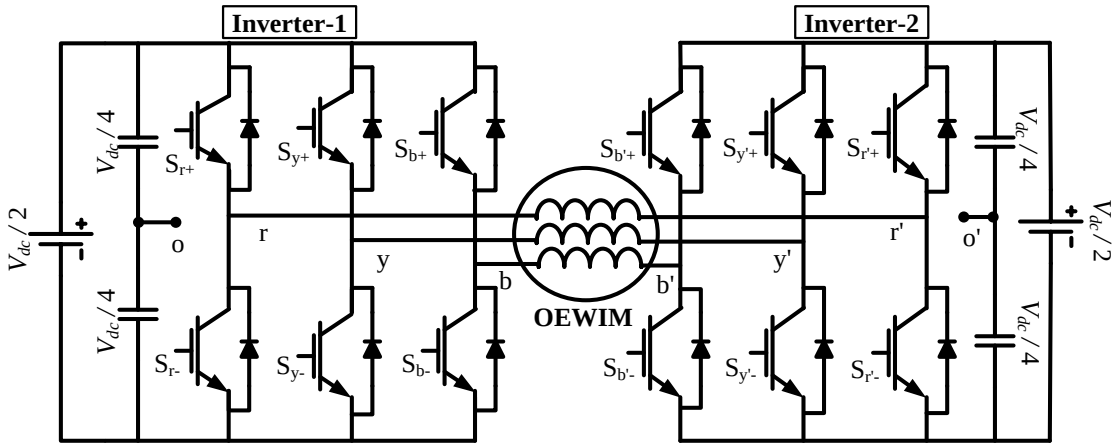

Figure 2.1 Power circuit of OEWIM drive for two and three-level inversion

The voltage space vector of Inverter-1 is given by (2.7), whereas the voltage space vector of Inverter-2 is given by (2.8) and the resultant voltage space vector (2.9) of dual inverter configuration is obtained by using (2.7) and (2.8).

$$v_{s1} = \frac{2}{3}\frac{V_{dc}}{2}\left(S_r + S_y e^{j2\pi/3} + S_b e^{j4\pi/3} \right) \tag{2.7}$$

$$v_{s2} = \frac{2}{3}\frac{V_{dc}}{2}\left(S_{r'} + S_{y'} e^{j2\pi/3} + S_{b'} e^{j4\pi/3} \right) \tag{2.8}$$

$$\text{and } v_s = \left(v_{s1} - v_{s2}\right) \tag{2.9}$$

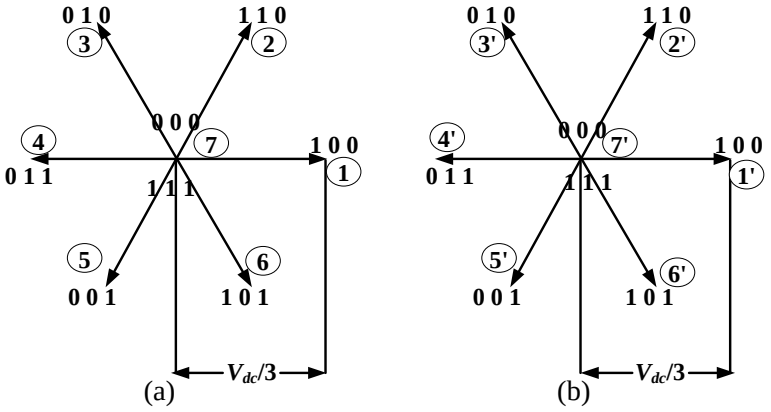

Figure 2.2 Voltage space vector combinations: (a) Inverter-1 and (b) Inverter-2

The voltage space vectors of Inverter-1 and Inverter-2 are determined for all possible combinations of switching states. Inverter-1 has 8 switching states and Inverter-2 has 8 switching states, hence the dual inverter configuration provides 64 possible switching states. All possible switching combinations of Inverter-1 and Inverter-2 are shown in Table 2.1. With these 64 possible switching states, 19 space vector locations can be obtained. These 19 space vector locations are chosen based on the number of switch transitions and the effect of CMV. Out of these 19 space vectors, 18 space vectors are called active voltage vectors and one is null vector. The voltage space vectors used in this chapter are shown in Table 2.2 and 2.3. The voltage space vector utilized in DTC of OEWIM drive with two-level inversion is shown in Table 2.2, whereas Table 2.3 represents voltage space vectors used for three-level inversion.

The following is an example to determine resultant space vector for switching combinations of (1,0,0) & (0,1,1) for inverters 1 and 2. Where '1' refers to the top switch of the respective leg of voltage source inverter is ON, '0' indicates the bottom switch of the respective leg of inverter is ON. The output voltages of inverters are given by (2.7) and (2.8). The voltage space vector v_s is obtained from the resultant of pole voltages of Inverter-1 and Inverter-2 (2.9). If the switching combinations are (1,1,0) and (0,1,0) then the voltage space vector has a magnitude of $V_{dc}/2$, and it is named as v_1. On arranging the switching combinations of dual inverter for two-level inversion, the obtained voltage space vector locations are shown in Figure 2.4.

2.3 Dynamic Model of OEWIM drive

The dynamic model of OEWIM is developed in stationary reference frame (Clarkes transformation). The dynamic equations used for DTC and PTC of OEWIM are given by (2.10)-(2.16). The stator and rotor voltage equations in complex form (space vector) are given by (2.10) and (2.11).

$$\begin{bmatrix} v_{s\alpha} \\ v_{s\beta} \end{bmatrix} = R_s \begin{bmatrix} i_{s\alpha} \\ i_{s\beta} \end{bmatrix} + p \begin{bmatrix} \psi_{s\alpha} \\ \psi_{s\beta} \end{bmatrix} \tag{2.10}$$

$$\begin{bmatrix} 0 \\ 0 \end{bmatrix} = R_r \begin{bmatrix} i_{r\alpha} \\ i_{r\beta} \end{bmatrix} + p \begin{bmatrix} \psi_{r\alpha} \\ \psi_{r\beta} \end{bmatrix} + \omega_e \begin{bmatrix} \psi_{r\beta} \\ -\psi_{r\alpha} \end{bmatrix} \tag{2.11}$$

Table 2.1 All possible switching combinations of dual inverter fed OEWIM drive with equal DC-link voltage

Inverter-1			**Inverter-2**			**Switching Combination**	**Realization**		**CMV (V)**
S_r	S_y	S_b	$S_{r'}$	$S_{y'}$	$S_{b'}$		v_α	v_β	Vo
0	0	0	0	0	0	1	0	0	0
0	0	0	1	0	0	2	-0.333	0	$-V_{dc}/6$
0	0	0	1	1	0	3	-0.1667	-0.2887	$-V_{dc}/3$
0	0	0	0	1	0	4	0.1667	-0.2887	$-V_{dc}/6$
0	0	0	0	1	1	5	0.333	0	$-V_{dc}/3$
0	0	0	0	0	1	6	0.1667	0.2887	$-V_{dc}/6$
0	0	0	1	0	1	7	-0.1667	0.2887	$-V_{dc}/3$
0	0	0	1	1	1	8	0	0	$-V_{dc}/2$
1	0	0	0	0	0	9	0.3333	0	$V_{dc}/6$
1	0	0	1	0	0	10	0	0	0
1	**0**	**0**	**1**	**1**	**0**	**11**	**0.1667**	**-0.2887**	$\mathbf{-V_{dc}/6}$
1	**0**	**0**	**0**	**1**	**0**	**12**	**0.5000**	**-0.2887**	**0**
1	**0**	**0**	**0**	**1**	**1**	**13**	**0.6667**	**0**	$\mathbf{-V_{dc}/6}$
1	0	0	0	0	1	14	0.5000	0.2887	0
1	0	0	1	0	1	15	0.1667	0.2887	$-V_{dc}/6$
1	0	0	1	1	1	16	0.333	0	$-V_{dc}/3$
1	1	0	0	0	0	17	0.1667	0.2887	$V_{dc}/3$
1	1	0	1	0	0	18	-0.1667	0.2887	$V_{dc}/6$
1	**1**	**0**	**1**	**1**	**0**	**19**	**0**	**0**	**0**
1	**1**	**0**	**0**	**1**	**0**	**20**	**0.333**	**0**	$\mathbf{V_{dc}/6}$
1	**1**	**0**	**0**	**1**	**1**	**21**	**0.5000**	**0.2887**	**0**
1	**1**	**0**	**0**	**0**	**1**	**22**	**0.3333**	**0.5774**	$\mathbf{V_{dc}/6}$
1	1	0	1	0	1	23	0	0.5774	0
1	1	0	1	1	1	24	0.1667	0.2887	$-V_{dc}/6$
0	1	0	0	0	0	25	-0.1667	0.2887	$V_{dc}/6$
0	1	0	1	0	0	26	-0.5000	0.2887	0
0	1	0	1	1	0	27	-0.3333	0	$-V_{dc}/6$
0	1	0	0	1	0	28	0	0	0
0	**1**	**0**	**0**	**1**	**1**	**29**	**0.1667**	**0.2887**	$\mathbf{-V_{dc}/6}$
0	**1**	**0**	**0**	**0**	**1**	**30**	**0**	**0.5774**	**0**
0	**1**	**0**	**1**	**0**	**1**	**31**	**-0.3333**	**0.5774**	$\mathbf{-V_{dc}/6}$
0	1	0	1	1	1	32	-0.1667	0.2887	$-V_{dc}/3$
0	1	1	0	0	0	33	-0.333	0	$V_{dc}/3$
0	**1**	**1**	**1**	**0**	**0**	**34**	**-0.6667**	**0**	$\mathbf{V_{dc}/6}$
0	1	1	1	1	0	35	-0.5	-0.2887	0
0	1	1	0	1	0	36	-0.1667	-0.2887	$V_{dc}/6$
0	1	1	0	1	1	37	0	0	0
0	**1**	**1**	**0**	**0**	**1**	**38**	**-0.1667**	**0.2887**	$\mathbf{V_{dc}/6}$
0	**1**	**1**	**1**	**0**	**1**	**39**	**-0.5**	**0.2887**	**0**
0	1	1	1	1	1	40	-0.333	0	$-V_{dc}/6$
0	0	1	0	0	0	41	-0.1667	-0.2887	$V_{dc}/6$
0	**0**	**1**	**1**	**0**	**0**	**42**	**-0.5**	**-0.2887**	**0**
0	**0**	**1**	**1**	**1**	**0**	**43**	**-0.333**	**-0.5774**	$\mathbf{-V_{dc}/6}$
0	0	1	0	1	0	44	0	-0.5774	0
0	0	1	0	1	1	45	0.1667	-0.2887	$-V_{dc}/6$
0	0	1	0	0	1	46	0	0	0
0	**0**	**1**	**1**	**0**	**1**	**47**	**-0.3333**	**0**	$\mathbf{-V_{dc}/6}$
0	0	1	1	1	1	48	-0.1667	-0.2887	$-V_{dc}/3$
1	0	1	0	0	0	49	0.1667	-0.2887	$V_{dc}/3$

1	**0**	**1**	**1**	**0**	**0**	**50**	**-0.1667**	**-0.2887**	**V_{dc}/6**
1	**0**	**1**	**1**	**1**	**0**	**51**	**0**	**-0.5774**	**0**
1	**0**	**1**	**0**	**1**	**0**	**52**	**0.3333**	**-0.5774**	**V_{dc}/6**
1	0	1	0	1	1	53	0.5	-0.2887	0
1	0	1	0	0	1	54	0.3333	0	V_{dc}/6
1	0	1	1	0	1	55	0	0	0
1	0	1	1	1	1	56	0.1667	-0.2887	-V_{dc}/6
1	1	1	0	0	0	57	0	0	V_{dc}/2
1	1	1	1	0	0	58	-0.3333	0	V_{dc}/3
1	1	1	1	1	0	59	-0.1667	-0.2887	V_{dc}/6
1	1	1	0	1	0	60	0.1667	-0.2887	V_{dc}/3
1	1	1	0	1	1	61	0.3333	0	V_{dc}/6
1	1	1	0	0	1	62	0.1667	0.2887	V_{dc}/3
1	1	1	1	0	1	63	-0.1667	0.2887	V_{dc}/6
1	1	1	1	1	1	64	0	0	0

Table 2.2 Voltage space vectors used to implement DTC of OEWIM drive with two-level inversion

Inverter-1			**Inverter-2**			**Voltage Space Vectors**	**Realization**		**CMV**
S_r	**S_y**	**S_b**	**$S_{r'}$**	**$S_{y'}$**	**$S_{b'}$**	***v_s***	**Magnitude**	**Angle (°)**	**Vo**
1	1	0	1	1	0	v_0	0	0	0
1	0	0	0	1	1	v_1	0.667V_{dc}	0	-V_{dc}/6
1	1	0	0	0	1	v_2	0.667V_{dc}	60	V_{dc}/6
0	1	0	1	0	1	v_3	0.667V_{dc}	120	-V_{dc}/6
0	1	1	1	0	0	v_4	0.667V_{dc}	180	V_{dc}/6
0	0	1	1	1	0	v_5	0.667V_{dc}	-120	-V_{dc}/6
1	0	1	0	1	0	v_6	0.667V_{dc}	-60	V_{dc}/6

Table 2.3 Voltage space vectors used to implement DTC of OEWIM drive with three-level inversion

Inverter-1			**Inverter-2**			**Voltage Space Vectors**	**Realization**		**CMV**	**Output voltage Level**
S_r	**S_y**	**S_b**	**$S_{r'}$**	**$S_{y'}$**	**$S_{b'}$**	***v_s***	**Magnitude**	**Angle (°)**	**Vo**	
1	1	0	1	1	0	v_0	0	0	0	Space vectors v_1-v_6, delivers Two-level output voltage
1	1	0	0	1	0	v_1	0.333V_{dc}	0	V_{dc}/6	
0	1	0	0	1	1	v_2	0.333V_{dc}	60	-V_{dc}/6	
0	1	1	0	0	1	v_3	0.333V_{dc}	120	V_{dc}/6	
0	0	1	1	0	1	v_4	0.333V_{dc}	180	-V_{dc}/6	
1	0	1	1	0	0	v_5	0.333V_{dc}	-120	V_{dc}/6	
1	0	0	1	1	0	v_6	0.333V_{dc}	-60	-V_{dc}/6	
1	0	0	0	1	1	v_7	0.667V_{dc}	0	-V_{dc}/6	Space vectors v_7-v_{18}, delivers Three-level output voltage
1	1	0	0	1	1	v_8	0.5774V_{dc}	30	0	
1	1	0	0	0	1	v_9	0.667V_{dc}	60	V_{dc}/6	
0	1	0	0	0	1	v_{10}	0.5774V_{dc}	90	0	
0	1	0	1	0	1	v_{11}	0.667V_{dc}	120	-V_{dc}/6	
0	1	1	1	0	1	v_{12}	0.5774V_{dc}	150	0	
0	1	1	1	0	0	v_{13}	0.667V_{dc}	180	V_{dc}/6	
0	0	1	1	0	0	v_{14}	0.5774V_{dc}	-150	0	
0	0	1	1	1	0	v_{15}	0.667V_{dc}	-120	-V_{dc}/6	
1	0	1	1	1	0	v_{16}	0.5774V_{dc}	-90	0	
1	0	1	0	1	0	v_{17}	0.667V_{dc}	-60	V_{dc}/6	
1	0	0	0	1	0	v_{18}	0.5774V_{dc}	-30	0	

Flux linkages of stator and rotor are given by (2.12) and (2.13), (2.14) represents magnitude of stator flux space vector [49].

$$\begin{bmatrix} \psi_{s\alpha} \\ \psi_{s\beta} \end{bmatrix} = L_s \begin{bmatrix} i_{s\alpha} \\ i_{s\beta} \end{bmatrix} + L_m \begin{bmatrix} i_{r\alpha} \\ i_{r\beta} \end{bmatrix} \tag{2.12}$$

$$\begin{bmatrix} \psi_{r\alpha} \\ \psi_{r\beta} \end{bmatrix} = L_r \begin{bmatrix} i_{r\alpha} \\ i_{r\beta} \end{bmatrix} + L_m \begin{bmatrix} i_{s\alpha} \\ i_{s\beta} \end{bmatrix} \tag{2.13}$$

$$\left|\psi_s\right| = \left|\psi_{s\alpha} + j\psi_{s\beta}\right| \tag{2.14}$$

Torque of OEWIM is given by (2.15)

$$T_e = \frac{3}{2}\frac{P}{2}\left(\psi_{s\alpha} i_{s\beta} - \psi_{s\beta} i_{s\alpha}\right) \tag{2.15}$$

Speed of OEWIM is obtained from state-space model (2.16)

$$\begin{cases} T_e - T_L = J\left(p\omega_m\right) \\ \left(p\omega_m\right) = \dfrac{1}{J}\left(T_e - T_L\right) \end{cases} \tag{2.16}$$

where R_s is stator resistance, L_s is stator inductance, L_r is rotor inductance, L_m is mutual inductance, ($v_{s\alpha}$, $v_{s\beta}$) are stator voltages, ($i_{s\alpha}$, $i_{s\beta}$) are stator currents, ($\psi_{s\alpha}$, $\psi_{s\beta}$) are stator flux in stationary reference frame, p is differential operator (d/dt), P is number of poles, T_e is electromagnetic torque, T_L is load torque, J is moment of inertia, ω_m is angular speed in mechanical rad/s, ω_e is angular speed in electrical rad/s.

2.4 DTC of OEWIM Drive with Two-level Inversion

The block diagram of two-level inversion fed direct torque controlled OEWIM drive is shown in Figure 2.3. In the block diagram, the induction motor is fed by two voltage source inverters. The difference of output voltage of two inverters is used to operate the motor. In the block diagram ω_{ref} is reference speed (rad/s), ω_e is actual speed of rotor (rad/s in electrical systems), ω_m is actual speed of rotor (rad/s in mechanical systems), T_{ref} is reference torque (Nm) obtained from speed PI controller, T_e is estimated torque (Nm), ψ_{ref} is reference flux (Wb), ψ_s is estimated stator flux (Wb), V_{dc} is the effective DC link Voltage of dual inverter configuration and i_r, i_y are the stator currents.

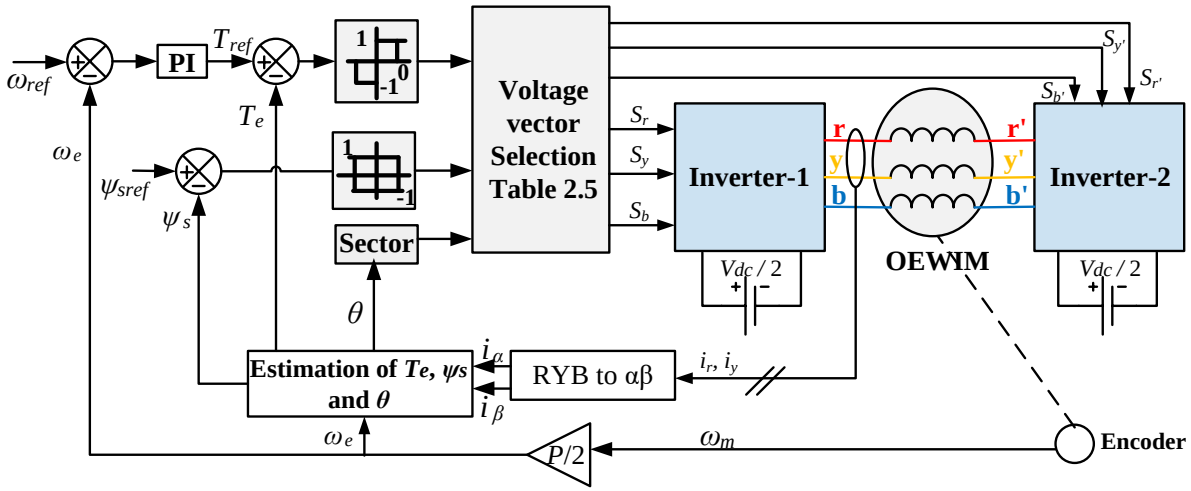

Figure 2.3 Block diagram of direct torque controlled OEWIM drive with two-level inversion

The operating principle of DTC of OEWIM drive with two-level inversion is same as classical DTC of induction motor. In two-level configuration of OEWIM drive, it uses seven voltage space vectors; out of these seven voltage space vectors, six voltage vectors are termed as active voltage vectors and one is null vector. These seven voltage vectors are used for all speeds of operation of OEWIM drive. The advantages of using seven voltage vectors are: (i) They can provide minimum CMV (0, $\pm V_{dc}/6$) (ii) The switching transitions between one voltage space vector to another space vector is less and (iii) There are only seven voltage vectors instead of eight voltage vectors. The location of voltage vectors and the division of sectors used to implement DTC of OEWIM drive with two-level inversion is shown in Figure 2.4.

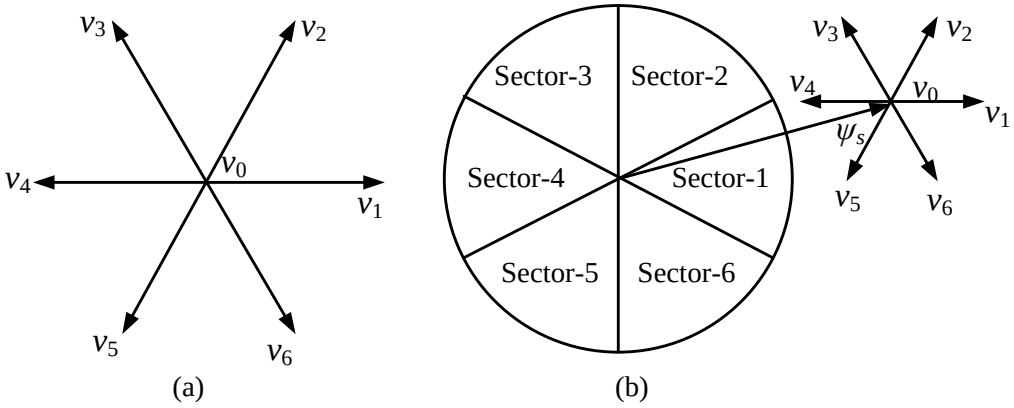

Figure 2.4 (a) Location of active voltage vectors for two-level inversion and (b) Classification of sectors

On combining the voltage vectors v_0 to v_7 it forms like hexagon as shown in Figure 2.4(a). The resultant voltage space vector (v_s) is divided into six sectors as shown in Figure 2.4(b). Each sector is divided with an angle of 60°. Sector-1 is from 330° to 30°. Sector-2 is from 30° to 90°. Sector-3 is from 90° to 150°. Sector-4 is from 150° to 210°. Sector-5 is from 210° to 270° and sector-6 is from 270° to 330°.

2.4.1 Operating Principle

The torque of OEWIM drive in stationary reference frames is given by (2.17)

$$T_e = \frac{3}{2}\frac{P}{2}\left(\psi_{s\alpha} i_{s\beta} - \psi_{s\beta} i_{s\alpha}\right) \tag{2.17}$$

On simplification (2.17) can be written as

$$T_e = \frac{3}{2}\frac{P}{2}\left(\psi_s i_s \sin\alpha\right) \tag{2.18}$$

where, P is the number of poles, ψ_s is stator flux linkages, i_s is stator current and α is angle between stator flux linkage and stator current space vector. From (2.18) the torque of induction motor is dependent on stator flux and stator current, hence the lower torque ripple can be obtained by maintaining lower stator flux ripple and lower current ripple.

The dynamic changes in torque can be obtained by performing the switching action of Inverters-1 and inverter-2. By performing switching action, the output voltage of inverter will be controlled. The switching states of inverter are selected in such a way that they should maintain low current ripple. The stator flux can be changed very quickly by applying suitable voltage vectors and the rotor flux is assumed to be constant in a sampling interval. The dynamical changes in torque can be obtained by quickly changing the angle between stator flux linkage and stator current. Table 2.4 represents the application of suitable voltage vectors to increase or decrease flux and torque by assuming stator flux is in sector-1. In Table 2.4, +++ refers to more increment, ++ to an increase while + indicates small increment, - indicates small decrement, -- decrease and --- a large decrement. Table 2.4 gives information about the effect of voltage space vectors on stator flux and angle between stator flux linkages and stator current. The voltage vectors have a direct impact on stator flux; the dynamic changes in flux cause dynamic variation in load angle and vary electromagnetic torque.

Table 2.4 Effect of voltage space vectors on electromagnetic torque and stator flux in sector-1

	v_1	v_2	v_3	v_4	v_5	v_6	v_0
Flux	+++	++	-	---	--	+	0
Torque	-	++	+++	+	--	---	0

An example is illustrated to indicate the impact of voltage vector by considering flux space vector in sector-1 shown in Figure 2.5. In Figure 2.5(a) the flux space vector is assumed to lie in between 0° and 30°. From Figure 2.5(a) it can be observed that, if the flux space vector is in sector-1, then by applying the voltage vector v_1, the magnitude of flux gets increases, whereas the torque reduces as the angle between stator flux and current decreases.

In Figure 2.5(b), the flux space vector is assumed to be in between 330° and 0°, then by applying v_1, stator flux gets increases whereas the torque decreases. In Figure 2.5(c), to increase torque and flux simultaneously it is assumed that voltage vector v_4 has to be applied; by applying v_4 flux decreases whereas torque increases by a small amount. If the flux space vector is in sector-1 then v_1, v_3, v_4 should not be applied to increase/decrease both flux and torque.

If it is required to increase torque and flux then voltage vector v_2 has to be applied. If it is required to decrease flux and torque of induction motor, voltage vector v_5 has to be applied. If it is required to increase torque and decrease flux then the suitable voltage vector to be applied is v_3. If it is required to decrease torque and increase flux, then voltage vector v_6 has to be applied.

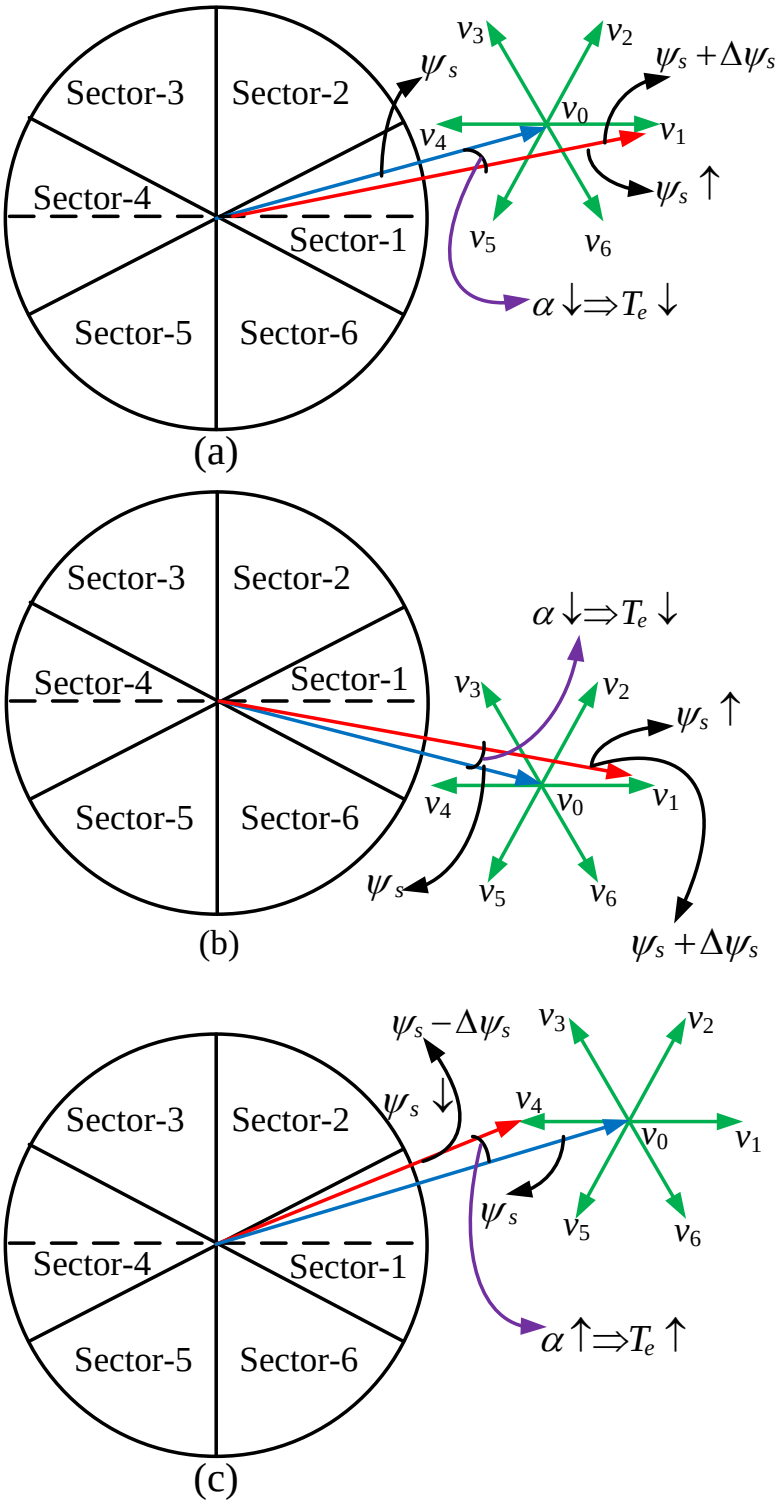

Figure 2.5 Effect of voltage space vectors v_1 and v_4 on torque and flux by assuming the flux space vector in sector-1: (a) Effect of v_1 by assuming flux space vector is in between 0° to 30°. (b) Effect of v_1 by assuming flux space vector is in between 330° and 0° and (c) Effect of v_4 on torque and flux

Table 2.5 Selection of voltage vectors based on torque error, flux error and sector

Flux Error	Torque Error	Sector					
		1	2	3	4	5	6
1	1	v_2	v_3	v_4	v_5	v_6	v_1
	0	v_0	v_0	v_0	v_0	v_0	v_0
	-1	v_6	v_1	v_2	v_3	v_4	v_5
-1	1	v_3	v_4	v_5	v_6	v_1	v_2
	0	v_0	v_0	v_0	v_0	v_0	v_0
	-1	v_5	v_6	v_1	v_2	v_3	v_4

The proposed classical two-level inversion fed DTC utilizes three-level torque comparator and a two-level flux comparator and information of stator flux sector. It does not depend on exact location of flux space phasor; it needs to know in which sector the flux space phasor exists. Based on outputs of torque hysteresis controller and flux hysteresis controller and sector of flux space phasor suitable voltage vector is applied. The selection of active voltage vectors based on torque and flux errors are shown in Table 2.5. The flowchart to develop DTC of OEWIM drive with two-level inversion is shown in Figure 2.6.

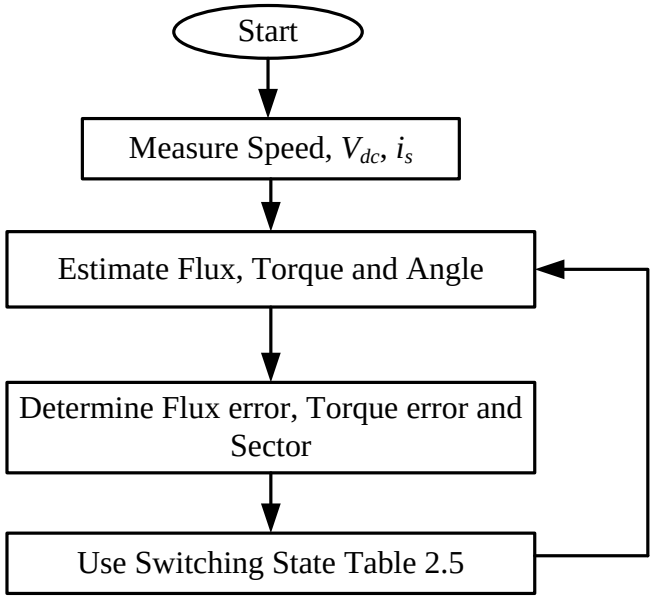

Figure 2.6 Flowchart of DTC of OEWIM with classical two-level inversion

2.5 DTC of OEWIM Drive with Three-level Inversion

The configuration of DTC of OEWIM drive with three-level inversion is shown in Figure 2.7; the motor is supplied with the difference of voltages obtained from two inverters.

Three-level inversion was obtained by operating two inverters with equal DC-link voltage. The advantage of OEWIM configuration is it uses two inverters and they are operated with half of the rated DC-link voltage. Table 2.3 shows the realization of voltage space vectors used to implement the proposed DTC algorithm. Switches are turned 'ON', to realize the switching states to obtain three-level output voltage.

In Figure 2.8, there are 18 non-zero voltage vectors (v_1 to v_{18}). The active vectors of OEWIM drive with three-level inversion are shown in Figure 2.8, (2.1) – (2.3) are used to realize voltage vectors. There exist 19 space vector locations for three-level inversion.

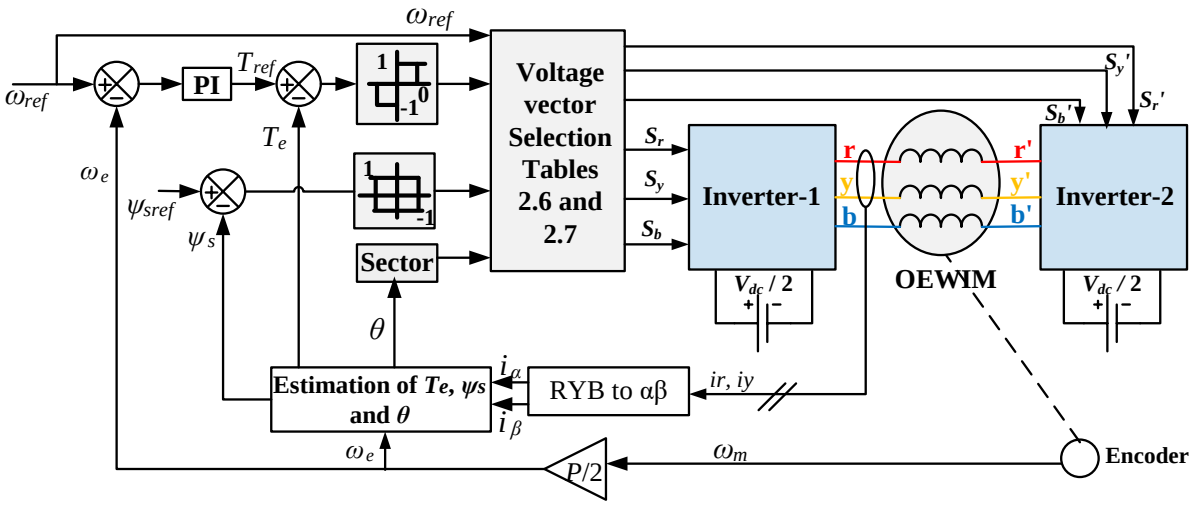

Figure 2.7 DTC of OEWIM with three-level inversion

On arranging all the vectors described in Table 2.3, it forms like a hexagon and it is shown in Figure 2.9; further the voltage space vectors are divided into 12-sectors. Sector-1 occupies (345°-15°) with respect to real-axis. Sector-2 is from (15°-45°). Sector-3 is from (45°-75°). Sector-4 is from (75°-105°). Sector-5 is from (105°-135°). Sector-6 is from (135°-165°). Sector-7 is from (165°-195°). Sector-8 is from (195°-225°). Sector-9 is from (225°-255°). Sector-10 is from (255°-285°). Sector-11 is from (285°-315°) and sector-12 is from (315°-345°).

From space vector diagram, the voltage vectors are categorized into two groups. Voltage vectors v_7 to v_{18} are used to operate at higher frequencies (more than 50% of ω_r).

Voltage space vectors v_1 to v_6 are used to operate the OEWIM drive with low (less than 50% of ω_r) and medium (between low-high) frequencies.

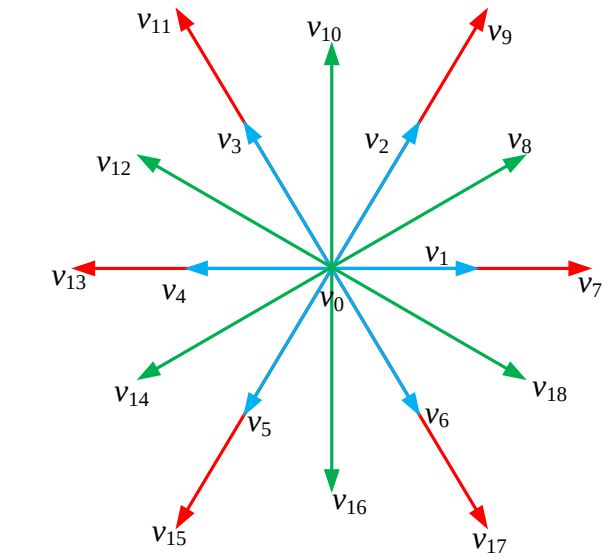

Figure 2.8 Active voltage vector locations of OEWIM drive for three-level inversion

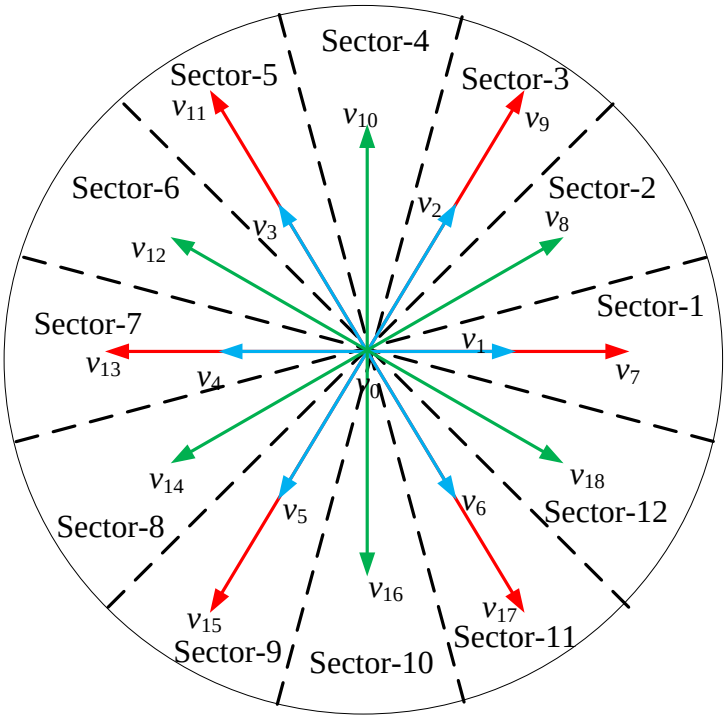

Figure 2.9 Classification of sector in three-level inversion fed DTC of OEWIM drive

2.5.1 High Speeds of Operation

The voltage space vectors v_7 to v_{18} and a null vector v_0 are used to control torque and flux of OEWIM drive for high frequencies of operation. In Figure 2.9, if the location of stator flux is in sector-1, then the voltage space vectors v_8, v_9, v_{17} and v_{18} are applied to increase its magnitude, whereas voltage space vectors v_{11}, v_{12}, v_{14} and v_{15} are applied to reduce its magnitude. For sector-1 to reduce positive torque error v_8, v_9 and v_{10} are utilized, whereas to reduce negative torque error v_{16}, v_{17} and v_{18} are utilized. In this mode of operation v_1 to v_6 should not be used and the selection of vectors is given in Table 2.6. By utilizing the voltage vectors v_7-v_{18} three-level output voltage can be obtained.

Table 2.6 Switching table of proposed three-level DTC for high speeds of operation

Flux Error	**Torque Error**	**Sector**											
		1	**2**	**3**	**4**	**5**	**6**	**7**	**8**	**9**	**10**	**11**	**12**
1	**1**	v_9	v_{10}	v_{11}	v_{12}	v_{13}	v_{14}	v_{15}	v_{16}	v_{17}	v_{18}	v_7	v_8
	-1	v_{17}	v_{18}	v_7	v_8	v_9	v_{10}	v_{11}	v_{12}	v_{13}	v_{14}	v_{15}	v_{16}
-1	**1**	v_{11}	v_{12}	v_{13}	v_{14}	v_{15}	v_{16}	v_{17}	v_{18}	v_7	v_8	v_9	v_{10}
	-1	v_{15}	v_{16}	v_{17}	v_{18}	v_7	v_8	v_9	v_{10}	v_{11}	v_{12}	v_{13}	v_{14}

2.5.2 Medium and Low Speeds of Operation

The voltage vectors v_1 to v_6 and null-vector v_0 are used to control torque and flux of OEWIM drive for medium and low frequencies. In Figure 2.9 if the location of stator flux vector is in sector-1 then the active voltage vectors v_2 and v_6 are applied to increase its magnitude, whereas voltage vectors v_3 and v_5 are applied to decrease its magnitude. In sector-1, to reduce positive torque error v_2 is utilized, whereas to reduce negative torque error v_5 is utilized. In this mode of operation v_7 to v_{18} should not be used as the choice of vectors is given in Table 2.7. By utilizing the voltage vectors v_1-v_6 two-level output voltage can be obtained.

2.5.3 Reduction of Torque and Flux ripple

The voltage ripple has a direct impact on the performance of OEWIM drive. Torque and flux ripples are dependent on voltage ripple. The output voltage of inverter is given by

$$v(t) = R_s i_s + L_s \frac{\mathrm{d}i_s}{\mathrm{dt}} + e_o \tag{2.19}$$

where, $v(t)$ is the output voltage of three-level inverter, and it has 18 voltage space vectors shown in Table 2.3. e_o is the EMF induced and it depends on the frequency of operation. L_s is self-inductance and i_s is current. On neglecting stator voltage drop in (2.19), can be rewritten as

$$\frac{\mathrm{d}i_s}{\mathrm{dt}} = \left(\frac{v(t) - e_o}{L_s} \right) \tag{2.20}$$

From (2.20), it is evident that the rate of change of stator current is dependent on the selection of inverter voltage vector for the respective operating frequency. Hence to get low current ripple at steady state, it is required to select suitable voltage vector which maintains $\mathrm{d}i_s/\mathrm{dt}$ as minimum. The rate of change of stator current is dependent on inverter voltage vector and back EMF. Therefore $\mathrm{d}i_s/\mathrm{dt}$ is independent of rotor flux magnitude. The rotor time constant is much too high when compared to stator time constant. The choice of active voltage vectors to reduce torque and flux ripples are shown in Table 2.6 and 2.7.

Figure 2.10 represents the deviation of current ripple for high and low frequencies of operation. Figure 2.10(a) gives the selection of voltage vector for high frequency of operation by assuming the flux space vector is in sector-1. Figure 2.10(b) represents the selection and impact of voltage vectors for low and medium frequencies. If the flux space vector is in sector-1 by applying vector v_{10} rather than vector v_9 it results in higher change of load angle. Hence, v_{10} should not be applied. To reduce torque and flux errors v_9 should be applied. For low and medium operating frequencies, if flux space vector is in sector-1 then voltage vector v_9 should not be applied to increase torque and flux, because it increases current ripple $\mathrm{d}i_s/\mathrm{dt}$. For low and medium frequencies, voltage vector v_2 should be applied. By applying v_9 and v_2 for high and medium range of frequencies, constant V/f ratio is maintained. The flow chart of direct torque controlled OEWIM drive with three-level inversion is shown in Figure 2.11.

Table 2.7 Switching table of proposed three-level DTC for low and medium speeds of operation

Flux Error	**Torque Error**	**Sector**											
		1	**2**	**3**	**4**	**5**	**6**	**7**	**8**	**9**	**10**	**11**	**12**
1	1	v_2	v_2	v_3	v_3	v_4	v_4	v_5	v_5	v_6	v_6	v_1	v_1
	-1	v_6	v_6	v_1	v_1	v_2	v_2	v_3	v_3	v_4	v_4	v_5	v_5
-1	1	v_3	v_3	v_4	v_4	v_5	v_5	v_6	v_6	v_1	v_1	v_2	v_2
	-1	v_5	v_5	v_6	v_6	v_1	v_1	v_2	v_2	v_3	v_3	v_4	v_4

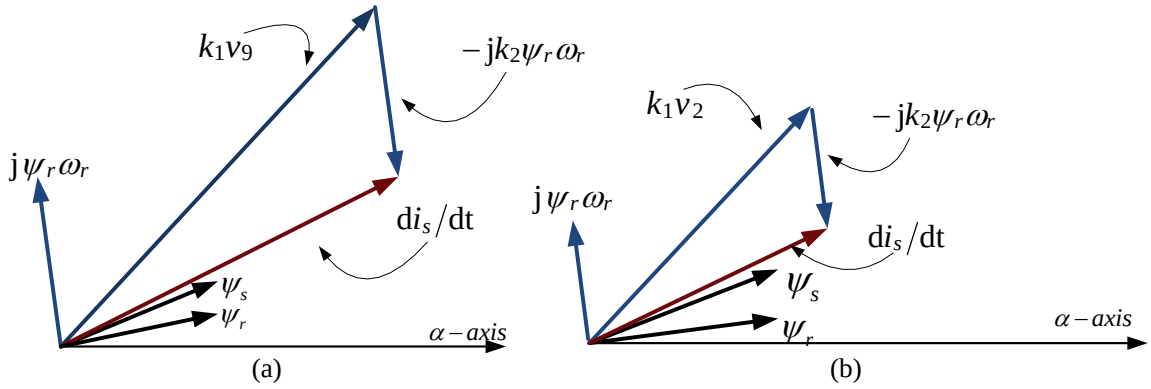

Figure 2.10 Rate of change of stator current to increase flux and torque for: (a) High Speeds of operation and (b) Medium and low speeds of operation

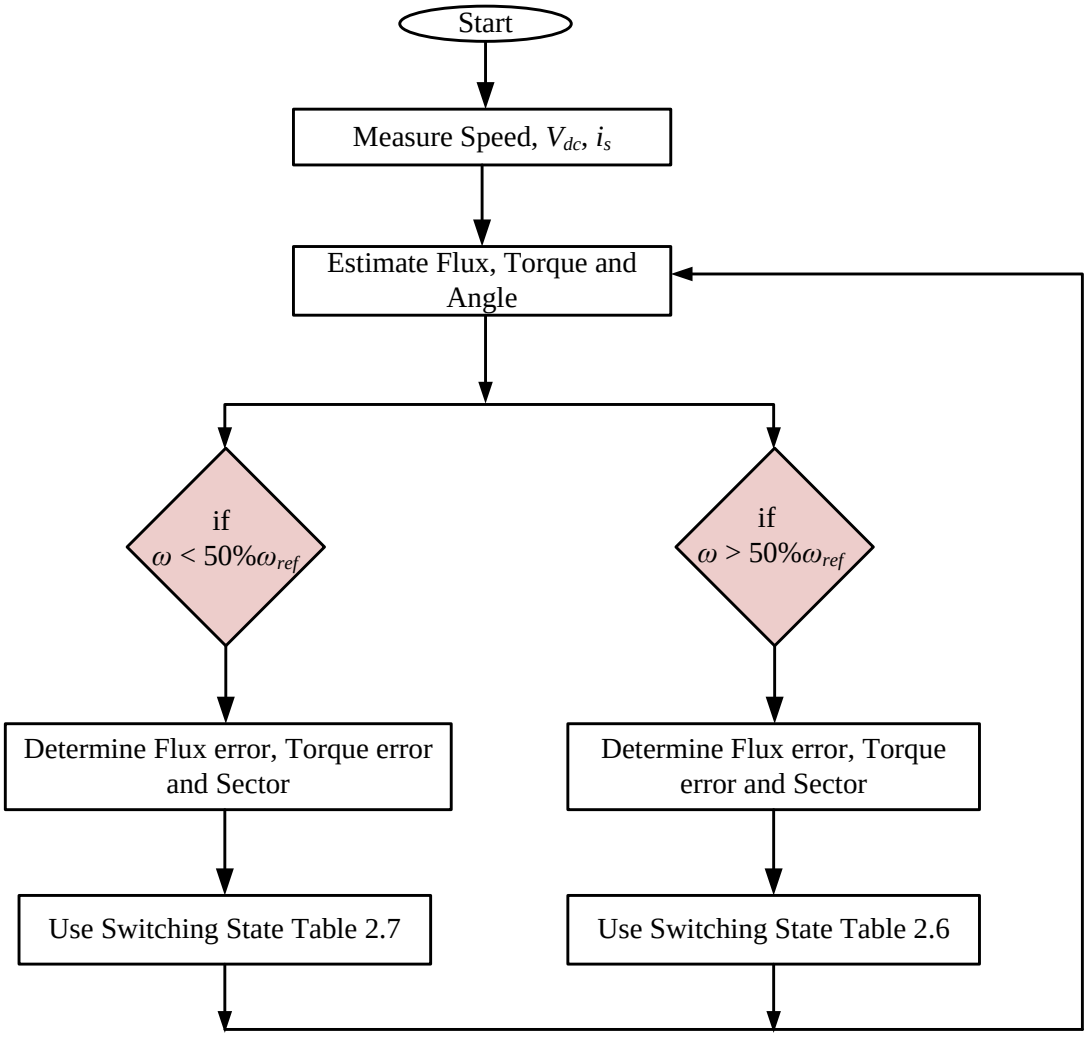

Figure 2.11 Flowchart of DTC of OEWIM drive with three-level inversion

2.6 Simulation and Experimental Results

2.6.1 Simulation Results

The proposed DTC algorithms are simulated in MATLAB/SIMULINK, to verify the performance of OEWIM drive. In the interest of brevity the simulation results are shown for speed variations of 100 rad/s, 200 rad/s and 300 rad/s in forward and reverse motoring modes. Figure 2.12 shows simulation results of OEWIM drive in forward motoring for speed variations of 100 rad/s, 200 rad/s and 300 rad/s with two-level inversion. Figure 2.12 describes speed, torque, flux and phase voltage of OEWIM drive for two-level inversion. The simulation studies are carried by assuming the inverters are operating at a voltage of 270 V. The flux reference used in two-level and three-level inversion is 0.8 Wb. The parameters of OEWIM used for simulation and experimentation are given in appendix Table A.1.

Figure 2.13 demonstrates speed, torque, flux and phase voltage of OEWIM in forward motoring for step change in speeds with three-level inversion. Figure 2.12 and Figure 2.13, shows classical two-level DTC and proposed three-level DTC algorithms for OEWIM drive in forward motoring for speeds of 100 rad/s, 200 rad/s and 300 rad/s. From Figure 2.12 and Figure 2.13, it is observed that the three-level DTC gives fewer ripples in torque and flux when compared with two-level DTC and eliminates several limitations of classical DTC. From Figure 2.13 it is also clear that the proposed three-level inversion operates with specific voltage vectors. In Figure 2.13, for the speed of 100 rad/s OEWIM drive operates with two-level inversion (v_1 to v_6), whereas for 200 rad/s and 300 rad/s the motor operates with three-level inversion (v_7 to v_{18}). Figures 2.14 and 2.15 show simulation results of classical two-level and proposed three-level DTC algorithms of OEWIM drive for step change in speed variation of 200 rad/s to -200 rad/s. Figures 2.14 and 2.15 describe speed, torque, flux, current and voltage of OEWIM drive with two-level and three-level inversion. In Figure 2.15 the proposed three-level DTC algorithm operates with 200 rad/s (more than 50 % of rated speed), hence the dual inverter configuration gives three-level output voltage, and it is also observable from Figure 2.15. From Figure 2.15 it is observed that the proposed DTC algorithms gives the same characteristics as that of two-level DTC; when compared to classical DTC, the proposed DTC gives lower ripple in torque and flux.

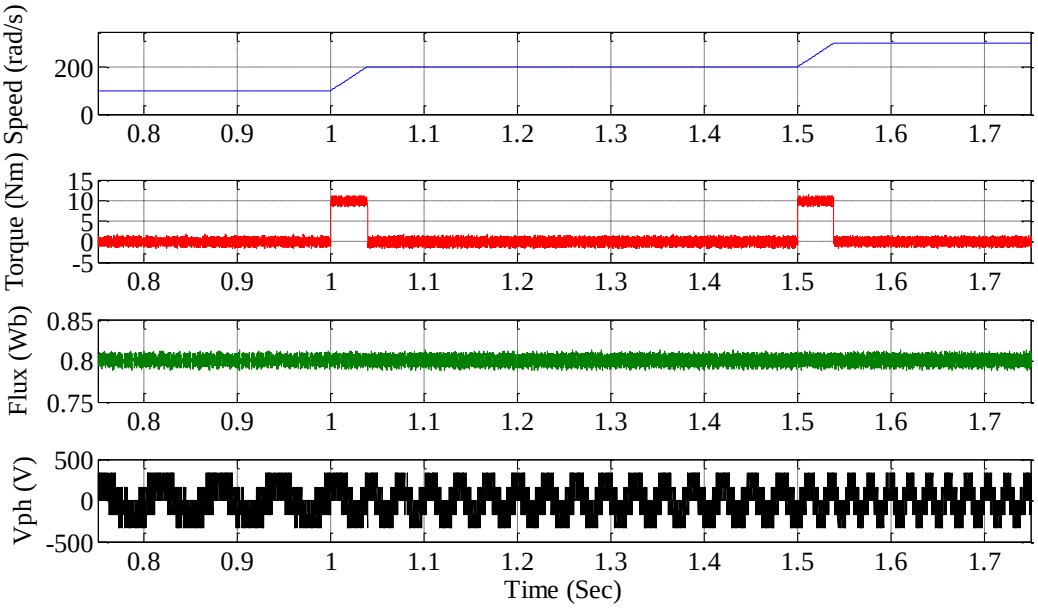

Figure 2.12 Simulation results of speed, torque, flux and phase voltage of OEWIM drive in forward motoring for speeds of 100 rad/s, 200 rad/s and 300 rad/s in forward motoring with proposed two-level inversion

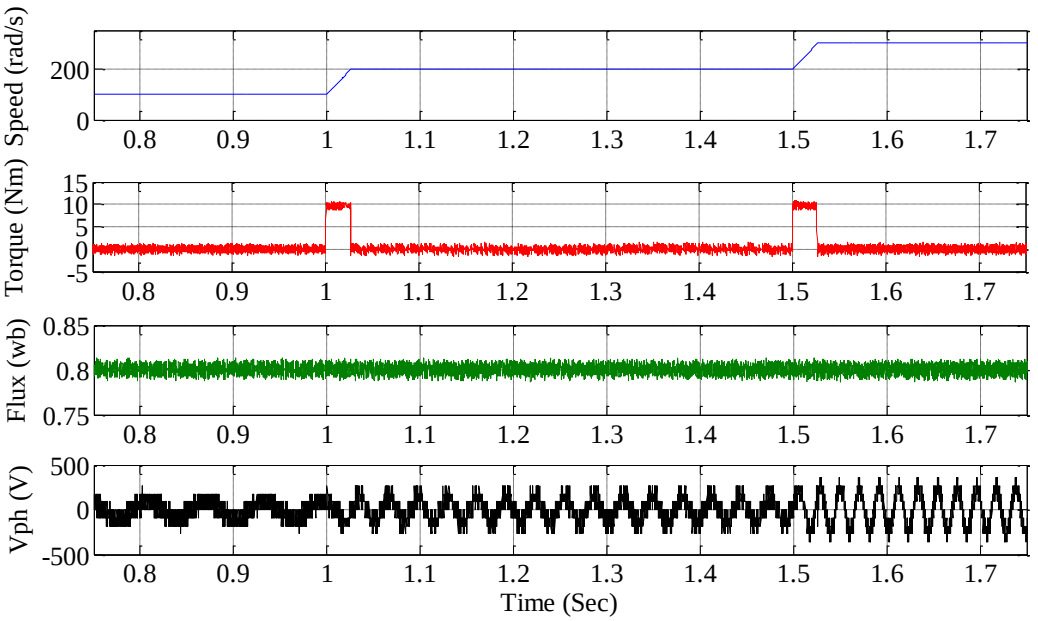

Figure 2.13 Simulation results of speed, torque, flux and phase voltage of OEWIM drive in forward motoring for speeds of 100 rad/s, 200 rad/s and 300 rad/s in forward motoring with proposed three-level inversion

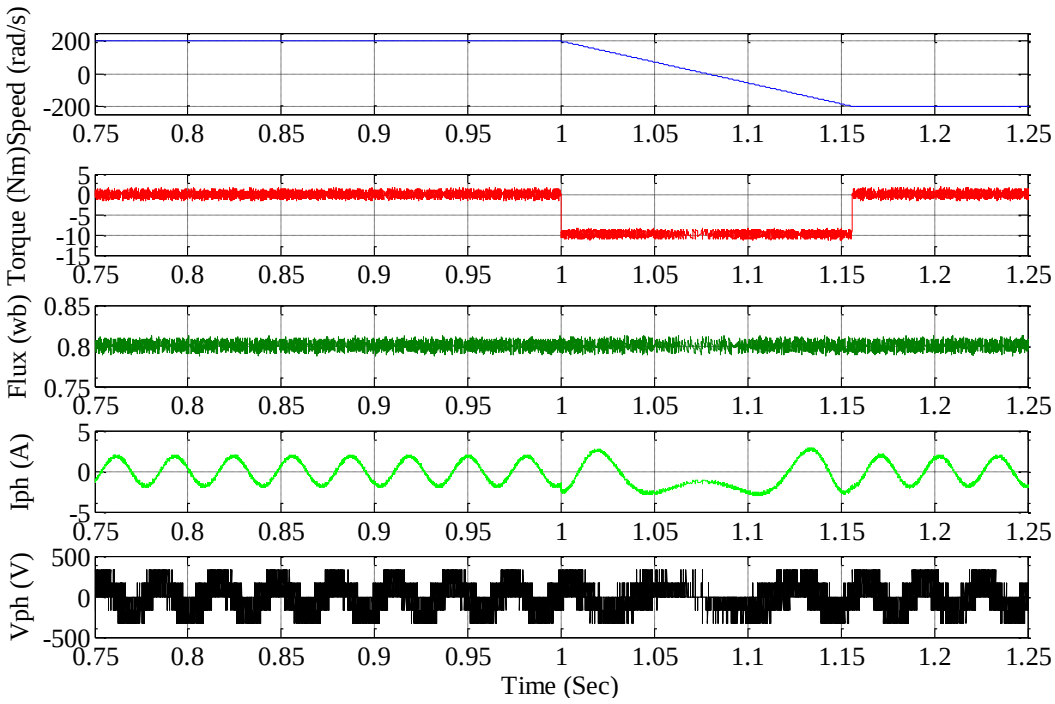

Figure 2.14 Simulation results of speed, torque, flux and phase voltage of OEWIM drive for speed variations of 200 rad/s and -200 rad/s with proposed two-level inversion (forward to reverse motoring)

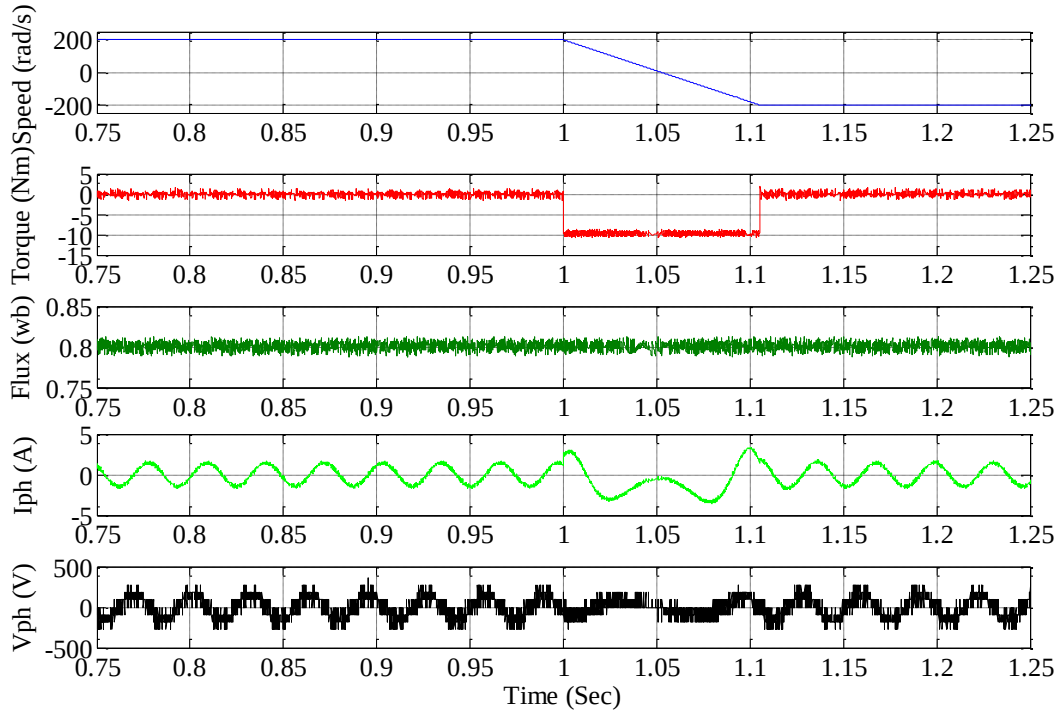

Figure 2.15 Simulation results of speed, torque, flux and phase voltage of OEWIM drive for speed variations of 200 rad/s and -200 rad/s with proposed three-level inversion (forward to reverse motoring)

2.6.2 Experimental Results

The proposed two-level and three-level DTC strategies are implemented by using dSPACE-1104 control board with MATLAB/SIMULINK real time interface. In order to develop the proposed DTC strategies, 3.7 kW OEWIM is used and it is coupled to a 3.7 kW DC generator. The developed DTC strategies in MATLAB are interfaced with dSPACE-1104 controller for experimental validation. To develop the DTC strategies following feedback signals are used: (i) Speed feedback from the encoder, (ii) Current feedback from current sensors (LA-25) and (iii) Effective DC-link voltage from voltage sensor (LV-25). These feedback signals are given to dSPACE controller by BNC connectors to ADC channels. The digital I/O signals are used to deliver the pulses for inverters from the switching states of voltage vector selection table. An experiment is conducted on OEWIM drive to verify the effectiveness of the proposed DTC algorithm at various rotor speeds. In the interest of brevity, experimental results are shown for low (100 rad/s), medium (200 rad/s) and high frequencies (300 rad/s) of operation in forward and reverse motoring.

Figure 2.16 represents actual speed and flux of OEWIM drive for two-level and proposed three-level DTC respectively. Figure 2.17 represents speed and torque of OEWIM drive for two-level and the proposed three-level DTC, respectively. Figure 2.18 presents phase voltage, CMV, phase current of OEWIM drive at a steady speed of 250 rad/s. Figures 2.16(a) and 2.16(b) represents actual speed and flux of motor in forward motoring for step change in speed variations of 100 rad/s, 200 rad/s and 300 rad/s. Figures 2.16(c) and 2.16(d) represents speed and flux of motor in reverse motoring for speed variations of -100 rad/s, -200 rad/s and -300 rad/s. Figures 2.16(e) and 2.16(f) represents flux locus of two-level and proposed DTC, respectively. From Figure 2.16 it is evident that the proposed three-level DTC gives low flux ripple when compared with two-level DTC and it provides better dynamic response for high speed variations. Figures 2.17(a) and 2.17(b) represent actual speed and torque of motor in forward motoring for step change in speed variations of 100 rad/s, 200 rad/s and 300 rad/s. Figures 2.17(c) and 2.17(d) represent actual speed and torque of OEWIM drive for the speed variations of -100 rad/s, -200 rad/s and -300 rad/s. Figure 2.17(e) and 2.17(f) represents actual speed and torque of OEWIM drive for the speed variation from 100 rad/s to 200 rad/s and 100 rad/s.

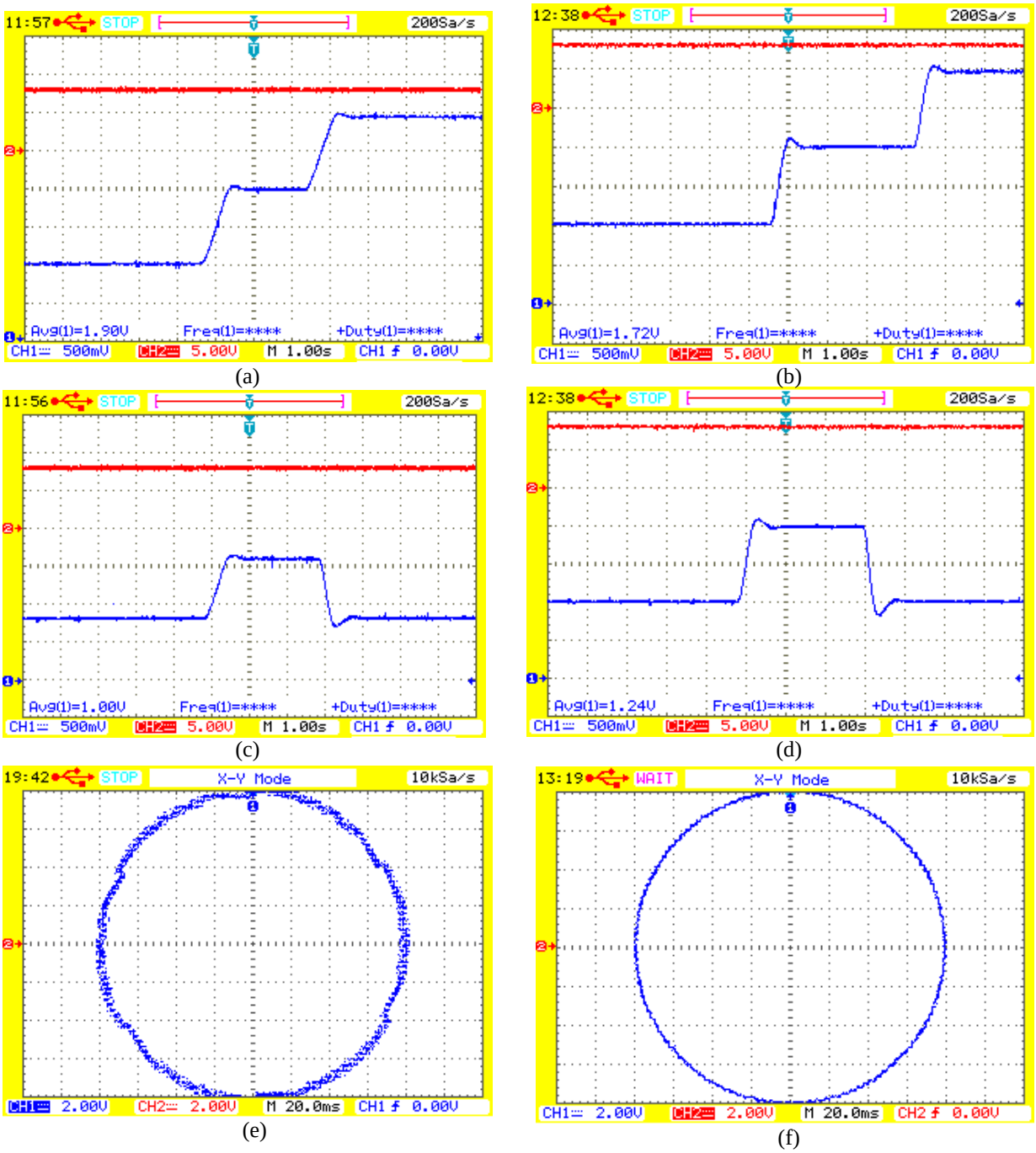

Figure 2.16 Experimental results of two-level and proposed DTC: (a), (b) Speed and flux in forward motoring. (c), (d) Speed and flux for variation of speed (blue-speed-50 rad/s/div), (red-flux-0.5 Wb/div). (e), (f) Flux locus (0.2 Wb/div)

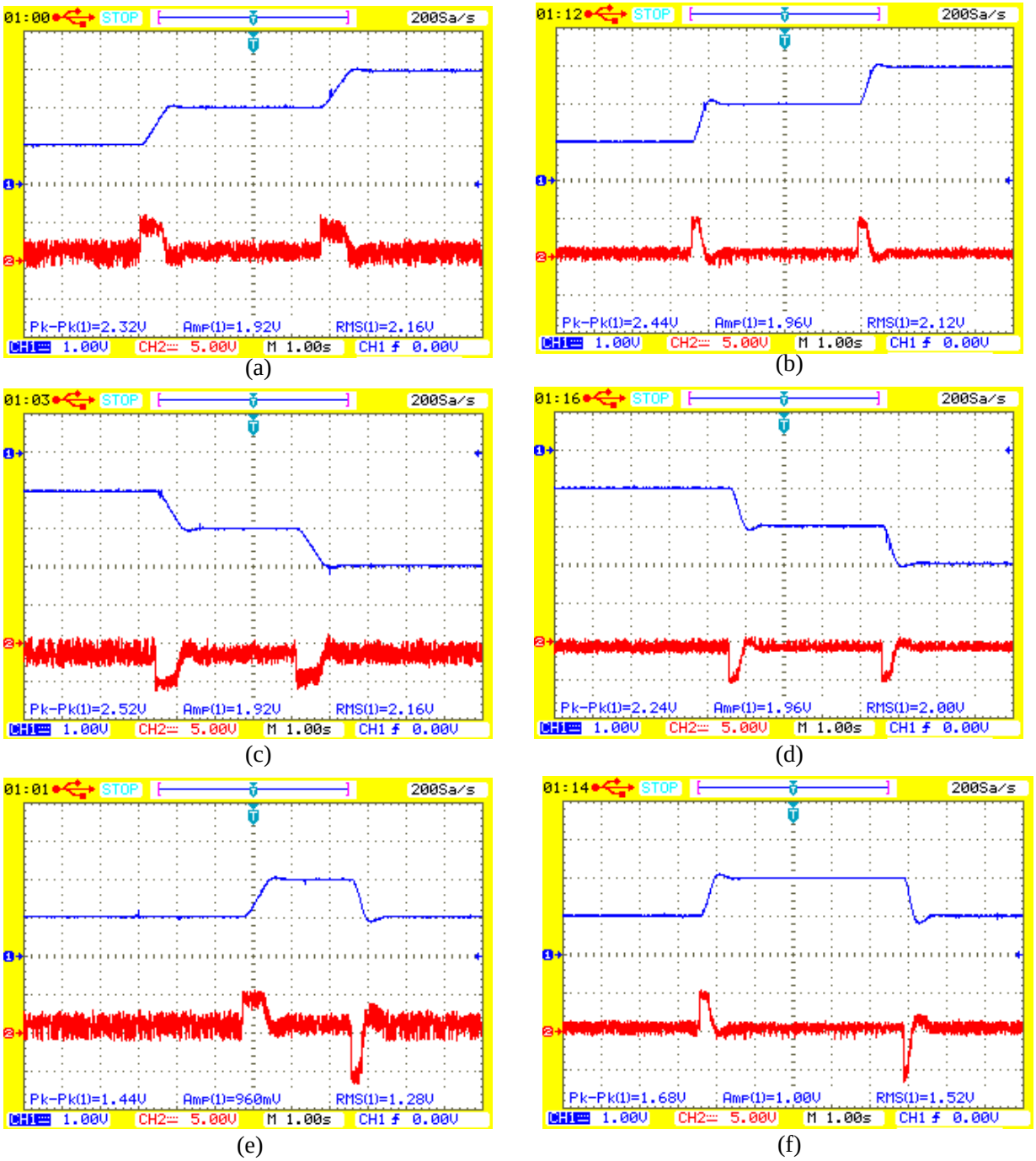

Figure 2.17 Experimental results of two-level and proposed three-level DTC: (a), (b) Speed and torque in forward motoring. (c), (d) Speed and torque in reverse motoring. (e), (f) Speed and torque for variation of speed from 100 rad/s to 200 rad/s. (blue-speed-100 rad/s/div), (red-torque - 5 Nm/div)

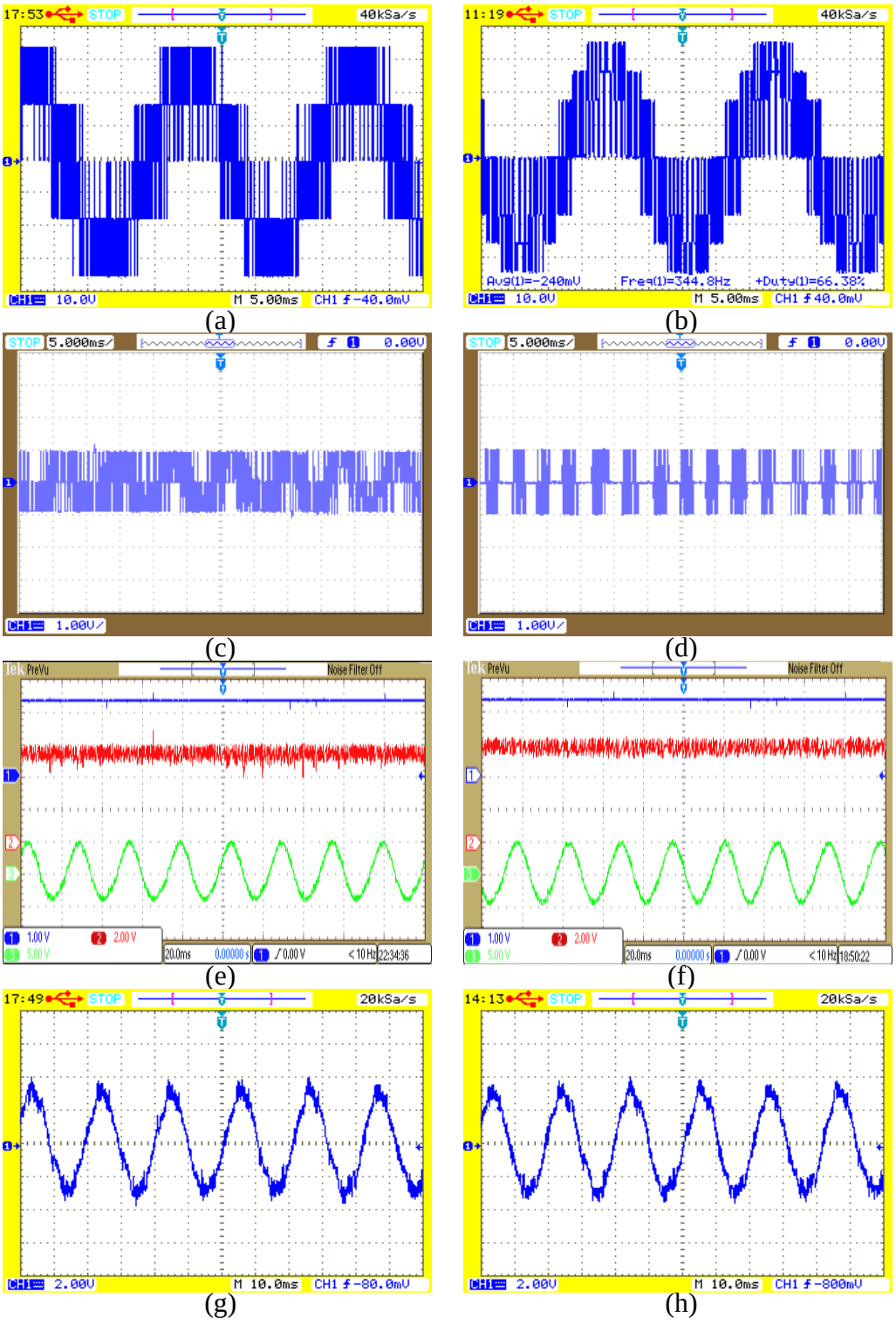

Figure 2.18 Voltage, CMV and phase current of OEWIM drive for two-level and proposed three-level inversion: (a), (b) R-phase voltage of OEWIM drive at a speed of 250 rad/s (Voltage/phase:100V/div). (c), (d) CMV of OEWIM drive at 250 rad/s. (100 V/div) (e), (f) Speed, torque and current/phase at a load torque of 14 Nm. (blue- speed 100 rad/s/div, red- torque 5 Nm/div and green- 5A/div) (g), (h) Current/phase at a speed of 300 rad/s under no-load condition (1A/div)

From Figure 2.17, it is evident that the steady-state torque ripple in the proposed DTC algorithm is very less when compared with two-level inversion. Figures 2.18(a) and 2.18(b) represent r-phase voltage of OEWIM drive and common mode voltage (CMV) of two-level DTC at a speed of 300 rad/s. Figures 2.18(c) and 2.18(d) represent r-phase voltage of OEWIM drive and CMV of proposed three-level DTC at a speed of 250 rad/s. Figures 2.18(e) and 2.18(f) represent r-phase of OEWIM drive at a load torque of 14 Nm at a steady speed of 250 rad/s. Figure 2.18(g) and 2.18(h) represents r-phase current of OEWIM drive for two-level and proposed DTC respectively at a speed of 300 rad/s. Table 2.8 represents quantified torque ripple and flux ripple under steady state condition at different operating frequencies. The torque and flux ripples are calculated by considering the sum of the difference between the measured and reference over 200 samples. Computation of % torque and flux ripple is given in Appendix-B. From Figure 2.17, it is clear that the proposed-three level DTC gives low torque ripple when compared with two-level DTC for all operating speeds; for the sake of brevity only three speeds of operation is reported in this chapter.

Table 2.8 Steady-state torque and flux ripple of OEWIM drive with two-level and three-level inversion

Speed (rad/s)	**2-level Inversion**					**3-level Inversion**				
	Torque ripple		**Flux ripple**		**CMV (V)**	**Torque ripple**		**Flux ripple**		**CMV (V)**
	Nm	**%**	**Wb**	**%**		**Nm**	**%**	**Wb**	**%**	
100	3.5	14.29	0.057	5.7	155.62	2.5	10.21	0.045	4.5	102.85
200	3.25	13.27	0.042	4.2	141.82	2.32	9.47	0.038	3.8	97.25
300	3.0	12.25	0.036	3.6	131	2.2	8.98	0.036	3.6	89.24

2.7 Summary

In this chapter, a modified three-level voltage switching scheme is implemented for OEWIM drive with the help of two two-level inverters to reduce torque and flux ripples at different speed conditions. The proposed scheme is closer to conventional DTC, so it has all the features of DTC. The two two-level inverters are operated with individual DC sources, so it is easy to interface with PV arrays. The intents of this chapter are: (i) Implement an effective voltage switching state scheme for an OEWIM drive with three-level inversion, (ii) Classify the voltage vectors based on rotor speed, (iii) Reduce the problems encountered at low speeds and (iv) Limit the ripples in torque and flux. The effectiveness of the proposed algorithm was verified experimentally by operating OEWIM drive in forward and reverse motoring at low

(100 rad/s), medium (200 rad/s) and high (300 rad/s) speeds. From hardware results, the proposed three-level DTC gives low torque and flux ripples when compared with two-level DTC for all speeds of operation.

Chapter 3

An Effective Four-level Voltage Switching State Algorithm for Direct Torque Controlled Open-end Winding Induction Motor Drive by using Two Two-level Inverters

Chapter 3

An Effective Four-level Voltage Switching State Algorithm for Direct Torque Controlled Open-end Winding Induction Motor Drive by using Two Two-level Inverters

3.1 Introduction

In the previous chapter, a modified voltage switching state algorithm for three-level inversion fed OEWIM drive was developed by considering two inverters operating with equal DC link voltages. Another possibility of OEWIM drive configuration was operating the dual inverter configuration with unequal DC link voltages to obtain four-level inversion [101]. In the previous chapter, it was observed that there was a possibility to reduce torque and flux ripples further, hence four-level inversion fed DTC algorithm is introduced for OEWIM drive. In this chapter the active voltage vectors are classified into three categories rather than two, which was considered in chapter 2. This chapter provides location of active voltage space vectors for four-level inversion and their classification accordingly. The experimental results show that the proposed algorithm reduces torque and flux ripples without losing features of classical DTC and it also provides multi-level operation.

In this chapter, mathematical modelling of dual inverter fed OEWIM drive is introduced and the locations of voltage space vectors to obtain four-level inversion are also represented. The possible switching combinations of Inverter-1 and Inverter-2 are presented in Table 3.1; from all 64 possible switching combinations, 37 voltage space vectors are used to develop the proposed DTC strategy. The voltage vectors are classified into various categories to reduce torque and flux ripples based on operating frequencies.

The intents of this chapter are: implementing an effective voltage switching state algorithm for an OEWIM drive to reduce torque and flux ripple with the help of four-level inversion based on two two-level inverters, locating voltage space vectors, applying voltage space vectors based on operating frequencies, utilizing necessary mathematical models, algorithm for reduction of torque and flux ripple and hardware implementation of proposed

scheme to observe its behaviour. The proposed algorithm has been developed with four-level configuration, so that it has low d*v*/dt stress.

The open-end winding configuration is developed with two independent DC sources and the effects of CMV are reduced. In this chapter experimental verification is performed for DTC of OEWIM drive with two-level inverter configuration and four-level configuration. The two-level configuration is obtained by operating the inverters with DC link voltage of 1:1 ratio as shown in Table 2.2, whereas four-level configuration was obtained by operating the inverters with 2:1 ratio. Finally, it is noticed that the proposed algorithm reduces torque and flux ripples at all frequencies of operation of motor drive without losing the features of classical two-level DTC.

3.2 Proposed Four-Level DTC

The power circuit diagram and the block diagram of the proposed four-level DTC strategy are shown in Figures 3.1 and 3.2 respectively. The four-level inversion scheme is obtained by energizing OEWIM with two- two level inverters on both sides with asymmetrical configuration. The asymmetrical configuration is obtained by feeding the two inverters with voltages $2V_{dc}/3$ and $V_{dc}/3$.

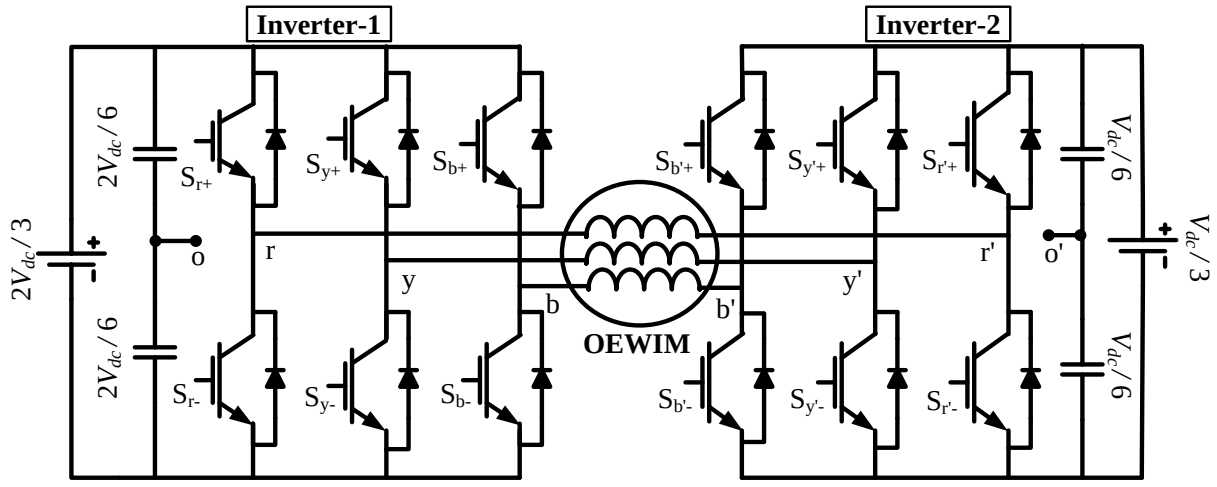

Figure 3.1 Power circuit diagram of OEWIM drive with four-level inversion

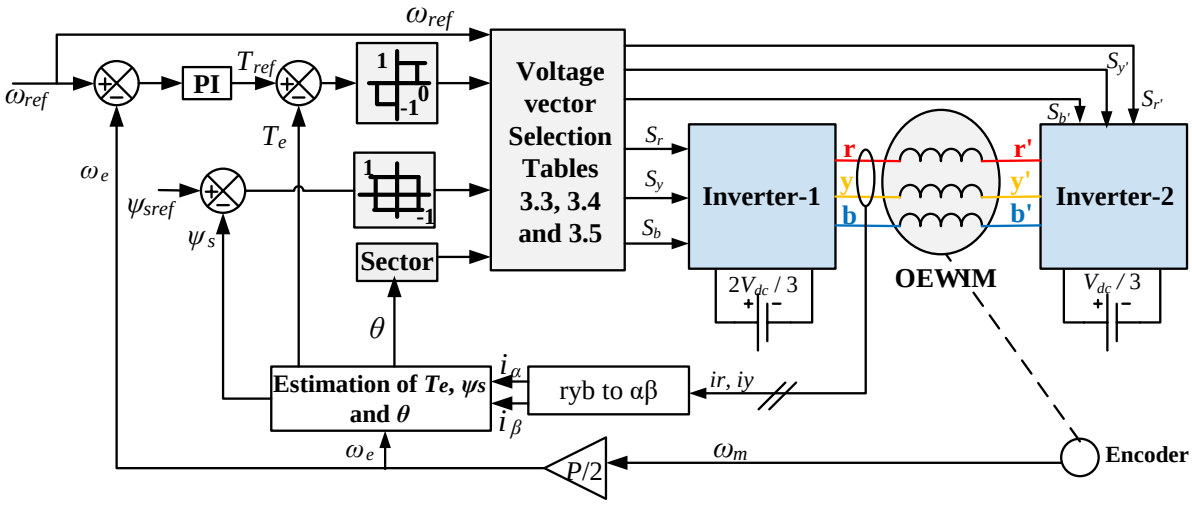

Figure 3.2 Block diagram of direct torque controlled OEWIM drive with four-level inversion

In Figure 3.1 two voltage source inverters are energized with DC link voltage ratio of 2:1. The dual inverter configuration gives 64 switching combinations. Out of these 64 switching combinations, the configuration gives 36 active voltage space vectors and a null vector because the OEWIM configuration leads to high redundancy of switching states.

Table 3.1 indicates all possible switching states of individual switches used in the inverter. The switches are turned to realize all switching states of two inverters. The switching states of inverter for two-level configuration is calculated using following equations,

$$v_{s1} = \frac{2}{3}\frac{2V_{dc}}{3}\left(S_r + S_y e^{j\frac{2\pi}{3}} + S_b e^{j\frac{4\pi}{3}}\right) \tag{3.1}$$

$$\text{and } v_{s2} = \frac{2}{3}\frac{V_{dc}}{3}\left(S_{r'} + S_{y'} e^{j\frac{2\pi}{3}} + S_{b'} e^{j\frac{4\pi}{3}}\right) \tag{3.2}$$

The space vector locations of the proposed four-level inverter are shown in Figure 3.3. To obtain four-level configuration the two inverters are operated with unequal DC link voltages and they are operated in duality mode. Table 3.2 indicates active voltage space vector locations of dual inverter configuration with four-level inversion. The switches are turned on to realize all switching states of the two inverters. Therefore, from mathematical calculations, four-level inverter produces 37 voltage space vector locations and these are represented in Figure 3.3 and

are shown in Table 3.2. The active voltage space vectors of the four-level inverter are obtained from all combinations of the switching states of inverter.

An example is illustrated to show that how to find the voltage space vector. The voltage space vector v_1 is obtained by operating Inverter-1 with switching states of (1,0,0) and Inverter-2 with switching states of (1,0,0). Then by using equations (3.1) and (3.2) the voltage space vector v_1 can be written as

$$v_s = (v_{s1} - v_{s2}) \tag{3.3}$$

The resultant voltage space vector for all the switching states of inverter is obtained by using (3.3). On simplifying (3.3) with switching states of (1,0,0) and (1,0,0) the resultant voltage vector is obtained, with a magnitude of $V_{dc}/3$ and phase angle of zero; hence it is named as v_1. Likewise, on applying switching states (1,0,0) and (1,1,1) voltage space vector v_7 is obtained. By applying the switching states of (1,0,0) and (0,1,1) voltage space vector v_{19} is obtained. The equation used to find CMV is same as that of (2.4). The phase voltages of OEWIM drive are shown in chapter 2 (2.1) to (2.6). The only modifications are input DC-link voltages, to obtain four-level inversion the inverters are fed by $2V_{dc}/3$ and $V_{dc}/3$, therefore the pole voltages obtained at the terminals of Inverter-1 and Inverter-2 are $\pm V_{dc}/3$ and $\pm V_{dc}/6$. By using pole voltages, the CMV can be estimated and it is given by (2.4). On applying all possible switching states to the inverter, 37 active voltage space vectors are obtained. The voltage space vectors shown in Figure 3.3 are divided into three groups for different frequencies of operation. Voltage space vectors v_{19} to v_{36} are applied for higher frequencies of operation. Voltage space vectors v_7 to v_{18} are applied for medium frequencies. The voltage space vectors v_1 to v_6 are applied for low frequencies of operation. These 37 space vector locations are divided into three groups to maintain constant V/f ratio and minimum current ripple.

The division of active voltage space vector corresponds to the operation at low, medium and high frequencies. In Figure 3.3, the active voltage space vector is divided into 18 sectors for high frequencies of operation and 12 sectors for medium and low frequencies of operation. For ease of representation, only 12 sectors are shown in Figure 3.3.

Table 3.1 All possible switching combinations of dual inverter configuration with un-equal DC link voltage for four-level inversion

Inverter-1			**Inverter-2**			**Switching Combination**	**Realization**		**CMV (V)**
S_r	S_y	S_b	$S_{r'}$	$S_{y'}$	$S_{b'}$		v_α	v_β	Vo
0	**0**	**0**	**0**	**0**	**0**	**1**	**0**	**0**	$\mathbf{-V_{dc}/6}$
0	0	0	1	0	0	2	-0.2222	0	$-5V_{dc}/18$
0	0	0	1	1	0	3	-0.1111	-0.1925	$-7V_{dc}/18$
0	0	0	0	1	0	4	0.1111	0.1925	$-5V_{dc}/18$
0	0	0	0	1	1	5	0.2222	0	$-7V_{dc}/18$
0	0	0	0	0	1	6	0.1111	0.1925	$-7V_{dc}/18$
0	0	0	1	0	1	7	-0.1111	0.1925	$-7V_{dc}/18$
0	0	0	1	1	1	8	0	0	$-V_{dc}/2$
1	0	0	0	0	0	9	0.4444	0	$V_{dc}/18$
1	**0**	**0**	**1**	**0**	**0**	**10**	**0.2222**	**0**	$\mathbf{-V_{dc}/18}$
1	**0**	**0**	**1**	**1**	**0**	**11**	**0.3333**	**-0.1925**	$\mathbf{-V_{dc}/6}$
1	**0**	**0**	**0**	**1**	**0**	**12**	**0.5556**	**-0.1925**	$\mathbf{-V_{dc}/18}$
1	**0**	**0**	**0**	**1**	**1**	**13**	**0.6667**	**0**	$\mathbf{-V_{dc}/6}$
1	**0**	**0**	**0**	**0**	**1**	**14**	**0.5556**	**0.1925**	$\mathbf{-V_{dc}/18}$
1	**0**	**0**	**1**	**0**	**1**	**15**	**0.3333**	**0.1925**	$\mathbf{-V_{dc}/6}$
1	**0**	**0**	**1**	**1**	**1**	**16**	**0.4444**	**0**	$\mathbf{-V_{dc}/6}$
1	1	0	0	0	0	17	0.2222	0.3849	$5V_{dc}/18$
1	1	0	1	0	0	18	0	0.3849	$V_{dc}/6$
1	**1**	**0**	**1**	**1**	**0**	**19**	**0.1111**	**0.1925**	$\mathbf{V_{dc}/18}$
1	1	0	0	1	0	20	0.3333	0.1925	$V_{dc}/6$
1	**1**	**0**	**0**	**1**	**1**	**21**	**0.4444**	**0.3849**	$\mathbf{V_{dc}/18}$
1	**1**	**0**	**0**	**0**	**1**	**22**	**0.3333**	**0.5774**	$\mathbf{V_{dc}/6}$
1	**1**	**0**	**1**	**0**	**1**	**23**	**0.1111**	**0.5774**	$\mathbf{V_{dc}/18}$
1	**1**	**0**	**1**	**1**	**1**	**24**	**0.2222**	**0.3849**	$\mathbf{V_{dc}/18}$
0	1	0	0	0	0	25	-0.2222	0.3849	$V_{dc}/18$
0	**1**	**0**	**1**	**0**	**0**	**26**	**-0.4444**	**0.3849**	$\mathbf{-V_{dc}/18}$
0	**1**	**0**	**1**	**1**	**0**	**27**	**-0.3333**	**0.1925**	$\mathbf{-V_{dc}/6}$
0	**1**	**0**	**0**	**1**	**0**	**28**	**-0.1111**	**0.1925**	$\mathbf{-V_{dc}/18}$
0	**1**	**0**	**0**	**1**	**1**	**29**	**0**	**0.3849**	$\mathbf{-V_{dc}/6}$
0	**1**	**0**	**0**	**0**	**1**	**30**	**-0.1111**	**0.5774**	$\mathbf{-V_{dc}/18}$
0	**1**	**0**	**1**	**0**	**1**	**31**	**-0.3333**	**0.5774**	$\mathbf{-V_{dc}/6}$
0	**1**	**0**	**1**	**1**	**1**	**32**	**-0.2222**	**0.3849**	$\mathbf{-V_{dc}/6}$
0	1	1	0	0	0	33	-0.4444	0	$3V_{dc}/18$
0	**1**	**1**	**1**	**0**	**0**	**34**	**-0.6667**	**0**	$\mathbf{V_{dc}/6}$
0	**1**	**1**	**1**	**1**	**0**	**35**	**-0.5556**	**-0.1925**	$\mathbf{V_{dc}/18}$
0	1	1	0	1	0	36	-0.3333	-0.1925	$V_{dc}/6$
0	**1**	**1**	**0**	**1**	**1**	**37**	**-0.2222**	**0**	$\mathbf{V_{dc}/18}$
0	1	1	0	0	1	38	-0.3333	0.1925	$V_{dc}/6$
0	**1**	**1**	**1**	**0**	**1**	**39**	**-0.5556**	**0.1925**	$\mathbf{V_{dc}/18}$
0	**1**	**1**	**1**	**1**	**1**	**40**	**-0.4444**	**0**	$\mathbf{V_{dc}/18}$
0	0	1	0	0	0	41	-0.2222	-0.3849	$V_{dc}/18$
0	**0**	**1**	**1**	**0**	**0**	**42**	**-0.4444**	**-0.3849**	$\mathbf{-V_{dc}/18}$
0	**0**	**1**	**1**	**1**	**0**	**43**	**-0.3333**	**-0.5774**	$\mathbf{-V_{dc}/6}$
0	**0**	**1**	**0**	**1**	**0**	**44**	**-0.1111**	**-0.5774**	$\mathbf{-V_{dc}/18}$
0	**0**	**1**	**0**	**1**	**1**	**45**	**0**	**-0.3849**	$\mathbf{-V_{dc}/6}$
0	**0**	**1**	**0**	**0**	**1**	**46**	**-0.1111**	**-0.1925**	$\mathbf{-V_{dc}/18}$
0	**0**	**1**	**1**	**0**	**1**	**47**	**-0.3333**	**-0.1925**	$\mathbf{-V_{dc}/6}$

0	**0**	**1**	**1**	**1**	**1**	**48**	**-0.2222**	**-0.3849**	**$-V_{dc}/6$**
1	0	1	0	0	0	49	0.2222	-0.3849	$5V_{dc}/18$
1	0	1	1	0	0	50	0	-0.3849	$V_{dc}/6$
1	**0**	**1**	**1**	**1**	**0**	**51**	**0.1111**	**-0.5774**	**$V_{dc}/18$**
1	**0**	**1**	**0**	**1**	**0**	**52**	**0.3333**	**-0.5774**	**$V_{dc}/6$**
1	**0**	**1**	**0**	**1**	**1**	**53**	**0.4444**	**-0.3849**	**$V_{dc}/18$**
1	0	1	0	0	1	54	0.3333	-0.1925	$V_{dc}/6$
1	**0**	**1**	**1**	**0**	**1**	**55**	**0.1111**	**-0.1925**	**$V_{dc}/18$**
1	**0**	**1**	**1**	**1**	**1**	**56**	**0.2222**	**-0.3849**	**$V_{dc}/18$**
1	1	1	0	0	0	57	0	0	$V_{dc}/2$
1	1	1	1	0	0	58	-0.2222	0	$7V_{dc}/18$
1	1	1	1	1	0	59	-0.1111	-0.1925	$5V_{dc}/18$
1	1	1	0	1	0	60	0.1111	-0.1925	$7V_{dc}/18$
1	1	1	0	1	1	61	0.2222	0	$5V_{dc}/18$
1	1	1	0	0	1	62	0.1111	0.1925	$7V_{dc}/18$
1	1	1	1	0	1	63	-0.1111	0.1925	$5V_{dc}/18$
1	1	1	1	1	1	64	0	0	$V_{dc}/6$

For high frequencies of operation each sector is divided into 20°. The division of sectors is explained below. Sector-1 of active voltage space vector is from 350° to 10°. Sector-2 of active voltage space vector is from 10° to 30°. Sector-3 of active voltage space vector is from 30° to 50°. Sector-4 of active voltage space vector is from 50° to 70°. Sector-5 of active voltage space vector is from 70° to 90°. Sector-6 of active voltage space vector is from 90° to 110°. Sector-7 of active voltage space vector is from 110° to 130°. Sector-8 of active voltage space vector is from 130° to 150°. Sector-9 of active voltage space vector is from 150° to 170°. Sector-10 of active voltage space vector is from 170° to 190°. Sector-11 of active voltage space vector is from 190° to 210°. Sector-12 of active voltage space vector is from 210° to 230°. Sector-13 of active voltage space vector is from 230° to 250°. Sector-14 of active voltage space vector is from 250° to 270°. Sector-15 of active voltage space vector is from 270° to 290°. Sector-16 of active voltage space vector is from 290° to 310°. Sector-17 of active voltage space vector is from 310° to 330°. Sector-18 of active voltage space vector is from 330° to 350°.

For medium and low frequencies of operation, each sector is divided into 30°. The division of sectors is explained below. Sector-1 of active voltage space vector is from 345° to 15°. Sector-2 of active voltage space vector is from 15° to 45°. Sector-3 of active voltage space vector is from 45° to 75°. Sector-4 of active voltage space vector is from 75° to 105°. Sector-5 of active voltage space vector is from 105° to 135°. Sector-6 of active voltage space vector is from 135° to 165°. Sector-7 of active voltage space vector is from 165° to 195°. Sector-8 of active voltage space vector is from 195° to 225°. Sector-9 of active voltage space vector is from

225° to 255°. Sector-10 of active voltage space vector is from 255° to 285°. Sector-11 of active voltage space vector is from 285° to 315°. Sector-12 of active voltage space vector is from 315° to 345°.

Table 3.2 Active voltage space vector locations for four-level inversion

Inverter-1			**Inverter-2**			**Space Vector**	**Realization**	**CMV**	**Output Voltage Level**
S_r	S_y	S_b	$S_{r'}$	$S_{y'}$	$S_{b'}$	(v_s)	(Complex Form)	V_o	
0	0	0	0	0	0	v_0	0	$-V_{dc}/6$	Space vectors v_1-v_6, delivers Two-level output voltage
1	0	0	1	0	0	v_1	$V_{dc}(0.222)$	$-V_{dc}/18$	
1	1	0	1	1	0	v_2	$V_{dc}(0.11+0.193i)$	$V_{dc}/18$	
0	1	0	0	1	0	v_3	$V_{dc}(-0.11+0.19i)$	$-V_{dc}/18$	
0	1	1	0	1	1	v_4	$V_{dc}(-0.222)$	$V_{dc}/18$	
0	0	1	0	0	1	v_5	$V_{dc}(-0.11-0.193i)$	$-V_{dc}/18$	
1	0	1	1	0	1	v_6	$V_{dc}(0.11-0.193i)$	$V_{dc}/18$	
1	0	0	1	1	1	v_7	$V_{dc}(0.444)$	$-V_{dc}/6$	Space vectors v_7-v_{18}, delivers Three-level output voltage
1	0	0	1	0	1	v_8	$V_{dc}(0.33+0.193i)$	$-V_{dc}/6$	
1	1	0	1	1	1	v_9	$V_{dc}(0.22+0.385i)$	$V_{dc}/18$	
0	1	0	0	1	1	v_{10}	$V_{dc}(0.385i)$	$-V_{dc}/6$	
0	1	0	1	1	1	v_{11}	$V_{dc}(-0.22+0.38i)$	$-V_{dc}/6$	
0	1	0	1	1	0	v_{12}	$V_{dc}(-0.33+0.19i)$	$-V_{dc}/6$	
0	1	1	1	1	1	v_{13}	$V_{dc}(-0.444)$	$V_{dc}/18$	
0	0	1	1	0	1	v_{14}	$V_{dc}(-0.33-0.193i)$	$-V_{dc}/6$	
0	0	1	1	1	1	v_{15}	$V_{dc}(-0.22-0.385i)$	$-V_{dc}/6$	
0	0	1	0	1	1	v_{16}	$V_{dc}(-0.385i)$	$-V_{dc}/6$	
1	0	1	1	1	1	v_{17}	$V_{dc}(0.22-0.385i)$	$V_{dc}/18$	
1	0	0	1	1	0	v_{18}	$V_{dc}(0.33-0.193i)$	$-V_{dc}/6$	
1	0	0	0	1	1	v_{19}	$V_{dc}(0.667)$	$-V_{dc}/6$	Space vectors v_{19}-v_{36}, delivers Four-level output voltage
1	0	0	0	0	1	v_{20}	$V_{dc}(0.55+0.193i)$	$-V_{dc}/18$	
1	1	0	0	1	1	v_{21}	$V_{dc}(0.44+0.385i)$	$V_{dc}/18$	
1	1	0	0	0	1	v_{22}	$V_{dc}(0.33+0.577i)$	$V_{dc}/6$	
1	1	0	1	0	1	v_{23}	$V_{dc}(0.11+0.577i)$	$V_{dc}/18$	
0	1	0	0	0	1	v_{24}	$V_{dc}(-0.11+0.57i)$	$-V_{dc}/18$	
0	1	0	1	0	1	v_{25}	$V_{dc}(-0.33+0.57i)$	$-V_{dc}/6$	
0	1	0	1	0	0	v_{26}	$V_{dc}(-0.44+0.38i)$	$-V_{dc}/18$	
0	1	1	1	0	1	v_{27}	$V_{dc}(-0.55+0.19i)$	$V_{dc}/18$	
0	1	1	1	0	0	v_{28}	$V_{dc}(-0.667)$	$V_{dc}/6$	
0	1	1	1	1	0	v_{29}	$V_{dc}(-0.55-0.19i)$	$V_{dc}/18$	
0	0	1	1	0	0	v_{30}	$V_{dc}(-0.44-0.38i)$	$-V_{dc}/18$	
0	0	1	1	1	0	v_{31}	$V_{dc}(-0.33-0.57i)$	$-V_{dc}/6$	
0	0	1	0	1	0	v_{32}	$V_{dc}(-0.11-0.577i)$	$-V_{dc}/18$	
1	0	1	1	1	0	v_{33}	$V_{dc}(0.11-0.577i)$	$V_{dc}/18$	
1	0	1	0	1	0	v_{34}	$V_{dc}(0.33-0.577i)$	$V_{dc}/6$	
1	0	1	0	1	1	v_{35}	$V_{dc}(0.44-0.385i)$	$V_{dc}/18$	
1	0	0	0	1	0	v_{36}	$V_{dc}(0.55-0.193i)$	$-V_{dc}/18$	

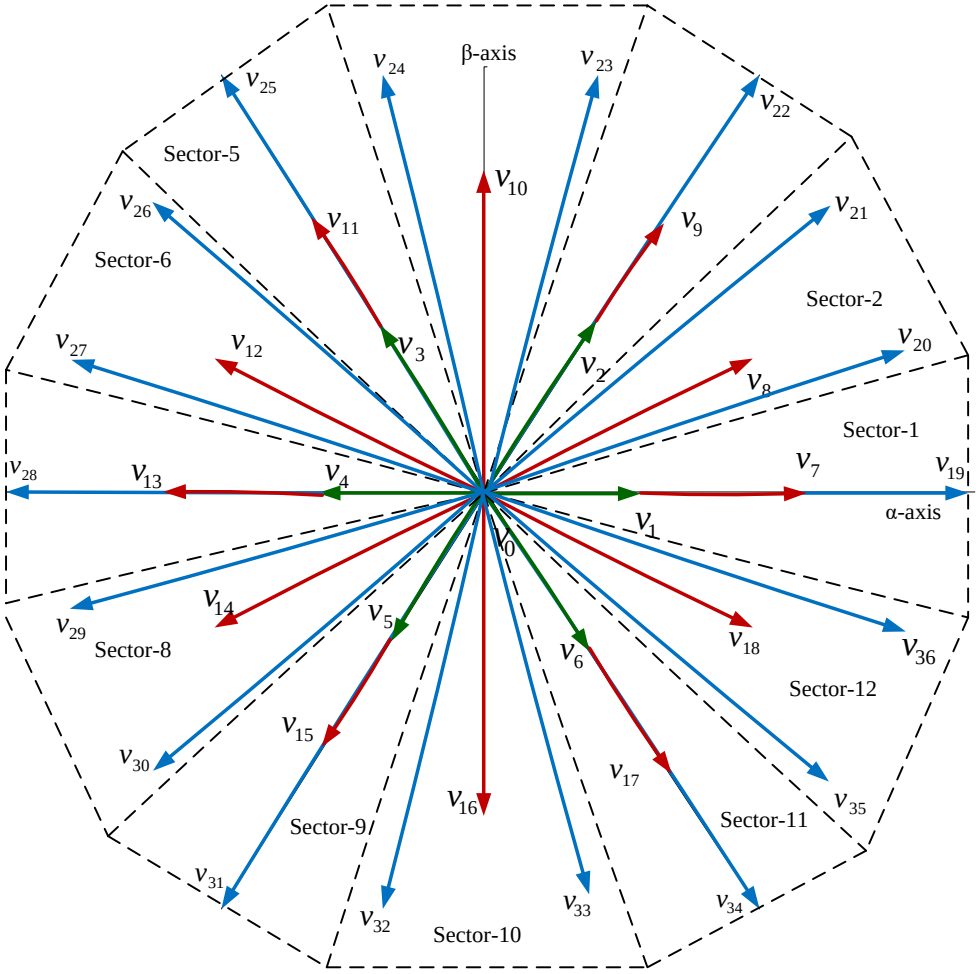

Figure 3.3 Classification of voltage vectors based on different operating frequencies

3.2.1 High Frequency of Operation (Above 70% of Rated Speed)

During high frequency of operation of OEWIM drive, to control stator flux and torque the voltage space vectors v_{19} to v_{36} and a null vector v_0 are utilized to realize the resultant space vector. In Figure 3.3, if the resultant stator flux vector ψ_s is in sector-1, then by applying voltage space vectors v_{20}, v_{21}, v_{22} and v_{36} its magnitude increases, whereas by applying v_{24}, v_{25}, v_{31} and v_{32} its magnitude decreases. In the same sector, to reduce positive torque error, v_{21}, v_{22} and v_{23} are utilized, whereas for the reduction of negative torque error, v_{34}, v_{35} and v_{36} are used. In high speed operation, to maintain constant V/f ratio, voltage vectors v_1 to v_{18} should not be applied. The selection of voltage vectors for high frequencies shown in Table 3.3.

Table 3.3 Selection of active voltage vectors for high speeds of operation

Flux Error	Torque Error	Sector																	
		1	2	3	4	5	6	7	8	9	10	11	12	13	14	15	16	17	18
1	1	v_{22}	v_{23}	v_{24}	v_{25}	v_{26}	v_{27}	v_{28}	v_{29}	v_{30}	v_{31}	v_{32}	v_{33}	v_{34}	v_{35}	v_{36}	v_{19}	v_{20}	v_{21}
	-1	v_{34}	v_{35}	v_{36}	v_{19}	v_{20}	v_{21}	v_{22}	v_{23}	v_{24}	v_{25}	v_{26}	v_{27}	v_{28}	v_{29}	v_{30}	v_{31}	v_{32}	v_{33}
-1	1	v_{25}	v_{26}	v_{27}	v_{28}	v_{29}	v_{30}	v_{31}	v_{32}	v_{33}	v_{34}	v_{35}	v_{36}	v_{19}	v_{20}	v_{21}	v_{22}	v_{23}	v_{24}
	-1	v_{31}	v_{32}	v_{33}	v_{34}	v_{35}	v_{36}	v_{19}	v_{20}	v_{21}	v_{22}	v_{23}	v_{24}	v_{25}	v_{26}	v_{27}	v_{28}	v_{29}	v_{30}

3.2.2 Medium Frequency of Operation (In Between 35% to 70% of Rated Speed)

In the medium frequency range, to control stator flux and torque of OEWIM drive, the voltage space vectors v_7 to v_{18} and a null vector v_0 are used to realize the resultant space vector. In Figure 3.3, if the resultant stator flux vector ψ_s is in sector-1, then by applying voltage space vectors v_8, v_9, v_{17} and v_{18} its magnitude increases, whereas by applying v_{11}, v_{12}, v_{14} and v_{15} its magnitude decreases. In the same sector, to reduce positive torque error, v_8, v_9 and v_{10} are utilized, whereas for the reduction of negative torque error, v_{16}, v_{17} and v_{18} are used. In medium speed operation, to maintain constant V/f ratio, the voltage vectors v_1 to v_6 and v_{19} to v_{36} should not be applied. The selection of active voltage vectors for medium frequencies of operation are shown in Table 3.4.

Table 3.4 Selection of active voltage vectors for medium speeds of operation

Flux Error	Torque Error	Sector											
		1	2	3	4	5	6	7	8	9	10	11	12
1	1	v_9	v_{10}	v_{11}	v_{12}	v_{13}	v_{14}	v_{15}	v_{16}	v_{17}	v_{18}	v_7	v_8
	-1	v_{17}	v_{18}	v_7	v_8	v_9	v_{10}	v_{11}	v_{12}	v_{13}	v_{14}	v_{15}	v_{16}
-1	1	v_{11}	v_{12}	v_{13}	v_{14}	v_{15}	v_{16}	v_{17}	v_{18}	v_7	v_8	v_9	v_{10}
	-1	v_{15}	v_{16}	v_{17}	v_{18}	v_7	v_8	v_9	v_{10}	v_{11}	v_{12}	v_{13}	v_{14}

3.2.3 Low Frequency of Operation (Less-than 35% of Rated Speed)

In the low frequency range, to control stator flux and torque of OEWIM drive, the voltage space vectors v_1 to v_6 and a null vector v_0 are used to realize the resultant space vector. In Figure 3.3, if the resultant flux vector ψ_s is in sector-1, then by applying voltage space vectors v_2 and v_6, its magnitude increases, whereas by applying v_5 and v_3 its magnitude decreases. In the same sector, to reduce positive torque error, v_2 and v_3 are utilized, whereas for the reduction of negative torque error, v_5 and v_6 are used. In low speed operation, to maintain

constant V/f ratio, the voltage vectors v_7 to v_{36} should not be applied. The selection of active voltage vectors for low frequencies of operation are shown in Table 3.5.

Table 3.5 Selection of voltage vectors for low speeds of operation

Flux Error	Torque Error	Sector											
		1	2	3	4	5	6	7	8	9	10	11	12
1	1	v_2	v_2	v_3	v_3	v_4	v_4	v_5	v_5	v_6	v_6	v_1	v_1
	-1	v_6	v_6	v_1	v_1	v_2	v_2	v_3	v_3	v_4	v_4	v_5	v_5
-1	1	v_3	v_3	v_4	v_4	v_5	v_5	v_6	v_6	v_1	v_1	v_2	v_2
	-1	v_5	v_5	v_6	v_6	v_1	v_1	v_2	v_2	v_3	v_3	v_4	v_4

3.2.4 Algorithm to Reduce Torque and Flux Ripple

From [4], the torque equation of induction motor in stationary reference frames is given by:

$$T_e = \frac{3}{2}\frac{P}{2}\left(\overline{\psi_s} \otimes \overline{i_s}\right) \tag{3.4}$$

Simplification of (3.4) gives

$$T_e = \frac{3}{2}\frac{P}{2}\left(\psi_{s\alpha} i_{s\beta} - \psi_{s\beta} i_{s\alpha}\right) \tag{3.5}$$

From (3.5), to obtain low torque ripple, it is required to maintain low current and flux ripples. By controlling the flux of the induction motor torque can be controlled. Therefore torque and flux ripples are dependent on voltage. If the voltage ripple is decreased, it reduces flux ripple. The stator voltage equation of open end winding induction motor (output voltage of inverter) is given by

$$v(t) = R_s i_s + L_s \frac{\mathrm{d}i_s}{\mathrm{dt}} + e \tag{3.6}$$

where, $v(t)$ is inverter output voltage, The inverter output voltage $v(t)$ has 36 locations for four-level inverter depending on its all possible switching states. Eq (3.6) can be rewritten as

$$\frac{\mathrm{d}i_s}{\mathrm{dt}} = \left(\frac{v(t) - e - R_s i_s}{L_s}\right) \tag{3.7}$$

On neglecting stator voltage drop ($R_s i_s$) of induction motor, the rate of change of stator current ($\mathrm{d}i_s/\mathrm{dt}$) is dependent on the inverter output voltage and the developed voltage of the motor. To obtain low current ripple, the rate of change of stator current should be low. It is maintained by selecting proper switching vectors. The rate of change of stator current ($\mathrm{d}i_s/\mathrm{dt}$)

plays an important role to reduce torque ripple in steady state and it is illustrated by (3.7). On simplification of (3.4) and from [4] and [32], the expressions of torque and rotor flux can be written as:

$$T_e = \frac{3}{2}\frac{P}{2}\frac{L_m}{kL_r}\left(\overline{\psi_r} \otimes \overline{\psi_s}\right) \tag{3.8}$$

$$\psi_r = \frac{L_r}{L_m}\psi_s - \sigma i_s \tag{3.9}$$

where, ψ_s is stator flux, ψ_r is rotor flux, L_m is mutual inductance, L_r is rotor inductance.

and $\sigma = \frac{L_s L_r - L_m^2}{L_m}; k = \frac{L_s L_r - L_m^2}{L_r}$.

Performing differentiation for (3.9) with respect to time, the equations can be written as

$$\frac{\mathrm{d}\psi_r}{\mathrm{dt}} = \frac{L_r}{L_m}\frac{\mathrm{d}\psi_s}{\mathrm{dt}} - \sigma\frac{\mathrm{d}i_s}{\mathrm{dt}} \tag{3.10}$$

$$\text{and}\,\frac{\mathrm{d}i_s}{\mathrm{dt}} = \left(k_1 v_s - \mathrm{j}k_2\psi_r\omega_r\right) \tag{3.11}$$

Here $k_1 = \frac{L_r}{\sigma L_m}$ and $k_2 = \frac{1}{\sigma}$.

From (3.10) and (3.11), the rate of change of stator current depends on the voltage applied to stator and speed of rotor flux. $\mathrm{d}i_s/\mathrm{dt}$ is independent of rotor flux so it is maintained constant by applying suitable voltage vector. If the rotor flux is kept constant, then torque of induction motor is dependent only on stator flux and current. By maintaining low current ripple, the ripples in flux and torque can be reduced significantly.

In the expression of $\mathrm{d}i_s/\mathrm{dt}$, the first component indicates stator voltage vector and the second component gives magnitude of back EMF. The back EMF depends on rotor flux speed ($\mathrm{j}k_2\psi_r\omega_r$) only while rotor flux is kept constant. The deviation of current ripple with respect to variation of operating frequencies is as shown in Figure 3.4.

For high speed operations, if the flux vector is assumed to be in sector-1, by applying v_{22} torque and flux can be increased. Applying v_{23} will result in rapid change of load angle so that torque can increase but flux will decrease rapidly. Hence, for high speed operation, if the

stator flux is in sector-1, then voltage vector v_{22} should be applied. To decrease torque and flux, v_{31} has to be applied.

For medium speeds of operation, if flux space vector is in sector-1, then the suitable voltage vector applied to increase flux and torque is v_9. For medium frequencies v_{22} should not be used; if voltage vector v_{22} is used for medium frequencies operation then V/f ratio should not be maintained constant. By applying v_9 voltage vector, the magnitude of voltage applied is low when compared with v_{22} and it also decreases variations in rate of change of stator current di_s/dt.

For low speeds of operation, if the flux space vector is in sector-1, then the suitable voltage vector applied to increase torque and flux is v_2. The voltage vector v_2 for low speeds of operation maintains: constant V/f ratio, reduced current ripple, constant rotor flux and less flux and torque ripple.

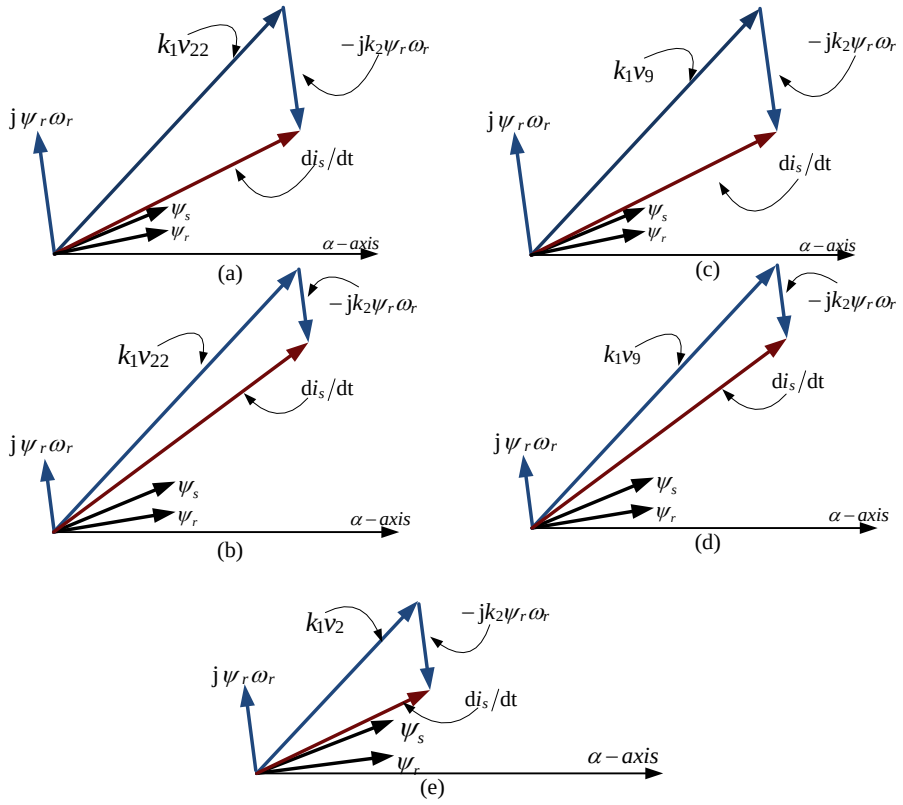

Figure 3.4 Incremental change in stator current to increase torque and flux: (a) High speeds of operation. (b), (c) Medium speeds of operation with large voltage vector, medium voltage vector and (d), (e) Low speeds of operation with medium voltage vector, low voltage vector

Figure 3.4 illustrates variation of current ripple with respect to high, medium and low speed of operation and application of suitable voltage vectors for flux space vector in sector-1. Tables 3.3 to 3.5 show the application of suitable voltage vectors with respect to rotor speed to maintain lower ripple in flux and torque. Figure 3.5 represents the steps to implement an effective voltage switching state algorithm based DTC of OEWIM drive with four-level inversion.

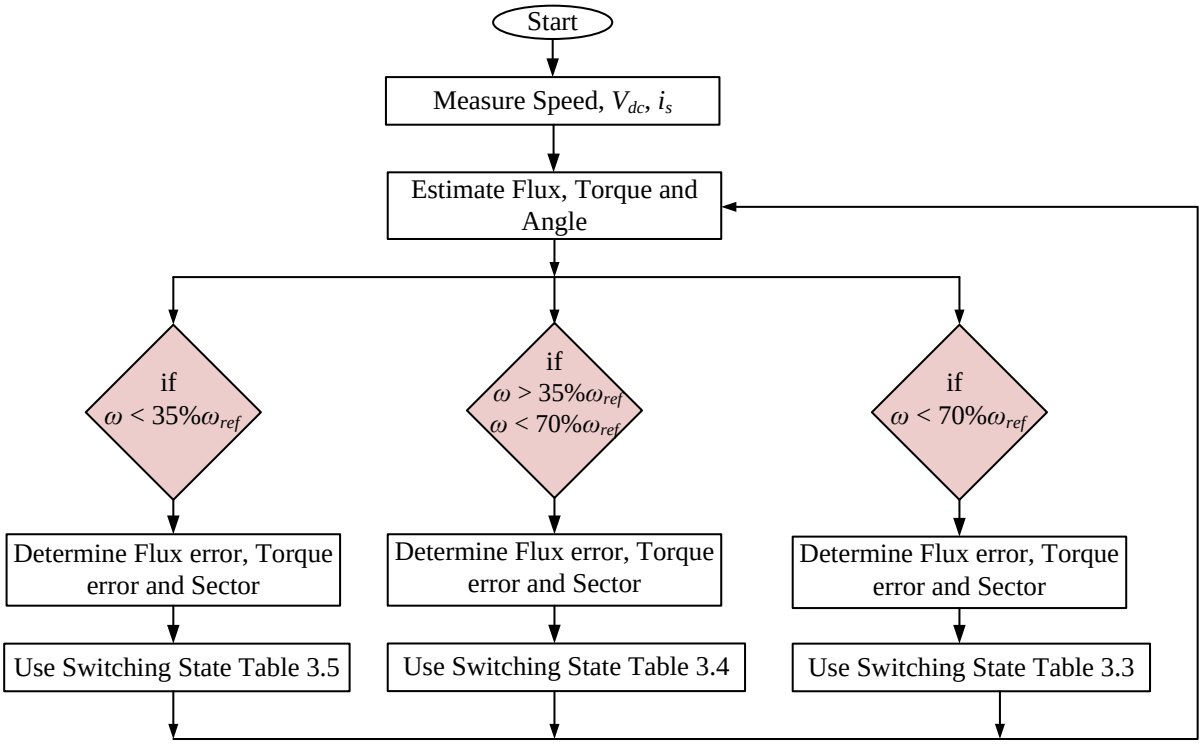

Figure 3.5 Flowchart of DTC of OEWIM with four-level inversion

3.3 Simulation and Experimental Results

The proposed DTC algorithms of OEWIM drive are simulated with MATLAB and the parameters of OEWIM that used to simulate are given in Table A.1 (Appendix). The simulation results are shown for various speeds of operation. The simulation results of OEWIM are shown for 80 rad/s, 160 rad/s and 250 rad/s in forward and reverse motoring modes. Figure 3.6 shows simulation results of OEWIM drive in forward motoring for classical two-level DTC strategy.

Figure 3.6 demonstrates speed, torque, flux and phase voltage of OEWIM in forward motoring for step change in speeds. Figures 3.6 and 3.7 show classical two-level DTC and

proposed four-level DTC algorithms for OEWIM in forward motoring for speeds of 80rad/s, 160 rad/s and 250 rad/s. From Figures 3.6 and 3.7, it is obvious that the four-level DTC gives fewer ripples in torque and flux when compared with two-level DTC and eliminates several limitations of classical DTC. From Figure 3.7 it is also clear that the proposed four-level inversion operates with specific voltage vectors. In Figure 3.7, for the speed of 80 rad/s OEWIM operates with two-level inversion (v_1 to v_6), whereas 160 rad/s and 250 rad/s operates with three-level inversion (v_7 to v_{18}) and four-level inversion (v_{19} to v_{36}) respectively. Figures 3.8 and 3.9 show simulation results of classical two-level and proposed four-level DTC algorithms of OEWIM drive for step change in speed variation of 200 rad/s to -200 rad/s.

Figures 3.8 and 3.9 describe speed, torque, flux, current and voltage of OEWIM drive with two-level and four-level inversion. In Figure 3.9 the proposed DTC algorithm operates with 200 rad/s (less than 70 % of rated speed), hence the dual inverter configuration gives three-level output voltage. From Figure 3.9 it is observed that the proposed DTC algorithms have the same characteristics as that of two-level DTC; when compared to classical DTC the proposed DTC gives lower ripple in torque and flux.

From the mathematical analysis of inverter and control circuit, the proposed algorithm is implemented with dSPACE-1104 system by interfacing it with MATLAB/SIMULINK. dSPACE-1104 is used to deliver gating signals for inverters. An experiment is conducted on the developed hardware to verify the proposed algorithm.

The experiment was conducted on OEWIM drive to operate at different speeds of operation. For convenience the results are shown for three different speeds of operation. For high speeds of operation the motor drive was set to operate at 250 rad/s, for medium speeds of operation it was set to operate at 160 rad/s and for low speeds of operation it was set to operate at 80 rad/s. The rated speed of motor drive is 1440 RPM, so it is approximately 300 rad/s (angular frequency in electrical rad/s). The behaviour of motor drive during forward and reverse motoring conditions is also exhibited. Figures 3.10 to 3.16 represent experimental waveforms of the proposed and DTC of induction motor using four-level and two-level inverter configuration. Figures 3.10 and 3.11 represent actual speed versus reference speed of motor drive for two-level and the proposed DTC respectively.

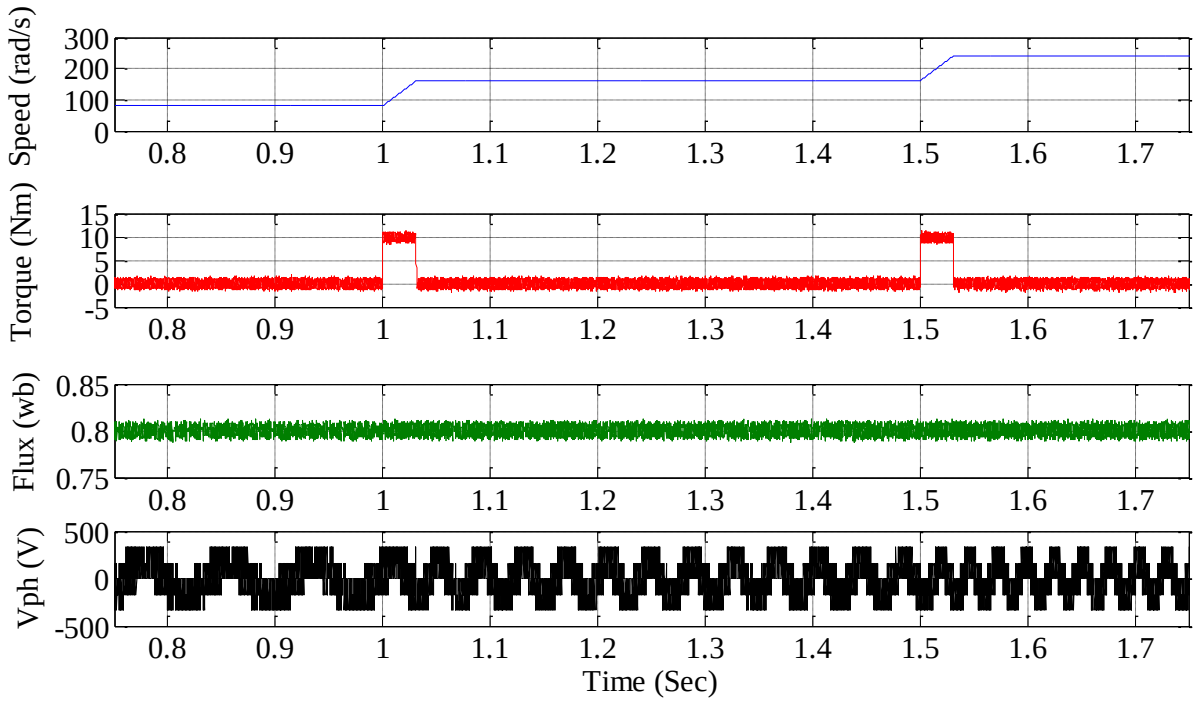

Figure 3.6 Simulation results of speed, torque, flux and voltage of OEWIM drive with two-level inversion

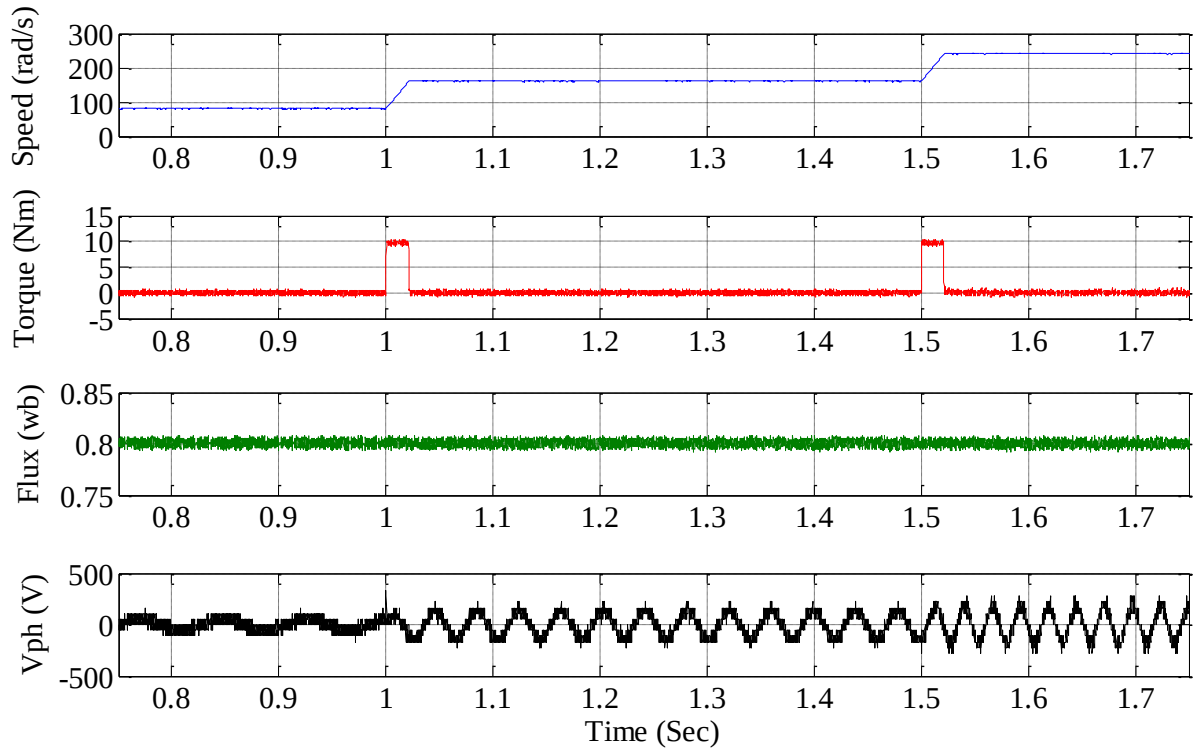

Figure 3.7 Simulation results of speed, torque, flux and voltage of OEWIM drive with four-level inversion

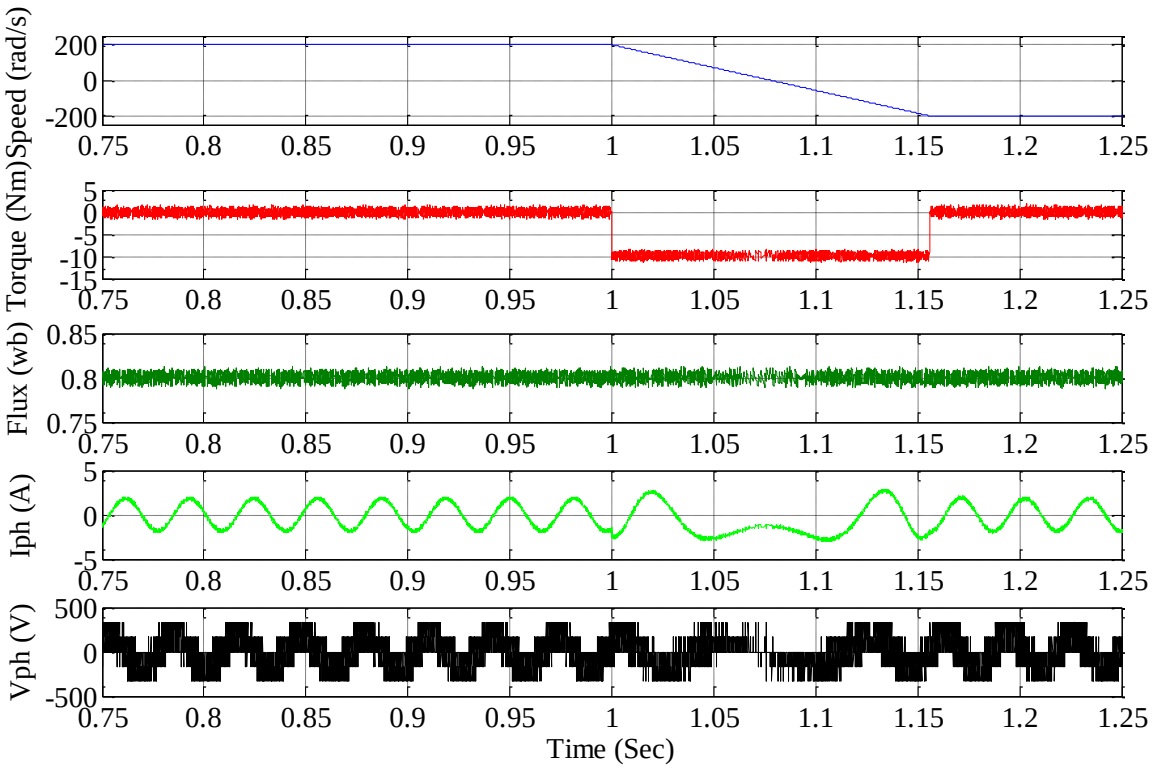

Figure 3.8 Simulation results of OEWIM drive in forward motoring to reverse motoring with two-level inversion

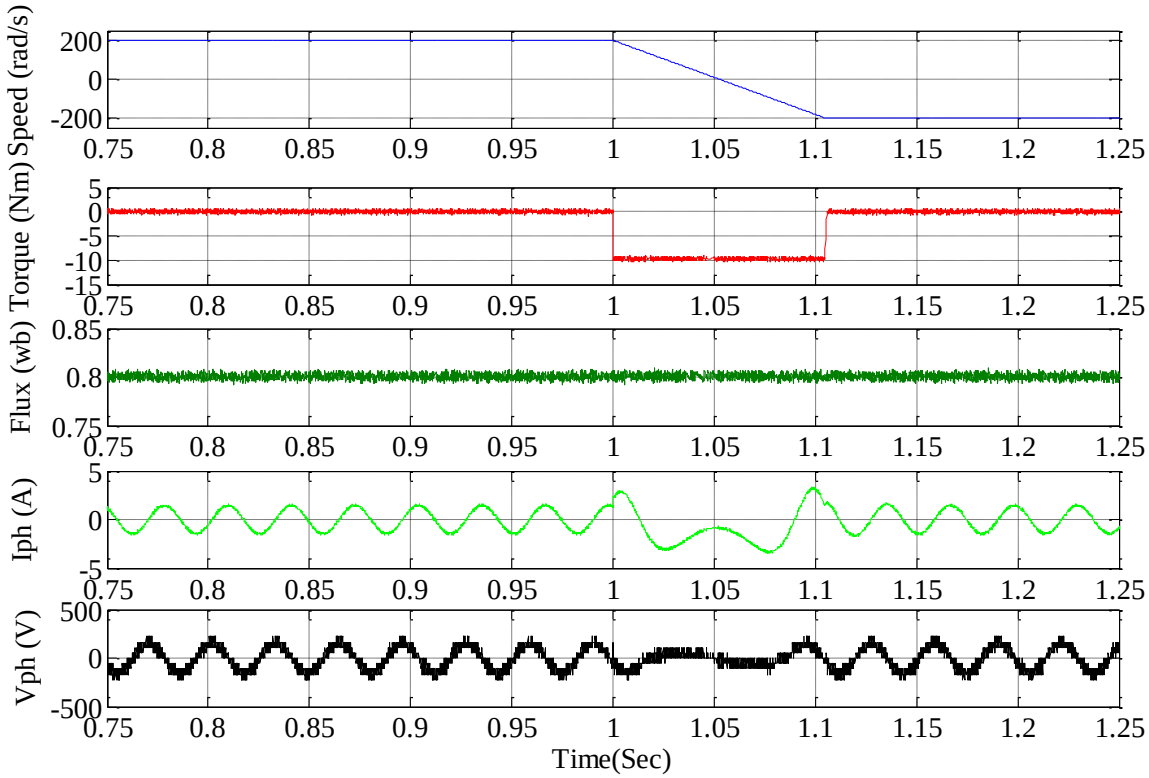

Figure 3.9 Simulation results of OEWIM drive in forward motoring to reverse motoring with four-level inversion

Figures 3.10(a) and 3.11(a) indicates forward motoring of drive at 80 rad/s, 160 rad/s and 250 rad/s for two-level DTC and the proposed DTC. Figures 3.10(b) and 3.11(b) represent forward motoring of drive at 250 rad/s, 160 rad/s and 80 rad/s for two-level and proposed DTC. Figures 3.10(c) and 3.11(c) indicate speed reversal of motor drive from -80 rad/s to 80 rad/s for two-level and proposed DTC. From the experimental results the proposed DTC provides less variation from actual speed to reference speed.

Figures 3.12 and 3.13 represent actual speed and flux of the motor drive in forward and reverse motoring conditions. The reference stator flux to motor drive is set at 0.8 Wb. Hence, the proposed and two-level DTC operates at 0.8 Wb. Figures 3.12(a) and 3.13(a) indicate actual speed and flux of motor drive in forward motoring and the motor drive is set to operate at 0.8 Wb with variation of speeds at 80 rad/s, 160 rad/s and 250 rad/s for two-level and proposed DTC. Figures 3.12(b) and 3.13(b) indicates actual speed and flux of motor drive in reverse motoring and motor drive is set to operate at 0.8 Wb with variation of speeds -80 rad/s, -160 rad/s and -250 rad/s for two-level and the proposed DTC. Figures 3.12(c) and 3.13(c) indicate the actual speed and flux of the motor drive in forward and reverse motoring with variations of speeds at 80 rad/s and -80 rad/s for two-level and the proposed DTC.

From experimental results the proposed four-level DTC gives low flux ripple in forward and reverse motoring conditions and the dynamic response of the proposed DTC is better. Figures 3.14(a) and 3.15(a) indicates actual speed and electromagnetic torque of motor drive in forward motoring with speed variations of 80 rad/s, 160 rad/s and 250 rad/s for two-level and the proposed DTC. Figures 3.14(b) and 3.15(b) indicate actual speed and torque of motor drive in reverse motoring with variations of speed at -80 rad/s 160 rad/s and 250 rad/s for two-level DTC and proposed DTC. From Figures 3.14 and 3.15, the proposed four-level DTC gives less torque ripple in steady-state during forward and reverse motoring modes when compared with two-level DTC. Figure 3.16 indicates r-phase voltage, CMV and r-phase current (during loaded and no-load) of two-level and the proposed DTC.

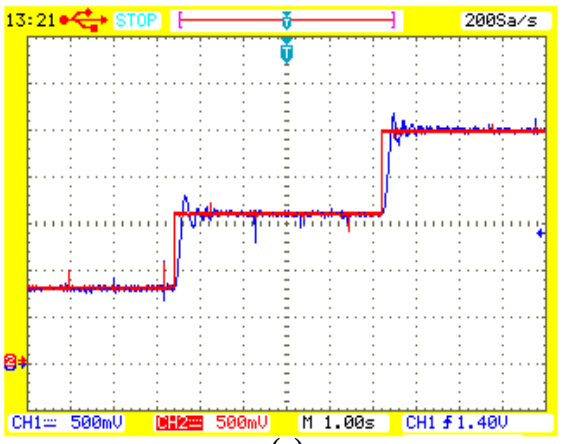

(a)

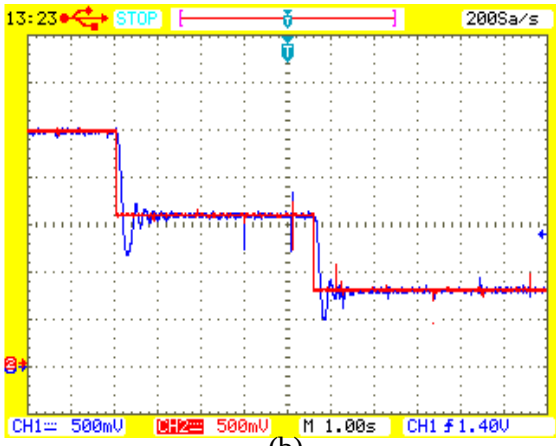

(b)

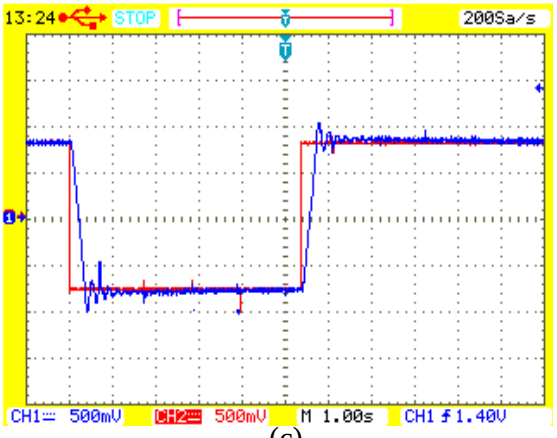

(c)

Figure 3.10 Experimental response of two-level DTC: (a) Forward motoring (speed increase). (b) Forward motoring (speed decrease) and (c) Variation of speed from reverse motoring to forward motoring. (red- reference speed and 1 div= 50 rad/s) (blue- actual speed and 1 div=50 rad/s)

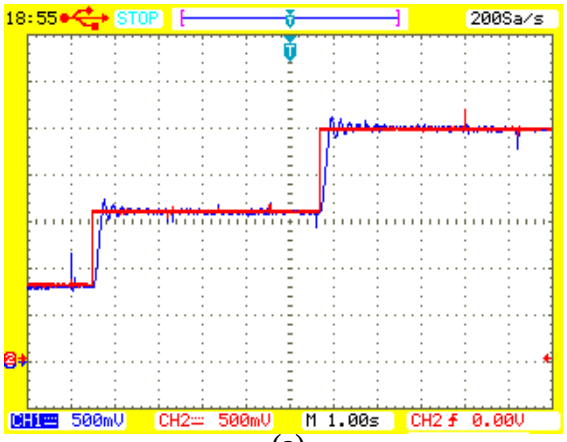

(a)

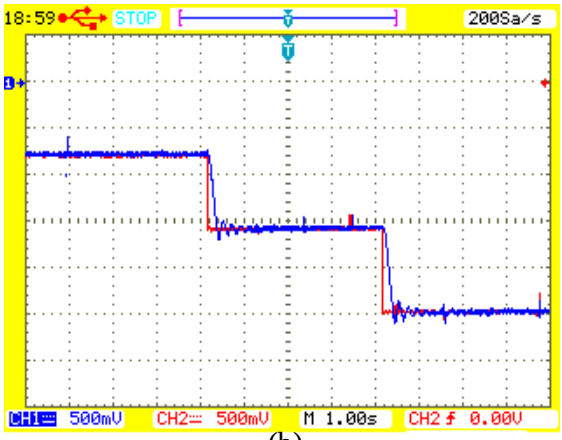

(b)

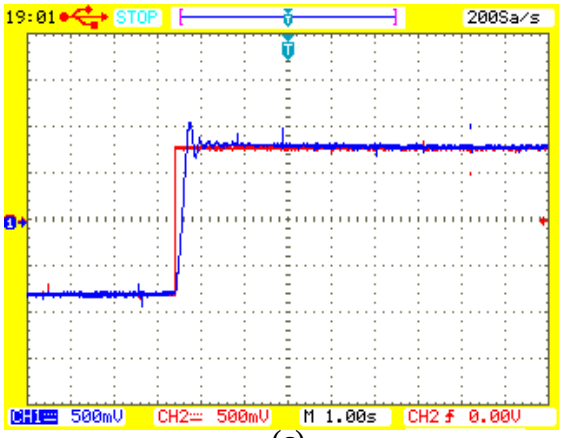

(c)

Figure 3.11 Experimental response of proposed four-level DTC: (a) Forward motoring (speed increase). (b) Forward motoring (speed decrease) and (c) Variation of speed from reverse motoring to forward motoring. (red- reference speed and 1 div= 50 rad/s) (blue- actual speed and 1 div=50 rad/s)

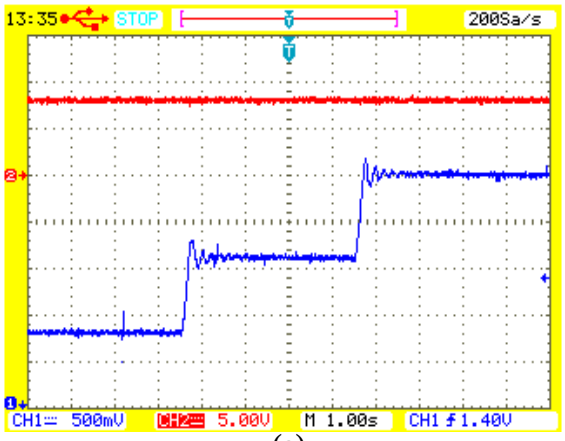

(a)

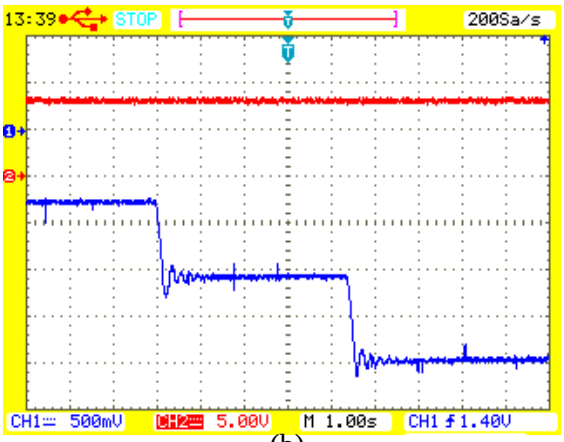

(b)

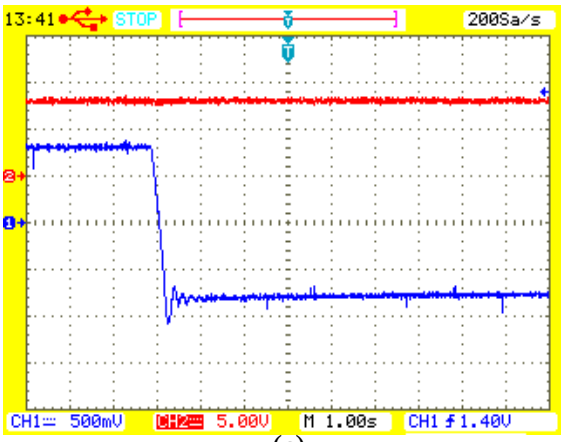

(c)

Figure 3.12 Experimental response of two-level DTC: (a) Actual speed and flux in forward motoring. (b) Actual speed and flux in reverse motoring and (c) Actual speed and flux during speed reversal. (red- flux and 1 div= 0.5 Wb) (blue- actual speed and 1 div=50 rad/s)

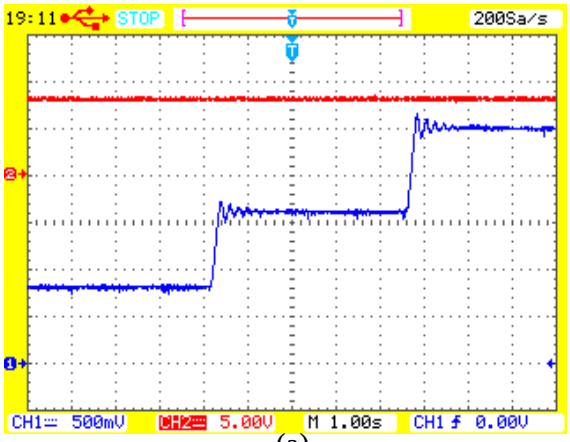

(a)

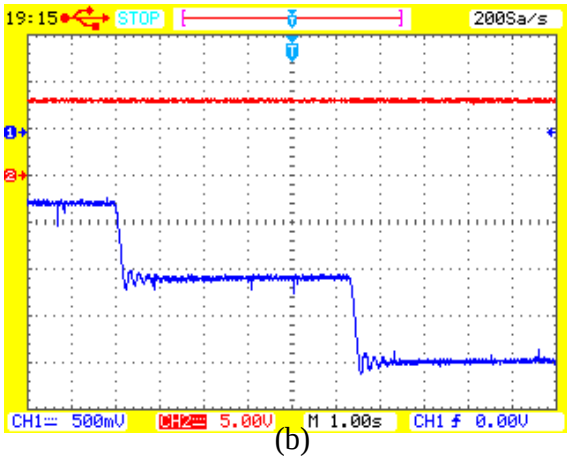

(b)

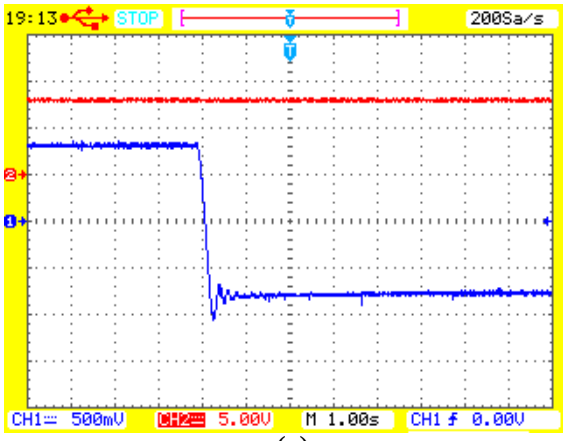

(c)

Figure 3.13 Experimental response of proposed four-level DTC: (a) Actual speed and flux in forward motoring. (b) Actual speed and flux in reverse Motoring and (c) Actual speed and flux during speed reversal. (red- flux and 1 div= 0.5 Wb) (blue- actual speed and 1 div=50 rad/s)

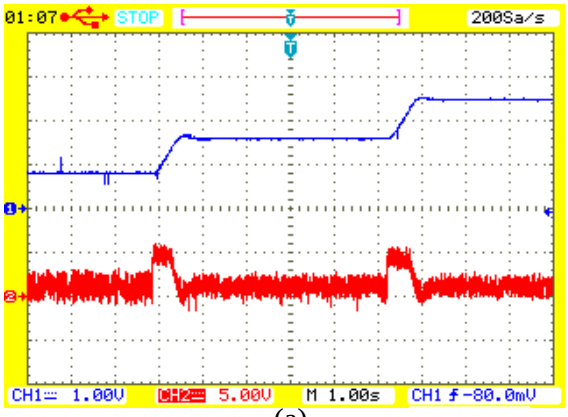

(a)

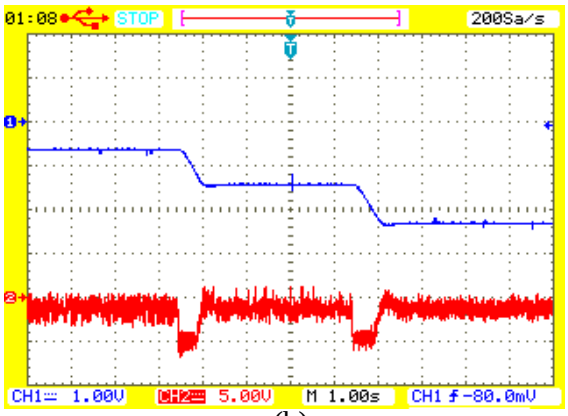

(b)

Figure 3.14 Experimental response of two-level DTC: (a) Actual speed and torque in forward motoring and (b) Actual speed and torque in reverse motoring (red-torque and 1 div=5 Nm) (blue-speed and 1 div=100 rad/s)

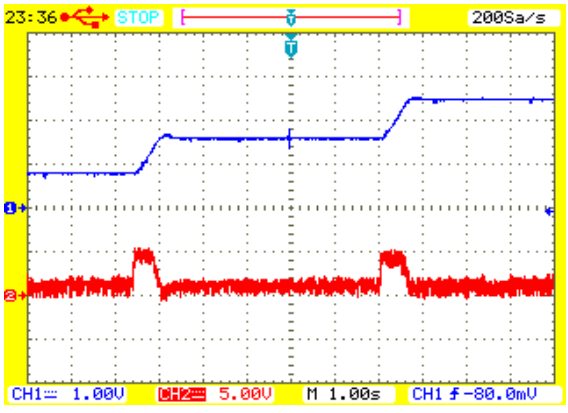

(a)

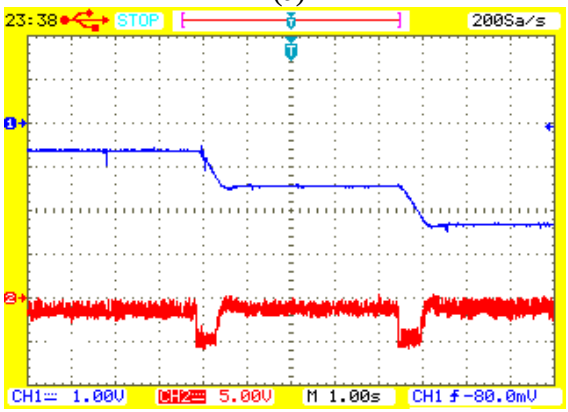

(b)

Figure 3.15 Experimental response of proposed four-level DTC: (a) Actual speed and torque in forward motoring and (b) Actual speed and torque in reverse motoring (red-torque and 1 div=5 Nm) (blue-speed and 1 div=100 rad/s)

Figures 3.16(a) and 3.16(b) represent r-phase voltage of OEWIM drive at a steady speed of 250 rad/s. Figures 3.16(c) and 3.16(d) represent CMV of OEIWM drive at 250 rad/s. Figures 3.16(e) and 3.16(f) represent r-phase current at a load torque of 14 Nm and 250 rad/s. Figures 3.16(g) and 3.16(h) present r-phase current of OEIWM drive during no-load condition at a steady speed of 300 rad/s. The numerical values of torque, flux ripple are obtained under steady state conditions and these are shown in Table 3.6. The torque and flux ripples are calculated by considering the sum of the difference between the measured and reference over 200 samples. Computation of % torque and flux ripple is given in Appendix-B, (B.1) and (B.2). From Figures 3.10 to 3.15 it is observed that at high speed (250 rad/s), medium speed (160 rad/s) and low speed (80 rad/s), the proposed four-level DTC gives lower flux and torque ripples during forward motoring and reverse motoring when compared with two-level DTC of OEWIM drive.

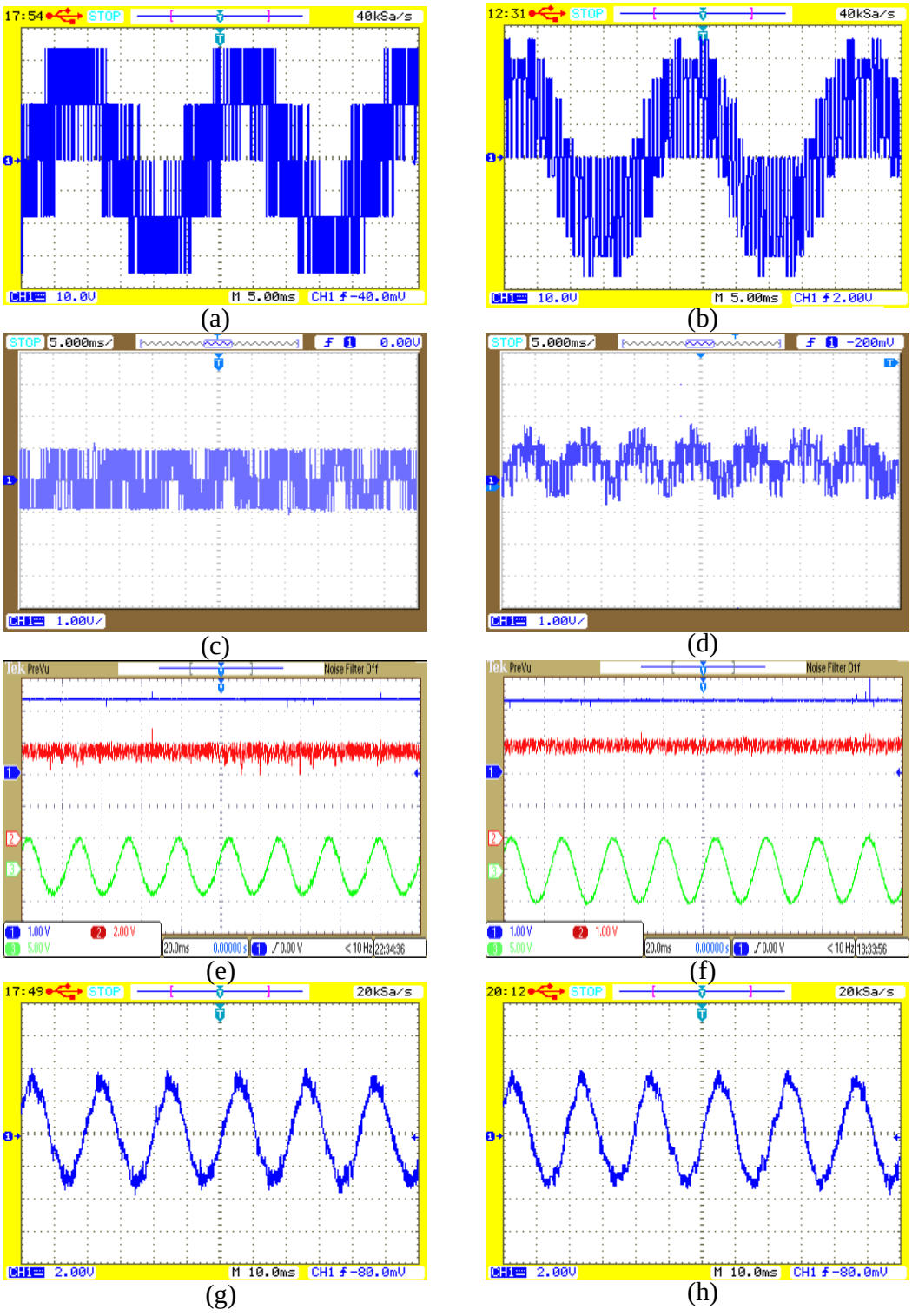

Figure 3.16 Experimental response of OEWIM drive for two-level (left) and proposed four-level DTC (right): (a), (b) R-phase voltage at a speed of 250 rad/s. (c), (d) CMV at a speed of 250 rad/s (1 div = 100V). (e),(f) Speed, torque and flux of OEWIM drive at a speed of 250 rad/s and 14 Nm (blue-speed 100 rad/s/div, red-torque 5Nm/div, green-5A/div) and (g), (h) R-phase current at 300 rad/s under no-load condition (1 div=1A)

Table 3.6 Steady-state torque and flux ripple of OEWIM drive with two-level and four-level inversion

Speed (rad/s)	2-level inversion					4-level inversion				
	Torque ripple		Flux ripple		CMV (V)	Torque ripple		Flux ripple		CMV (V)
	Nm	%	Wb	%		Nm	%	Wb	%	
80	3.65	14.91	0.061	6.1	158.12	2.25	9.19	0.048	4.8	81.35
160	3.3	13.48	0.044	4.4	146.28	2.1	8.57	0.03	3	76.46
250	3.15	12.86	0.038	3.8	131	1.95	7.96	0.028	2.8	65.48

3.4 Summary

In this chapter, an effective voltage switching state algorithm has been implemented for a four-level inverter fed direct torque controlled OEWIM drive to reduce torque and flux ripple at different operating speed conditions. In this study, the motor drive was tested at various speeds and the motor drive was operated in forward and reverse motoring conditions with speeds of 80 rad/s, 160 rad/s and 250 rad/s. The proposed DTC can be used in electric vehicles, industries, marines, ship propulsion and it can be used for high dynamic performance applications. From the experimental results, for all operating speeds the proposed DTC scheme reduces flux and torque ripples when compared with classical two-level DTC. Implementation of the proposed DTC is simple and it provides all features of conventional DTC. The proposed DTC is also applicable for permanent magnet synchronous motor (PMSM). The application part of model predictive control for the proposed DTC is left for future studies. The experiment has been carried out using two voltage sensors, two current sensors and a speed encoder while the reduction of the number of these sensors is left for future research.

Chapter 4

Predictive Torque Control of Open-end Winding Induction Motor Drive fed with Multi-level Inversion using Two Two-level Inverters

Chapter 4

Predictive Torque Control of Open-end Winding Induction Motor Drive Fed with Multi-level Inversion using Two Two-level Inverters

4.1 Introduction

In the previous chapters, the DTC of OEWIM drive with two, three and four-level inversion schemes were illustrated. In DTC of OEWIM drive with multi-level inversion, hysteresis controllers are used, it causes variable switching frequency and high ripples in torque and flux since the implementation of hysteresis controllers in discrete form is difficult [10]. In order to circumvent the problems of DTC, FCS-PTC was found to be an effective alternative to DTC [49]-[85]. From the literature, PTC also suffers from variable switching frequency, as well as higher ripples in torque and flux. To curtail torque and flux ripples it is better to use duty-cycle control [65]-[71] or MLI fed induction motor drives [61]-[63], [78], [79]. The multi-level inversion with less number of switches can be obtained by using open-end winding configuration. These are the motivating factor to implement PTC for OEWIM drive. Dual-inverter fed OEWIM drive is a better alternative for multi-level inversion schemes. The problems involved in the implementation of DTC of OEWIM for multi-level inversion can be easily addressed by PTC strategy.

The intents of this chapter are: implementation of discrete model of OEWIM drive, mathematical model of dual inverter configuration, formulation of switching states along with their space vector locations and their classification. In this chapter, OEWIM drive is programmed to operate with two-level and multi-level inversion. Hence, in this chapter, OEWIM drive is operated with two, three and four-level inversion schemes by classifying voltage vectors according to operating speed. The computational burden can be reduced by classifying the voltage vectors. A comparative study has been carried out on torque ripple for different inversion schemes. The proposed algorithms are implemented using dSPACE DS-1104 control board and the experimental results are compared with simulation results.

4.2 Discrete Model of Dual Inverter fed OEWIM Drive

The configuration of OEWIM to obtain multi-level inversion is shown in Figure 4.1. In the power circuit, by operating two inverters with equal DC-link voltages (x=y=1/2), it is easy to obtain two and three level output voltages, whereas by operating the two inverters in the ratio of 2:1 (x=2/3*; y*=1/3), four-level output voltage can be obtained [12]. To obtain four-level inversion, Inverter-1 is operated with a voltage of ($2V_{dc}$ / 3) and Inverter-2 is operated with a voltage of (V_{dc} / 3). The two inverters are operated with isolated DC sources and the net voltage at the terminals of OEWIM is a function of V_{dc}, and it is given by '$V_{dc} = xV_{dc}+yV_{dc}$'. In Figure 4.2(a) and 4.2(b), (1-8) represent voltage space vectors of Inverter-1 and (1'-8') represent voltage space vectors of Inverter-2. The voltage space vectors of Inverter-1 and Inverter-2 for equal DC-link voltage are shown in Figure 4.2(a) (two and three-level inversion), whereas Figure 4.2(b) represents voltage space vectors for unequal DC-link voltage (four-level inversion). Two-level VSI develops '8' switching states, the combination of two inverters develops (8X8) space vector locations. Out of these 64 voltage space vector locations, 37 active voltage vectors are obtained for four-level inversion. The location of active voltage vectors for two, three and four-level inversion are shown in Figure 4.5.

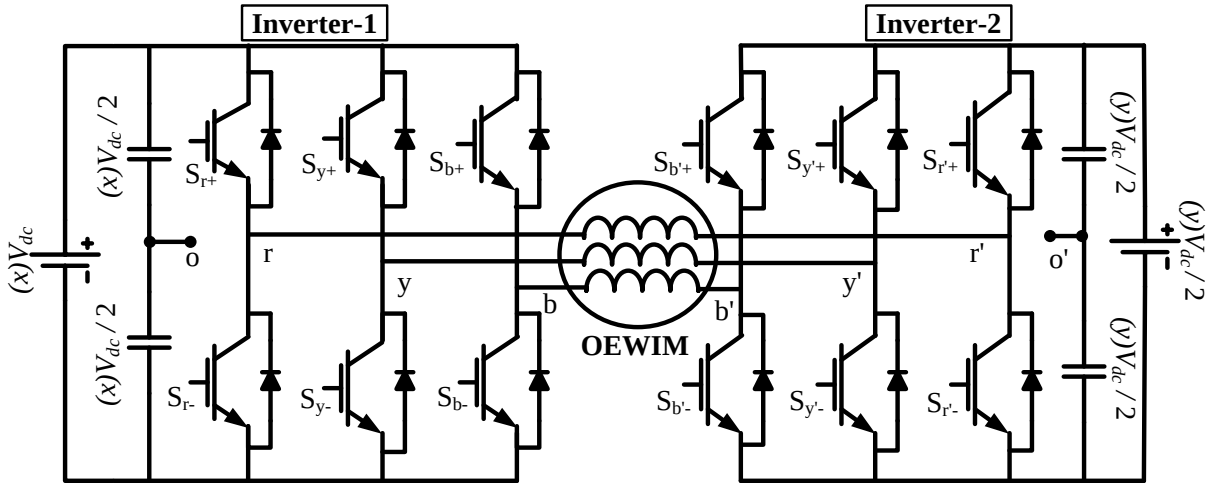

Figure 4.1 Power circuit diagram of OEWIM drive for multi-level inversion

The pole voltages of Inverter-1 are named as V_{ro}, V_{yo} and V_{bo}. The pole voltages of Inverter-2 are named as $V_{r'o'}$, $V_{y'o'}$ and $V_{b'o'}$ and the pole voltages are measured with respect to points o and o'. The pole voltage of Inverter-1 'V_{ro}' assumes xV_{dc}/2 or $-xV_{dc}$/2, similarly the

pole voltage of Inverter-2 '$V_{r'o'}$' is $yV_{dc}/2$ or $-yV_{dc}/2$ [12]. The phase voltages of OEWIM are obtained from the common mode voltage and difference of pole voltages.

$$\begin{bmatrix} V_{ro} \\ V_{yo} \\ V_{bo} \end{bmatrix} = \begin{cases} x\dfrac{V_{dc}}{2} \text{ when } S_r = S_y = S_b = 1 \\ -x\dfrac{V_{dc}}{2} \text{ when } S_r = S_y = S_b = 0 \end{cases} \tag{4.1}$$

$$\begin{bmatrix} V_{r'o'} \\ V_{y'o'} \\ V_{b'o'} \end{bmatrix} = \begin{cases} y\dfrac{V_{dc}}{2} \text{ when } S_{r'} = S_{y'} = S_{b'} = 1 \\ -y\dfrac{V_{dc}}{2} \text{ when } S_{r'} = S_{y'} = S_{b'} = 0 \end{cases} \tag{4.2}$$

The resultant pole voltages of dual inverter are given by (4.3). Pole voltages of Inverter-1 are given by (4.1) and pole voltages of Inverter-2 are given by (4.2). In (4.1) and (4.2), if S_r to S_b' =1 then the top switch of the respective leg is ON similarly when S_r to S_b'=0 the bottom switch of the respective leg is ON.

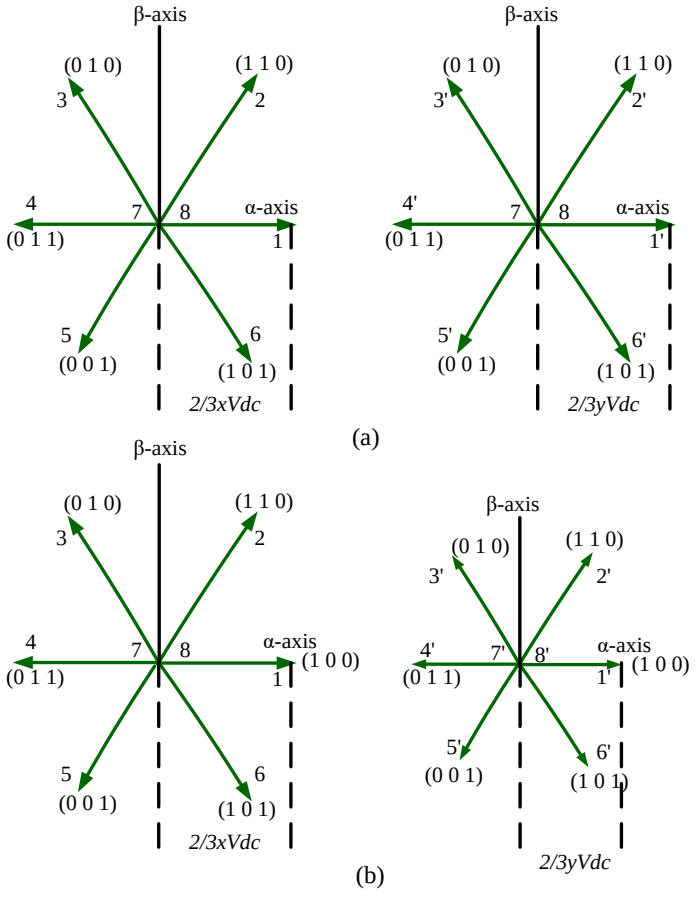

Figure 4.2 Location of space vectors for Inverter-1 and Inverter-2 (a) for two and three-level inversion (b) For four-level inversion

$$\begin{bmatrix} \Delta V_{rr'} \\ \Delta V_{yy'} \\ \Delta V_{bb'} \end{bmatrix} = \begin{bmatrix} V_{ro} - V_{r'o'} \\ V_{yo} - V_{y'o'} \\ V_{bo} - V_{b'o'} \end{bmatrix} \tag{4.3}$$

CMV of OEWIM is given by (4.4) and it is obtained from resultant pole voltages.

$$V_c = \frac{\left(\Delta V_{rr'} + \Delta V_{yy'} + \Delta V_{bb'}\right)}{3} \tag{4.4}$$

The phase voltages of OEWIM were obtained by taking the difference between resultant pole voltages and the common-mode voltage. The phase voltages of OEWIM are given by (4.5)

$$\begin{bmatrix} V_{rr'} \\ V_{yy'} \\ V_{bb'} \end{bmatrix} = \begin{bmatrix} \Delta V_{rr'} \\ \Delta V_{yy'} \\ \Delta V_{bb'} \end{bmatrix} - \begin{bmatrix} V_c \\ V_c \\ V_c \end{bmatrix} \tag{4.5}$$

From (4.5), the simplified inverter model in terms of pole voltages of Inverter-1 and Inverter-2 can be written as (4.6)

$$\begin{bmatrix} V_{rr'} \\ V_{yy'} \\ V_{bb'} \end{bmatrix} = \frac{1}{3}\begin{bmatrix} 2 & -1 & -1 \\ -1 & 2 & -1 \\ -1 & -1 & 2 \end{bmatrix}\begin{bmatrix} \Delta V_{rr'} \\ \Delta V_{yy'} \\ \Delta V_{bb'} \end{bmatrix} \tag{4.6}$$

4.2.1 Discretized Model of OEWIM drive

Discrete model of OEWIM is implemented in stationary reference frame and is shown in Figure 4.3. Stator and rotor voltages of OEWIM in stationary reference frames are given by (4.7) and (4.8). The voltage equations of stator and rotor are obtained by applying abc-αβ transformation [3].

$$\begin{bmatrix} v_{s\alpha}(k) \\ v_{s\beta}(k) \end{bmatrix}_m = R_s \begin{bmatrix} i_{s\alpha}(k) \\ i_{s\beta}(k) \end{bmatrix}_m + p\begin{bmatrix} \psi_{s\alpha}(k) \\ \psi_{s\beta}(k) \end{bmatrix}_m \tag{4.7}$$

$$\begin{bmatrix} 0 \\ 0 \end{bmatrix} = R_r \begin{bmatrix} i_{r\alpha}(k) \\ i_{r\beta}(k) \end{bmatrix}_m + p\begin{bmatrix} \psi_{r\alpha}(k) \\ \psi_{r\beta}(k) \end{bmatrix}_m + \omega_e \begin{bmatrix} \psi_{r\beta}(k) \\ -\psi_{r\alpha}(k) \end{bmatrix}_m \tag{4.8}$$

where: p is d/dt,

Flux linkages of stator and rotor are given by (4.9) and (4.10); (4.11) represents magnitude of stator flux space vector [49].

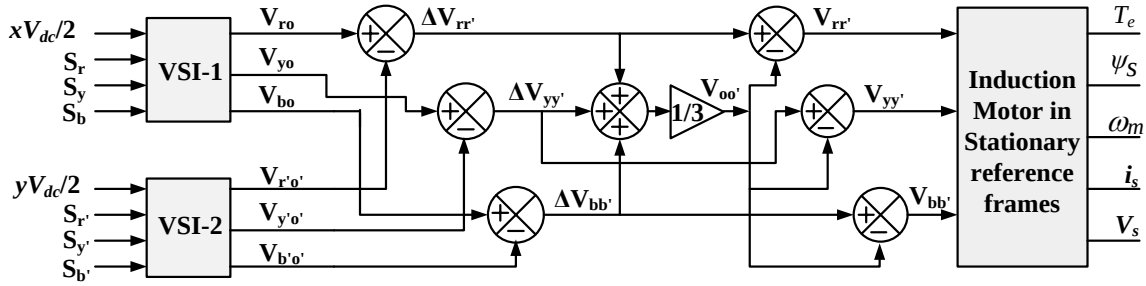

Figure 4.3 CMV model and OEWIM configuration in stationary reference frames

$$\begin{bmatrix}\psi_{s\alpha}(k)\\ \psi_{s\beta}(k)\end{bmatrix}_m = L_s\begin{bmatrix}i_{s\alpha}(k)\\ i_{s\beta}(k)\end{bmatrix}_m + L_m\begin{bmatrix}i_{r\alpha}(k)\\ i_{r\beta}(k)\end{bmatrix}_m \tag{4.9}$$

$$\begin{bmatrix}\psi_{r\alpha}(k)\\ \psi_{r\beta}(k)\end{bmatrix}_m = L_r\begin{bmatrix}i_{r\alpha}(k)\\ i_{r\beta}(k)\end{bmatrix}_m + L_m\begin{bmatrix}i_{s\alpha}(k)\\ i_{s\beta}(k)\end{bmatrix}_m \tag{4.10}$$

$$\left|\psi_s(k)\right|_m = \left|\psi_{s\alpha}(k) + j\psi_{s\beta}(k)\right| \tag{4.11}$$

Torque of OEWIM is given by (4.12),

$$T(k)_m = \frac{3}{2}\frac{P}{2}\left(\psi_{s\alpha}(k)_m i_{s\beta}(k)_m - \psi_{s\beta}(k)_m i_{s\alpha}(k)_m\right) \tag{4.12}$$

Speed of OEWIM is obtained from state-space model (4.13)

$$\begin{cases} T(k)_m - T_L = J\left(p\omega_m\right) \\ \left(p\omega_m\right) = \dfrac{1}{J}\left(T(k)_m - T_L\right) \end{cases} \tag{4.13}$$

4.3 Proposed FCS-PTC strategy

The block diagram of the proposed PTC is shown in Figure 4.4. For an induction motor, stator flux and electromagnetic torque can be varied by choosing proper voltage vector. The voltage vector should vary the magnitude of torque and flux either to increase or to decrease with the help of angle between stator flux and stator current. In PTC the same principle of DTC is used. In PTC the future values of stator flux and torque are predicted. The predicted torque and flux are compared with the reference torque and flux by using cost function. The cost function is evaluated for all possible switching states of the inverter configuration. The switching state which gives minimum value of cost function is considered to be an optimal switching state and it is applied to inverter in the sequential control interval.

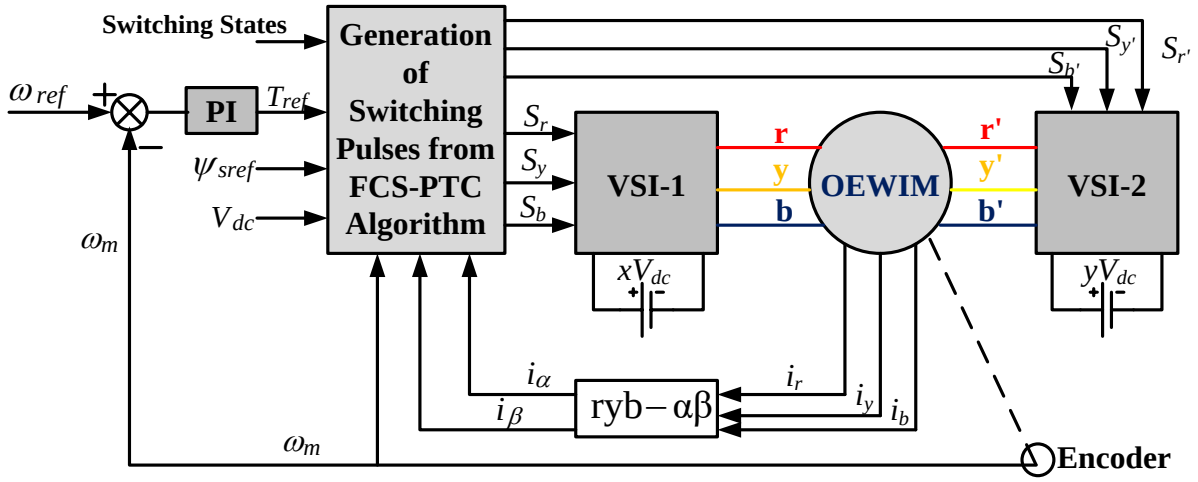

Figure 4.4 Block diagram of proposed predictive torque control of OEWIM drive fed with multi-level inversion

In this chapter PTC algorithm for OEWIM drive has been divided into three modes based on output voltage from the inverter, Mode-1: two-level output voltage, Mode-2: three-level output voltage and Mode-3: Four-level output voltage. DTC of OEWIM drive with two-level output voltage and the switching states of inverter is described in chapter-2. The voltage space vectors of OEWIM inverter for multi-level inversion can be determined using (4.14), (4.15) and (4.16).

The resultant voltage space vector (4.16) is obtained by using (4.14) and (4.15). The output voltage of Inverter-1 is given by (14), whereas (15) gives output voltage of Inverter-2.

$$v_{s1} = \frac{2}{3} x V_{dc} \left(S_r + S_y e^{j2\pi/3} + S_b e^{j4\pi/3} \right) \tag{4.14}$$

$$v_{s2} = \frac{2}{3} y V_{dc} \left(S_{r'} + S_{y'} e^{j2\pi/3} + S_{b'} e^{j4\pi/3} \right) \tag{4.15}$$

$$\text{and } v_s = v_{s1} - v_{s2} \tag{4.16}$$

In (4.16), v_{s1} indicates voltage space vector of Inverter-1, v_{s2} indicates voltage space vector of Inverter-2 and v_s indicates resultant voltage space vector of dual-inverter. Table 4.1 depicts switching states of OEWIM drive for two-level inversion, whereas Tables 4.2 and 4.3 show switching states and realization of space vectors for three and four-level inversion configuration.

Voltage space vectors are obtained from the switching states of Inverter-1 and Inverter-2. If Inverter-1 and Inverter-2 are operated with equal DC link voltages (i.e. $x=y=1/2$), then it gives two-level (6 active space vector locations) and three-level (18 active space vector locations) output voltage, whereas four-level output voltage can be obtained by operating inverters of unequal DC link voltages (i.e. $x=2/3$; $y=1/3$). In switching tables '1' indicates that the upper switch in respective leg is ON whereas '0' indicates that the lower switch is 'ON'. Based on switching states of Inverter-1 and Inverter-2 shown in Tables 4.1, 4.2 and 4.3, the locations of voltage space vectors are shown in Figure 4.5(a), 4.5(b) and 4.5(c) for two-level, three-level and four-level inversion are obtained.

The classical DTC of induction motor requires three-level torque hysteresis controller; if it is desired to operate the induction motor for more than two-level inversion then it requires multi-level hysteresis controllers and modifications of look-up table which this is tedious. To circumvent this problem and also to operate induction motor with multi-level inversion, OEWIM drive is a better alternative to meet the features of ASDs. In the proposed PTC strategy, the voltage space vector locations are classified into various groups. In case of two-level inversion mode there are 6 active vector locations, while the computational burden involved in this mode is less when compared to three and four-level inversion mode.

In three-level inversion mode, the active voltage space vector has 18 locations wherein locations v_1 to v_6 are used for speeds less than 50% of rated speed. The active vector locations v_7 to v_{18} are used for speeds for more than 50% of rated speed.

In four-level inversion, the active voltage space vector has 36 locations where locations v_1 to v_6 are used for speeds less than 35% of rated speed, locations v_7 to v_{18} are used for speeds between 35% of rated speed to 70% of rated speed and locations v_{19} to v_{36} are used for speeds more than 70% of rated speed. For multi-level inversion, PTC involves large computational burden; to handle this problem, voltage space vector is classified into various categories. Once the switching states and their realizations are calculated, it is easy to predict torque and flux of OEWIM.

Table 4.1 Realization of active voltage space vectors for two-level inversion

Inverter-1			Inverter-2			Space Vector	Realization	CMV
S_r	S_y	S_b	$S_{r'}$	$S_{y'}$	$S_{b'}$	v_s	Complex Form	V_c
0	0	0	0	0	0	v_0	0	0
1	0	0	0	1	1	v_1	V_{dc}(0.667)	-V_{dc}/6
1	1	0	0	0	1	v_2	V_{dc}(0.333+0.577i)	V_{dc}/6
0	1	0	1	0	1	v_3	V_{dc}(-0.33+0.577i)	-V_{dc}/6
0	1	1	1	0	0	v_4	V_{dc}(-0.667)	V_{dc}/6
0	0	1	1	1	0	v_5	V_{dc}(-0.33-0.577i)	-V_{dc}/6
1	0	1	0	1	0	v_6	V_{dc}(0.333-0.577i)	V_{dc}/6

Table 4.2 Realization of active voltage space vectors for three-level inversion

Inverter-1			Inverter-2			Space Vector	Realization	CMV
S_r	S_y	S_b	$S_{r'}$	$S_{y'}$	$S_{b'}$	v_s	Complex Form	V_c
1	1	0	1	1	0	v_0	0	0
1	1	0	0	1	0	v_1	V_{dc}(0.333)	V_{dc}/6
0	1	0	0	1	1	v_2	V_{dc}(0.167-0.287i)	-V_{dc}/6
0	1	1	0	0	1	v_3	V_{dc}(-0.167+0.28i)	V_{dc}/6
0	0	1	1	0	1	v_4	V_{dc}(-0.333)	-V_{dc}/6
1	0	1	1	0	0	v_5	V_{dc}(-0.167-0.28i)	V_{dc}/6
1	0	0	1	1	0	v_6	V_{dc}(0.167-0.287i)	-V_{dc}/6
1	0	0	0	1	1	v_7	V_{dc}(0.667)	-V_{dc}/6
1	1	0	0	1	1	v_8	V_{dc}(0.5-0.287i)	0
1	1	0	0	0	1	v_9	V_{dc}(0.333+0.577i)	V_{dc}/6
0	1	0	0	0	1	v_{10}	V_{dc}(0.577)	0
0	1	0	1	0	1	v_{11}	V_{dc}(-0.33+0.577i)	-V_{dc}/6
0	1	1	1	0	1	v_{12}	V_{dc}(-0.5+0.287i)	0
0	1	1	1	0	0	v_{13}	V_{dc}(-0.667)	V_{dc}/6
0	0	1	1	0	0	v_{14}	V_{dc}(0.333-0.577i)	0
0	0	1	1	1	0	v_{15}	V_{dc}(-0.33-0.577i)	-V_{dc}/6
1	0	1	1	1	0	v_{16}	V_{dc}(-0.577i)	0
1	0	1	0	1	0	v_{17}	V_{dc}(0.333-0.577i)	V_{dc}/6
1	0	0	0	1	0	v_{18}	V_{dc}(0.5-0.287i)	0

4.3.1 Prediction Algorithm

The concept of PTC depends on measurements, estimation and prediction of behaviour of the OEWIM in the next control cycle. In the previous section, discrete model of OEWIM is shown in stationary reference frames at k^{th} instant, for prediction of torque and flux at (k+1) instant, it require speed and current measurements. If currents are measured then by using stator voltage flux linkages of stator (4.17) can be estimated. The stator flux of OEWIM drive is

estimated by sensing DC-link voltages of Inverter-1 and inverter-2. The effective DC-link voltage is given by $V_{dc}=x\ V_{dc}+yV_{dc}$.

Table 4.3 Realization of active voltage vectors for four-level inversion

Inverter-1			**Inverter-2**			**Space Vector**	**Realization**	**CMV**
$\mathbf{S_r}$	$\mathbf{S_y}$	$\mathbf{S_b}$	$\mathbf{S_{r'}}$	$\mathbf{S_{y'}}$	$\mathbf{S_{b'}}$	$\boldsymbol{v_s}$	**Complex Form**	$\mathbf{V_c}$
0	0	0	0	0	0	v_0	0	$-V_{dc}/6$
1	0	0	1	0	0	v_1	$V_{dc}(0.222)$	$-V_{dc}/18$
1	1	0	1	1	0	v_2	$V_{dc}(0.11+0.193i)$	$V_{dc}/18$
0	1	0	0	1	0	v_3	$V_{dc}(-0.11+0.19i)$	$-V_{dc}/18$
0	1	1	0	1	1	v_4	$V_{dc}(-0.222)$	$V_{dc}/18$
0	0	1	0	0	1	v_5	$V_{dc}(-0.11-0.193i)$	$-V_{dc}/18$
1	0	1	1	0	1	v_6	$V_{dc}(0.11-0.193i)$	$V_{dc}/18$
1	0	0	1	1	1	v_7	$V_{dc}(0.444)$	$-V_{dc}/6$
1	0	0	1	0	1	v_8	$V_{dc}(0.33+0.193i)$	$-V_{dc}/6$
1	1	0	1	1	1	v_9	$V_{dc}(0.22+0.385i)$	$V_{dc}/18$
0	1	0	0	1	1	v_{10}	$V_{dc}(0.385i)$	$-V_{dc}/6$
0	1	0	1	1	1	v_{11}	$V_{dc}(-0.22+0.38i)$	$-V_{dc}/6$
0	1	0	1	1	0	v_{12}	$V_{dc}(-0.33+0.19i)$	$-V_{dc}/6$
0	1	1	1	1	1	v_{13}	$V_{dc}(-0.444)$	$V_{dc}/18$
0	0	1	1	0	1	v_{14}	$V_{dc}(-0.33-0.193i)$	$-V_{dc}/6$
0	0	1	1	1	1	v_{15}	$V_{dc}(-0.22-0.385i)$	$-V_{dc}/6$
0	0	1	0	1	1	v_{16}	$V_{dc}(-0.385i)$	$-V_{dc}/6$
1	0	1	1	1	1	v_{17}	$V_{dc}(0.22-0.385i)$	$V_{dc}/18$
1	0	0	1	1	0	v_{18}	$V_{dc}(0.33-0.193i)$	$-V_{dc}/6$
1	0	0	0	1	1	v_{19}	$V_{dc}(0.667)$	$-V_{dc}/6$
1	0	0	0	0	1	v_{20}	$V_{dc}(0.55+0.193i)$	$-V_{dc}/18$
1	1	0	0	1	1	v_{21}	$V_{dc}(0.44+0.385i)$	$V_{dc}/18$
1	1	0	0	0	1	v_{22}	$V_{dc}(0.33+0.577i)$	$V_{dc}/6$
1	1	0	1	0	1	v_{23}	$V_{dc}(0.11+0.577i)$	$V_{dc}/18$
0	1	0	0	0	1	v_{24}	$V_{dc}(-0.11+0.57i)$	$-V_{dc}/18$
0	1	0	1	0	1	v_{25}	$V_{dc}(-0.33+0.57i)$	$-V_{dc}/6$
0	1	0	1	0	0	v_{26}	$V_{dc}(-0.44+0.38i)$	$-V_{dc}/18$
0	1	1	1	0	1	v_{27}	$V_{dc}(-0.55+0.19i)$	$V_{dc}/18$
0	1	1	1	0	0	v_{28}	$V_{dc}(-0.667)$	$V_{dc}/6$
0	1	1	1	1	0	v_{29}	$V_{dc}(-0.55-0.19i)$	$V_{dc}/18$
0	0	1	1	0	0	v_{30}	$V_{dc}(-0.44-0.38i)$	$-V_{dc}/18$
0	0	1	1	1	0	v_{31}	$V_{dc}(-0.33-0.57i)$	$-V_{dc}/6$
0	0	1	0	1	0	v_{32}	$V_{dc}(-0.11-0.577i)$	$-V_{dc}/18$
1	0	1	1	1	0	v_{33}	$V_{dc}(0.11-0.577i)$	$V_{dc}/18$
1	0	1	0	1	0	v_{34}	$V_{dc}(0.33-0.577i)$	$V_{dc}/6$
1	0	1	0	1	1	v_{35}	$V_{dc}(0.44-0.385i)$	$V_{dc}/18$
1	0	0	0	1	0	v_{36}	$V_{dc}(0.55-0.193i)$	$-V_{dc}/18$

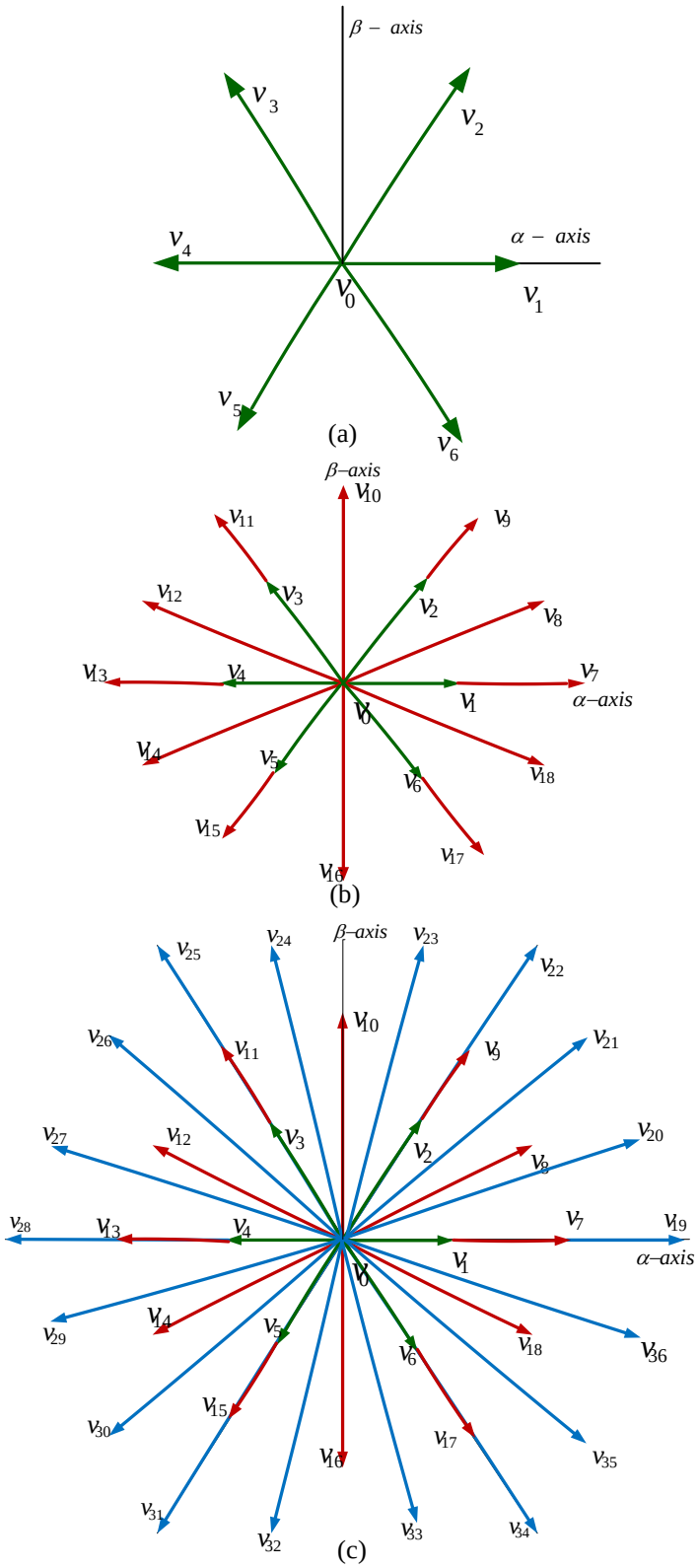

Figure 4.5 Voltage space vectors of dual inverter configuration: (a) Two-level inversion. (b) Three-level inversion and (c) Four-level inversion

The effective DC-link voltage has two functions: (i) It is used for the realisation of voltage space vectors in control algorithm and (ii) To estimate the phase voltages of OEWIM drive. From the total DC-link voltage, the phase voltages of OEWIM drive are estimated by using (4.4)-(4.9). $v_{s\alpha}(k)$ and $v_{s\beta}(k)$ are obtained by applying Clarke's transformation to phase voltages ($V_{rr'}$, $V_{yy'}$ and $V_{bb'}$). The stator flux of OEWIM drive is obtained by using (4.17) and (4.18).

The predicted values of torque and flux are obtained from the measurements and estimations at k^{th} instant.

$$p\begin{bmatrix}\psi_{s\alpha}(k)\\ \psi_{s\beta}(k)\end{bmatrix}_m = \begin{bmatrix}v_{s\alpha}(k)\\ v_{s\beta}(k)\end{bmatrix}_m - R_s\begin{bmatrix}i_{s\alpha}(k)\\ i_{s\beta}(k)\end{bmatrix}_m \tag{4.17}$$

$$\begin{bmatrix}\psi_{s\alpha}(k)\\ \psi_{s\beta}(k)\end{bmatrix}_m = \int\left(\begin{bmatrix}v_{s\alpha}(k)\\ v_{s\beta}(k)\end{bmatrix}_m - R_s\begin{bmatrix}i_{s\alpha}(k)\\ i_{s\beta}(k)\end{bmatrix}_m\right)dt \tag{4.18}$$

The predictions of torque and flux are developed by using forward Euler's approach [52] and it is shown in (4.19).

$$\frac{\mathrm{d}F}{\mathrm{d}t} = \frac{F(k+1)-F(k)}{T_s} \tag{4.19}$$

Therefore from (4.19) the next state can be predicted as:

$$F(k+1) = \frac{\mathrm{d}F}{\mathrm{d}t}T_s + F(k) \tag{4.20}$$

From (4.19) and (4.20):

$$\begin{bmatrix}\psi_{s\alpha}(k+1)\\ \psi_{s\beta}(k+1)\end{bmatrix}_m = T_s\left(\begin{bmatrix}v_{s\alpha}(k)\\ v_{s\beta}(k)\end{bmatrix}_m - R_s\begin{bmatrix}i_{s\alpha}(k)\\ i_{s\beta}(k)\end{bmatrix}_m\right) + \begin{bmatrix}\psi_{s\alpha}(k)\\ \psi_{s\beta}(k)\end{bmatrix}_m \tag{4.21}$$

$$p\begin{bmatrix}i_{s\alpha}(k)\\ i_{s\beta}(k)\end{bmatrix}_m = C\left[A\begin{bmatrix}\psi_{s\alpha}(k)\\ \psi_{s\beta}(k)\end{bmatrix}_m - E\begin{bmatrix}i_{s\alpha}(k)\\ i_{s\beta}(k)\end{bmatrix}_m + B\begin{bmatrix}\psi_{s\beta}(k)\\ -\psi_{s\alpha}(k)\end{bmatrix}_m - D\begin{bmatrix}i_{s\beta}(k)\\ i_{s\alpha}(k)\end{bmatrix}_m + F\begin{bmatrix}V_{s\alpha}(k)\\ V_{s\beta}(k)\end{bmatrix}_m\right] \tag{4.22}$$

Stator current can be predicted from (4.22) and it is given by:

$$\begin{bmatrix}i_{s\alpha}(k+1)\\ i_{s\beta}(k+1)\end{bmatrix}_m = T_s\left(C\begin{bmatrix}A\begin{bmatrix}\psi_{s\alpha}(k)\\ \psi_{s\beta}(k)\end{bmatrix}_m - E\begin{bmatrix}i_{s\alpha}(k)\\ i_{s\beta}(k)\end{bmatrix}_m + B\begin{bmatrix}\psi_{s\beta}(k)\\ -\psi_{s\alpha}(k)\end{bmatrix}_m\\ -D\begin{bmatrix}i_{s\beta}(k)\\ i_{s\alpha}(k)\end{bmatrix}_m + F\begin{bmatrix}V_{s\alpha}(k)\\ V_{s\beta}(k)\end{bmatrix}_m\end{bmatrix}\right) + \begin{bmatrix}i_{s\alpha}(k)\\ i_{s\beta}(k)\end{bmatrix}_m \tag{4.23}$$

$$T_e(k+1) = \frac{3}{2}\frac{P}{2}\left(\psi_{s\alpha}(k+1) i_{s\beta}(k+1) - \psi_{s\beta}(k+1) i_{s\alpha}(k+1)\right) \quad (4.24)$$

where, $A = \frac{R_r}{L_m}$, $B = \omega_e \frac{L_r}{L_m}$, $C = \frac{L_m}{L_s L_r - L_m^2}$, $D = \frac{\omega_e}{C}$, $E = \frac{1}{L_m}\left(R_r L_s - R_s L_r\right)$, $F = \frac{L_r}{L_m}$, m=[v_0, v_1, v_2..... v_{36}], T_s is sample time, ω_m indicates speed in mechanical rad/sec and ω_e indicates speed in electrical rad/sec.

4.3.2 Formulation of Cost Function

To obtain the switching states of inverter, optimization of cost function (g) is required. The pre-requisites of cost function are common-mode voltage (V_c), stator flux reference (ψ_{sref}), predicted values of stator flux ($\psi_s(k+1)$), torque reference (T_{ref}) and predicted value of electromagnetic torque ($T_e(k+1)$). The cost function of the proposed PTC is shown in (4.25).

$$g = \sigma_T \left|T_{ref} - T_e(k+1)\right| + \sigma_\psi \left|\psi_{sref} - \psi_s(k+1)\right| + \sigma_n \left|V_c\right| \quad (4.25)$$

The cost function (4.25) should be verified for all active voltage space vectors of OEWIM drive configuration. The optimization of cost function is in such a way that the selected stator voltage vector can produce fewer ripples in torque, flux and less CMV. In (4.25), σ_T, σ_ψ and σ_n are weighting factors of torque, flux and CMV. The weighting factors used for simulation and experiment are σ_T =1, σ_ψ =75 and σ_n = 0.01. The branch and bound algorithm is used to determine weighting factors and they are obtained from several offline simulations. The procedure to find weighting factors for CMV and stator flux is reported in [75] and [76]. In [75], the procedure to select stator flux weighting factor and its effect on the performance of induction motor drive was presented. The selection of weighting factor for CMV and its influence on current is reported in [76]. The steps to develop PTC of OEWIM with four-level inversion are shown in Figure 4.6.

4.4 Simulation and Experimental Results

To verify the effectiveness of the proposed PTC strategies of OEWIM shown in Figure 4.4, the model was simulated using MATLAB and verified experimentally by using dSPACE 1104 control board. VSIs used in OEWIM drive operated with DC link voltages of 270V and 270V respectively, for two and three-level inversion scheme, therefore the effective

DC link voltage was 540V. For four-level inversion, Inverter-1 and Inverter-2 are operated with DC link voltages of 360V and 180 V with an effective DC link voltage of 540V.

To verify the proposed PTC algorithms, the OEWIM drive is programmed to operate at various speeds; in the interest of brevity, the simulation and experimental results are shown for 100 rad/s, 200 rad/s and 250 rad/s in both forward and reverse motoring modes. The parameters of OEWIM drive used for verification of experimental response are given in Table A.1 (Appendix). The test bench used for verification of the proposed algorithms is described in Appendix-A. The focus of this chapter is to develop PTC for OEWIM drive with equal and unequal DC link voltages and also to show the simulation and experimental response for three inversion schemes.

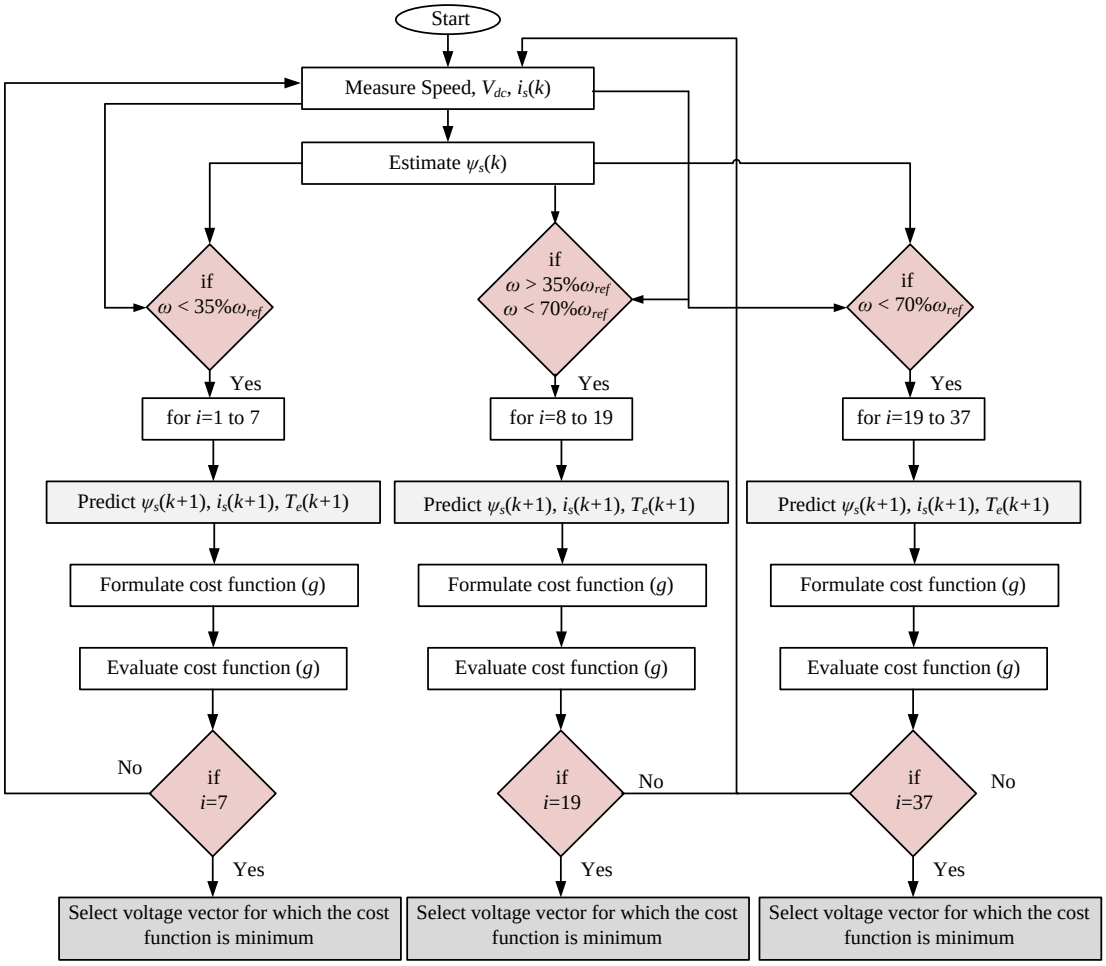

Figure 4.6 Flowchart of PTC of OEWIM with four-level inversion

It is well known that by operating induction motor drives with multi-level output voltages, the torque ripple and flux ripple decreases. To show comparison between two-level, three-level and four-level inversion schemes with PTC, an algorithm is presented with simulation and experimental results. OEWIM was tested under no-load condition; therefore the reference torque is zero in steady state condition and nominal/reference flux is 1 Wb. Torque ripple and flux ripple is estimated from the deviation of actual values of torque (4.12) and flux (4.11) with respect to reference torque and flux.

Figures 4.7 to 4.12 show simulated and experimental response of OEWIM drive at various speeds. The step change of speed response from 100 rad/s, 200 rad/s and 250 rad/s are shown in Figure 4.7 for two-level, three-level and four-level inversion respectively in forward motoring. From Figure 4.7, it can be observed that, if motor drive is operating with multi-level output voltage fed by inverter, it gives reduced ripple in torque and flux.

Figure 4.8 shows simulated and experimental response of OEWIM drive in reverse motoring mode for step change in speed. Figure 4.8 gives variation of torque and flux ripple for different output voltage levels of inverter and it gives higher ripple in torque and flux at -100 rad/s; as the speed of the motor drive increases, the input voltage to its stator terminals may increases and gives reduced ripple in torque and flux at -200 rad/s and -250 rad/s. Figure 4.8(a), is simulated and the experimental response of OEWIM drive in reverse motoring for two-level inversion is shown whereas Figures 4.8(b) and 4.8(c) represent simulated and experimental response of OEWIM for three-level and four-level inversion.

Simulated and experimental response of speed, torque and flux of OEWIM drive for a step change of 200 rad/s to -200 rad/s are shown in Figure 4.9, for two, three and four-level inversion respectively. Figure 4.10 shows simulated and experimental response of speed, current and voltage of OEWIM drive in forward motoring at a speed of 250 rad/s. Figure 4.11 shows simulated and experimental response of speed, voltage and CMV of OEWIM drive at a speed of 200 rad/s. Figure 4.12 illustrates r-phase current of OEWIM drive at a load torque of 14 Nm and flux loci of OEWIM for two, three and four-level inversion respectively.

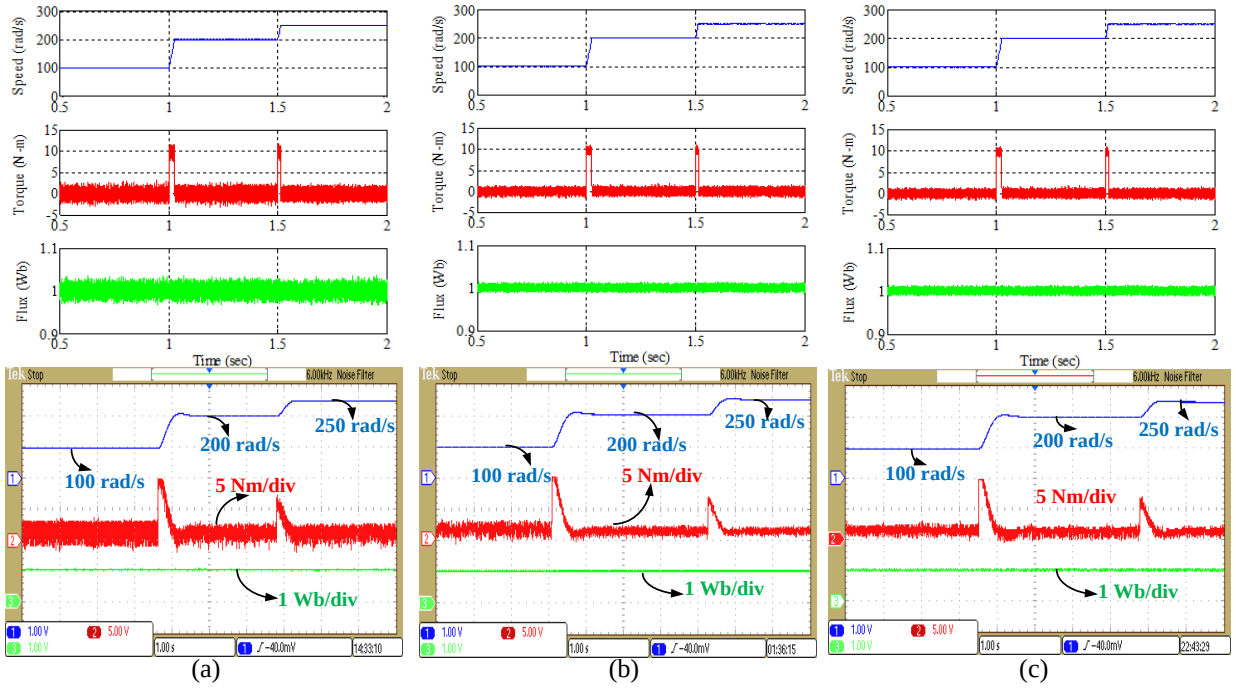

Figure 4.7 Speed, torque and flux in forward motoring of OEWIM drive for 100 rad/s, 200 rad/s and 250 rad/s. (a) Simulated and experimental response for two-level inversion. (b) Simulated and experimental response for three-level inversion. (c) Simulated and experimental response for four-level inversion

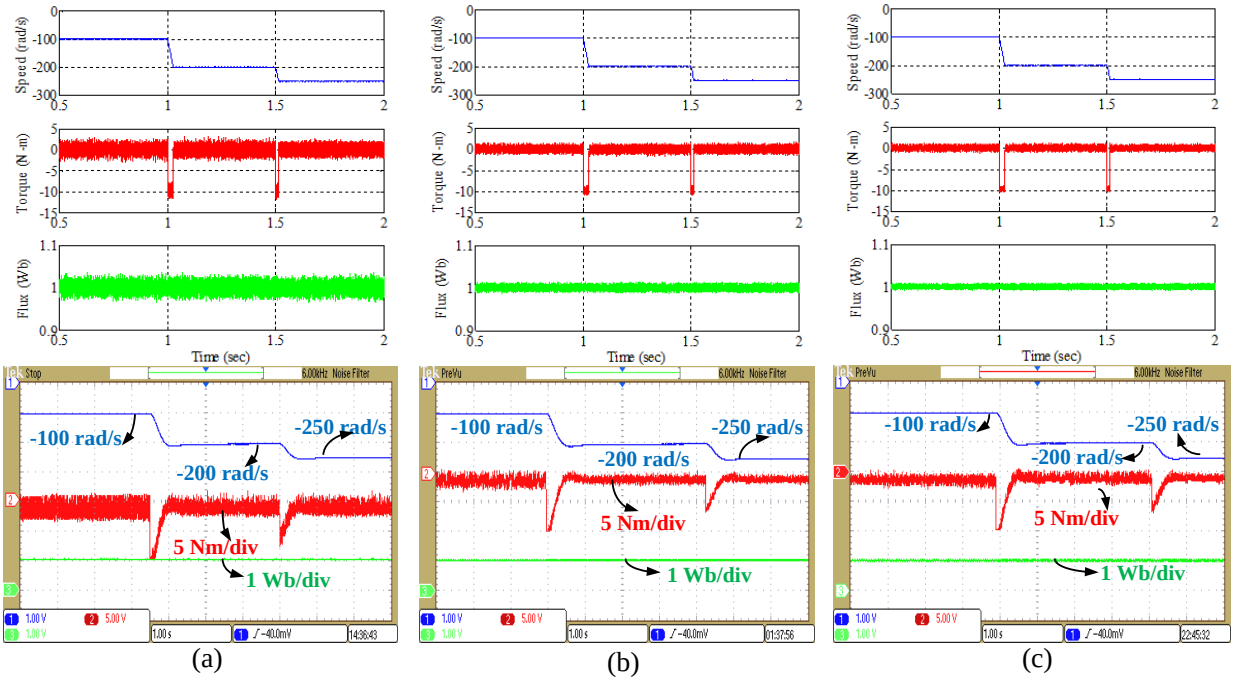

Figure 4.8 Speed, torque and flux in reverse motoring of OEWIM drive for -100 rad/s, -200 rad/s and -250 rad/s: (a) Simulated response and experimental response for two-level inversion. (b) Simulated and experimental response of three level inversion and (c) Simulated and experimental response for four-level inversion

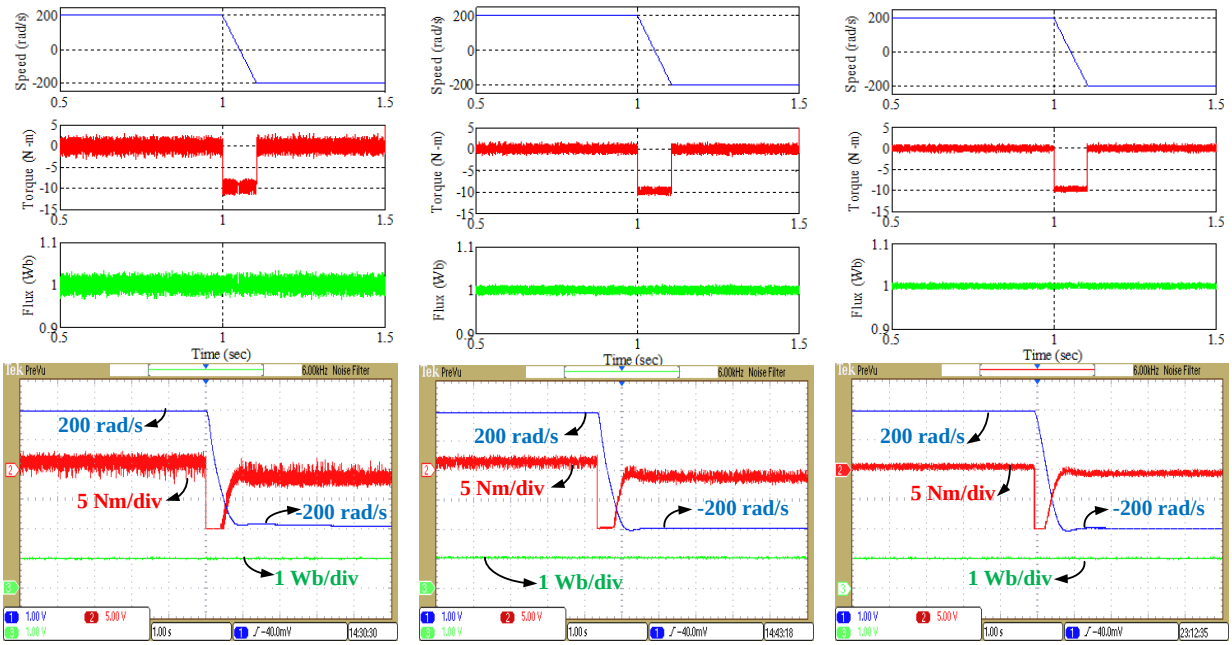

Figure 4.9 Speed, torque and flux in forward to reverse motoring of OEWIM drive for 200 rad/s to -200 rad/s: (a) Simulated and experimental response for two-level inversion. (b) Simulated and experimental response for three -level inversion and (c) Simulated and experimental response for four -level inversion

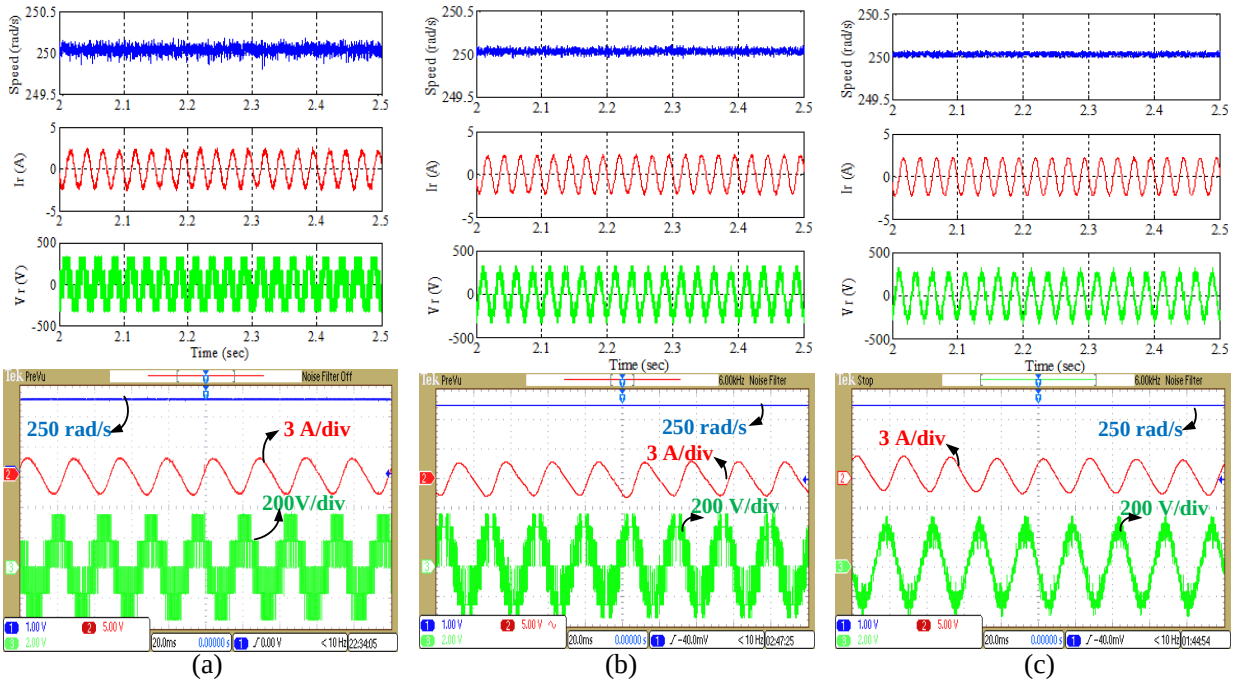

Figure 4.10 Speed, current and voltage of OEWIM drive: (a) Simulated and experimental response for two-level inversion. (b) Simulated and experimental response for three-level inversion and (c) Simulated and experimental response for four-level inversion

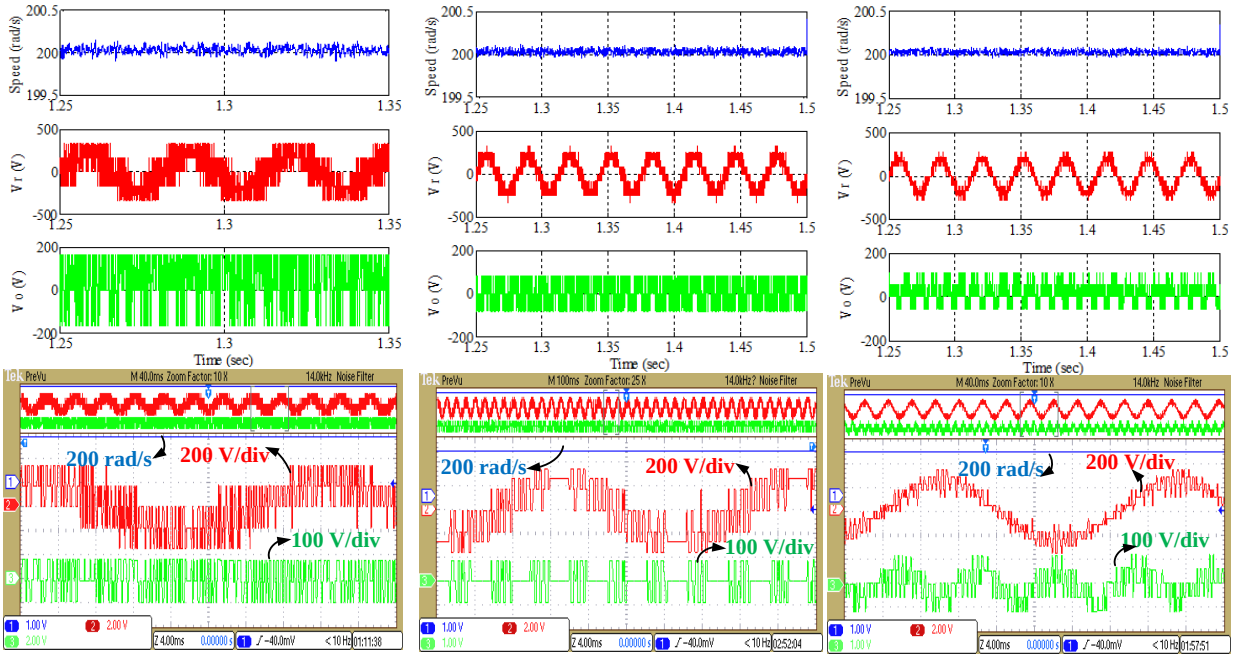

Figure 4.11 Speed, voltage and common-mode voltage of OEWIM drive: (a) Simulated and experimental response for two-level inversion. (b) Simulated and experimental response for three-level inversion and (c) Simulated and experimental response for four-level inversion

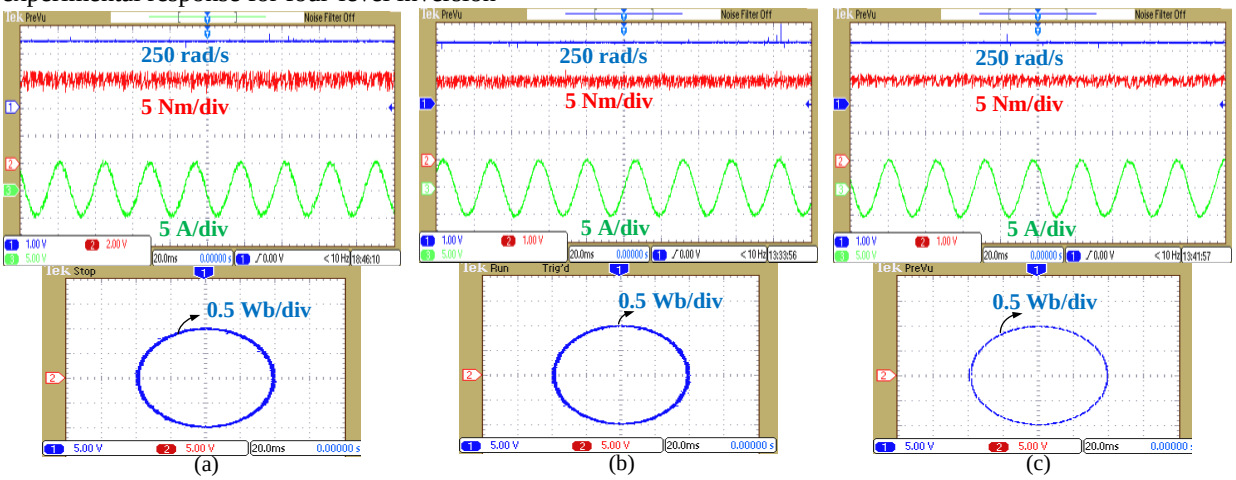

Figure 4.12 Speed, torque, phase-current and flux locus of OEWIM drive for (a) Two-level (b) Three-level and (c) Four-level inversion respectively

From Figure 4.9, torque and flux ripple reduces for four-level inversion when compared with two and three-level inversion. Figure 4.9 also illustrates the settling time required for four-level inversion is less when compared to two and three-level inversion. Figure 4.10(a) gives simulated and experimental response of OEWIM drive for a speed of 250 rad/s in forward motoring for two-level inversion, whereas Figures 4.10(b) and 4.10(c) represent simulated and experimental response of OEWIM drive for a speed of 250 rad/s in forward motoring for three

and four-level inversion respectively. Figure 4.11(a) shows speed, voltage and common mode voltage of OEWIM drive for a speed of 200 rad/s in forward motoring for two-level inversion whereas Figures 4.11(b) and 4.11(c) represent simulated and experimental response for three and four-level inversion schemes.

From Figure 4.11 it is evident that by operating OEWIM with three and four-level inversion, CMV can be reduced. In the cost function of the proposed algorithm, the CMV is added, by adding this term into cost function the switching states are chosen accordingly for minimum values of CMV. Therefore the effect of CMV is reduced from two-level inversion to four-level inversion.

From Figure 4.7 to Figure 4.9, it is clear that the torque and flux ripples decrease by using multi-level inversion scheme. To reduce the computational burden on the controller, the voltage vectors have been classified into different groups, whereas for two-level inversion or in the case of classical PTC, there are 6 active voltage vectors and a null vector. Therefore for two-level inversion and classical PTC, the 6 active voltage vectors are applied for all speed ranges whereas in the proposed three-level and four-level inversion schemes, the voltage vectors are classified to operate based on input reference speed; therefore classification of active voltage vectors not only reduces torque and flux ripple but also affects the computational burden of the controller.

Flux locus is obtained by estimating α-axis and β-axis flux with simple flux observer. By integrating (4.17), the real and imaginary components of the flux are estimated. From Figure 4.12(c), flux ripple is low when compared to two and three-level inversion. The peak-peak variations in steady-state torque and flux ripple of OEWIM drive for various speeds of operation is listed in Table 4.4. Computation of % torque and flux ripple (peak to peak variation) is given in Appendix-B, (B.3) and (B.4). The proposed PTC algorithms develop lower ripple in torque and flux when compared with classical DTC for OEWIM configuration.

Table 4.4 Experimental steady-state torque and flux ripple of OEWIM drive for different operating speeds

Control Algorithm	Speed (rad/s)	2-level Inversion				3-level Inversion				4-level Inversion			
		Torque ripple		Flux ripple		Torque ripple		Flux ripple		Torque ripple		Flux ripple	
		Nm	%	Wb	%	Nm	%	Wb	%	Nm	%	Wb	%
DTC	100	4.5	18.38	0.057	5.7	4.1	16.74	0.048	4.8	3.4	13.8	0.038	3.8
Proposed PTC		3.8	15.52	0.032	3.2	3.2	13.07	0.028	2.8	2.8	11.4	0.025	2.5
DTC	200	3.3	13.48	0.045	4.5	3	12.25	0.038	3.8	2.8	11.4	0.03	3
Proposed PTC		2.8	11.43	0.02	2	2.5	10.21	0.018	1.8	2	8.16	0.016	1.6
DTC	250	2.5	10.21	0.035	3.5	2.25	9.19	0.028	2.8	1.85	7.55	0.025	2.5
Proposed PTC		2	8.16	0.013	1.3	1.75	7.14	0.0125	1.25	1.4	5.71	0.01	1

4.5 Summary

This chapter develops the scheme of PTC for OEWIM drive using equal and unequal DC link voltages. It clearly describes implementation, mathematical modelling and analysis of PTC and the impact of classification of voltage vectors on speed, torque and flux. To reduce complexity and computational burden one step ahead prediction (prediction horizon N=1) is performed. The proposed algorithms are simple and extendable for more than four-level inversion by replacing two-level inverters with three-level NPC inverter. For three-level and four-level inversion the computational burden is high; the burden can be reduced by classifying the voltage vectors. By using OEWIM drive it is easy to implement PTC with reduced torque and flux ripples for multi-level inversion. The simulation and experimental results show the effectiveness of the proposed PTC algorithms and gives better steady-state response for multi-level inversion. In this chapter PTC of OEWIM drive is presented to show for two, three and four-level inversion schemes. The voltage vectors used in this chapter will provide minimum CMV; hence the CMV involved in the four-level inversion of OEWIM drive is much less when compared with two and three-level inversion.

Chapter 5

Improved Predictive Torque Control Strategies for an Open-end Winding Induction Motor Drive fed with Four-level Inversion

Chapter 5

Improved Predictive Torque Control Strategies for an Open-end Winding Induction Motor Drive fed with Four-level Inversion

5.1 Introduction

In the previous chapter, PTC of OEWIM drive was introduced with two, three and four-level inversion. The formulation of cost function in PTC is always chosen to track reference in classical PTC, whereas in the present trends, in addition to torque and flux control, reduction of CMV and balancing of neutral voltage potential are added in cost function for MLI fed induction motor drives [49]-[55]. The minimization of cost function is achieved by tuning the weighting factors involved in the cost function. There is no particular method to select the weighting factors; some of them use branch and bound algorithm to select the weighting factors [49], [53]-[57], [60]-[64]. In [49], the selection of flux weighting factor is given by the ratio of rated torque and flux; for real-time implementation further tuning is required. Multi-objective ranking based PTC algorithm was implemented to eliminate weighting factor selection [73], but it involves large computations when compared to classical PTC. In [74], weighting factors was eliminated by converting torque and flux reference into equivalent flux space phasor. In [82], the weighting factors of cost function are chosen by heuristic methods.

Based on the literature, the challenges in FCS-PTC are: variable switching frequency, tedious tuning of weighting factors and higher ripples in torque and flux. In order to overcome these limitations duty-cycle control, dead-beat control and MLI fed induction motor drives are implemented. In this chapter, an attempt is made to eliminate weighting factors, reduce switching frequency, torque and flux ripples by using MLI fed OEWIM configuration.

From the previous chapter and literature, it is identified that PTC requires tuning of weighting factors. The tuning of weighting factors is quite cumbersome, when compared with the tuning of PI controller [49], [79]. In order to tune weighting factors several off-line simulations are performed and the switching frequency involved in the implementation of PTC is very high when compared with DTC strategy. In order to address these two problems, this

chapter proposed a PTC algorithm with modified cost function and the tuning of weighting factors is simplified with the help of normalized weighted sum model (WSM), in addition, this chapter also proposed a simplified weighting factor eliminated PTC for the OEWIM drive.

In this chapter, four-level inversion is used to operate OEWIM drive; hence the cost function is evaluated for all 37 voltage space vector locations of dual inverter configuration. The switching frequency of dual inverter configuration is controlled by introducing an additional term into the cost function. In classical PTC, the switching frequency control is quite difficult and various methods are introduced to control switching frequency [66]-[69], [85]. The classical PTC uses torque and flux errors in cost function and hence it cannot control switching frequency. If it is required to add the other control objectives (constraints) into the cost function, then the tuning of multiple weighting factors is unavoidable.

In this chapter a simplified switching frequency control algorithm is used instead of complex control strategies [66]-[69], [78], [85]. The control algorithm is implemented by using difference of voltage space vector applied in the previous control cycle and the voltage space vector in the present control cycle. To simplify the selection of weighting factors and also to minimize multi-objective cost function one of the multi-criterion decision making algorithms is used. The WSM is a multi-criteria decision making algorithm and it is easy to implement [87], [88].

This chapter also proposed, a simplified weighting factor eliminated PTC strategy for the OEWIM drive. The weighting factor elimination is obtained by splitting the cost function into two individual functions. Cost function-I comprise flux control; the optimization of cost function gives a set of voltage space vectors, the voltage vectors obtained from the optimization of cost function are used in cost function-II. Cost function-II comprises torque control as an objective and the optimization of cost function-II gives optimum voltage vector to control torque and flux of OEWIM drive. The effectiveness of the proposed PTC algorithms was verified by implementing it with MATLAB/SIMULINK and experimentation. The experimentation was carried by implementing the proposed algorithms with dSPACE DS-1104 controller.

5.2 Classical FCS-PTC of OEWIM

Classical FCS-PTC of OEWIM can be implemented by using the following steps: (i) Implementing the dynamic model of VSI to identify all possible switching states (ii) Implementing discrete model of OEWIM to identify control variables (iii) Measuring the variables (speed and current) required for prediction (iv) Estimating the non-measurable variables (flux and torque) at k^{th} instant (v) Predicting the control variables for all possible switching combinations (vi) Implementing the cost function and (vii) Minimizing cost function to generate switching pulses. The flowchart to develop classical PTC of OEWIM drive is shown in Figure 5.1.

5.2.1 Prediction of Control Variables

The control variables in classical PTC are torque and flux. To predict control variables, forward Euler method (5.1) and (5.2) are used. The control variables are predicted for 37 possible space vector locations of OEWIM drive are given in Table 4.3. The state-space model of OEWIM drive is used to predict torque and flux of OEWIM by predicting stator current.

$$\frac{\mathrm{d}x}{\mathrm{dt}} = \frac{x(k+1) - x(k)}{T_s} \tag{5.1}$$

$$x(k+1) = \frac{\mathrm{d}x}{\mathrm{dt}} T_s + x(k) \tag{5.2}$$

The state-space equations of stator flux are obtained by using (4.9),

$$p\begin{bmatrix} \psi_{s\alpha}(k) \\ \psi_{s\beta}(k) \end{bmatrix}_m = \begin{bmatrix} v_{s\alpha}(k) \\ v_{s\beta}(k) \end{bmatrix}_m - R_s \begin{bmatrix} i_{s\alpha}(k) \\ i_{s\beta}(k) \end{bmatrix}_m \tag{5.3}$$

From (5.3), stator flux can be predicted as follows:

$$\begin{bmatrix} \psi_{s\alpha}(k+1) \\ \psi_{s\beta}(k+1) \end{bmatrix}_m = T_s \left(\begin{bmatrix} v_{s\alpha}(k) \\ v_{s\beta}(k) \end{bmatrix}_m - R_s \begin{bmatrix} i_{s\alpha}(k) \\ i_{s\beta}(k) \end{bmatrix}_m \right) + \begin{bmatrix} \psi_{s\alpha}(k) \\ \psi_{s\beta}(k) \end{bmatrix}_m \tag{5.4}$$

The simplified state-space equations of stator current are derived from (4.22)-(4.23).

$$p\begin{bmatrix} i_{s\alpha}(k) \\ i_{s\beta}(k) \end{bmatrix}_m = C\left[A\begin{bmatrix} \psi_{s\alpha}(k) \\ \psi_{s\beta}(k) \end{bmatrix}_m - E\begin{bmatrix} i_{s\alpha}(k) \\ i_{s\beta}(k) \end{bmatrix}_m + B\begin{bmatrix} \psi_{s\beta}(k) \\ -\psi_{s\alpha}(k) \end{bmatrix}_m - D\begin{bmatrix} i_{s\beta}(k) \\ i_{s\alpha}(k) \end{bmatrix}_m + F\begin{bmatrix} v_{s\alpha}(k) \\ v_{s\beta}(k) \end{bmatrix}_m \right] \tag{5.5}$$

Stator currents can be predicted from (5.5) and it is given by

$$\begin{bmatrix} i_{s\alpha}(k+1) \\ i_{s\beta}(k+1) \end{bmatrix}_m = T_s \left(C \begin{bmatrix} A \begin{bmatrix} \psi_{s\alpha}(k) \\ \psi_{s\beta}(k) \end{bmatrix}_m - E \begin{bmatrix} i_{s\alpha}(k) \\ i_{s\beta}(k) \end{bmatrix}_m + B \begin{bmatrix} \psi_{s\beta}(k) \\ -\psi_{s\alpha}(k) \end{bmatrix}_m \\ -D \begin{bmatrix} i_{s\beta}(k) \\ i_{s\alpha}(k) \end{bmatrix}_m + F \begin{bmatrix} v_{s\alpha}(k) \\ v_{s\beta}(k) \end{bmatrix}_m \end{bmatrix} \right) + \begin{bmatrix} i_{s\alpha}(k) \\ i_{s\beta}(k) \end{bmatrix}_m \tag{5.6}$$

If stator flux and current equations are known, then it is easy to predict torque of OEWIM

$$T(k+1)_m = \frac{3}{2}\frac{P}{2}\left(\psi_{s\alpha}(k+1)_m i_{s\beta}(k+1)_m - \psi_{s\beta}(k+1)_m i_{s\alpha}(k+1)_m\right) \tag{5.7}$$

From (5.4), the magnitude of predicted stator flux is given by

$$\psi_s(k+1)_m = \left|\left(\psi_{s\alpha}(k+1)_m + j\psi_{s\beta}(k+1)_m\right)\right| \tag{5.8}$$

where, $A = \frac{R_r}{L_m}$, $B = \omega_e \frac{L_r}{L_m}$, $C = \frac{L_m}{L_s L_r - L_m^2}$, $D = \frac{\omega_e}{C}$ $E = \frac{1}{L_m}\left(R_r L_s - R_s L_r\right)$, $F = \frac{L_r}{L_m}$,

m=[v_0, v_1, v_2..... v_{36}], T_s is sample time, ω_m indicates angular speed in mechanical rad/sec and ω_e indicates angular speed in electrical rad/s.

5.2.2 Formulation of Cost Function

In classical PTC, the cost function (g) comprises torque and flux control terms. The selection of switching states is made by minimization of cost function. The cost function is used to meet control law. In classical PTC, control law is defined to reduce torque ripple and flux ripple. The cost function is given by

$$g = w_1\left|\left(T_{ref} - T_e(k+1)_m\right)\right| + w_2\left|\left(\psi_{sref} - \psi_s(k+1)_m\right)\right| \tag{5.9}$$

Cost function of classical PTC consists of two parts. The first part is to reduce the torque error and second part of cost function is to minimize the flux error. In (5.9), w_1 and w_2 indicate weighting factors of torque and stator flux respectively.

The selection of w_1, w_2 plays a vital role on the performance of OEWIM. Initially w_1 and w_2 is taken as fixed value whereas for real time implementation tuning of w_1 and w_2 is required. Tuning of weighting factors is a cumbersome and tedious process.

Minimization of cost function is evaluated for all possible space vector combinations of the inverter. The switching frequency required in classical PTC is very high. In power converters, switching frequency is an effective measure of switching losses. As switching

frequency increases, number of commutations of power switches increase. To limit the number of commutations, switching frequency has to be reduced. In order to reduce the torque and flux ripples, multi-level inversion is used. The switching frequency is reduced by modifying cost function. This study uses normalized WSM to provide the same performance of classical PTC along with reduction of switching frequency and an attempt to reduce tedious tuning process of weighting factors.

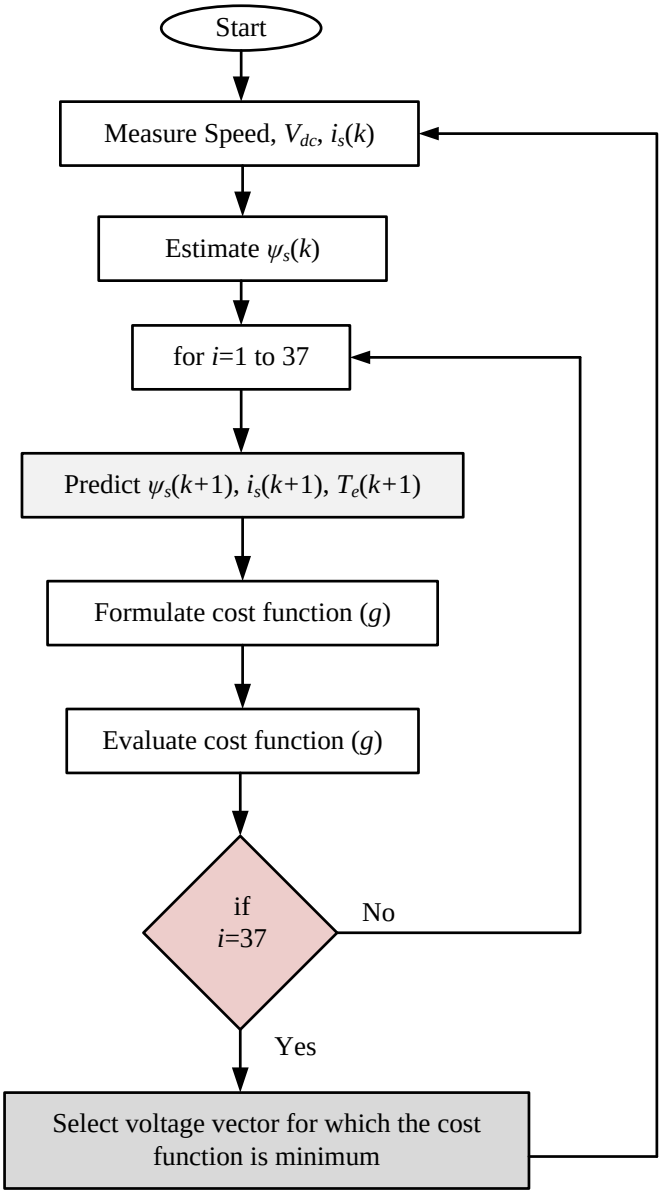

Figure 5.1 Flowchart of classical PTC of OEWIM with four-level inversion

5.3 PTC of OEWIM using Normalized Weighted Sum Model

The block diagram of the proposed PTC strategy is shown in Figure 5.2. In classical PTC cost function comprises only two control variables. For multi-level inversion, the number of switches is more, which increases commutations and causes switching losses. In order to reduce the switching frequency, cost function is reframed with three control objectives. The proposed PTC algorithm is implemented by considering multi-objective cost function. If the cost function consists of multiple control objectives then it is obvious to find weighting factors associated with each and every individual control objective and the tuning of these weighting factors becomes unavoidable. This chapter uses a multi-criteria decision making algorithm to simplify the selection of weighting factors by using normalized WSM as shown in Figure 5.3.

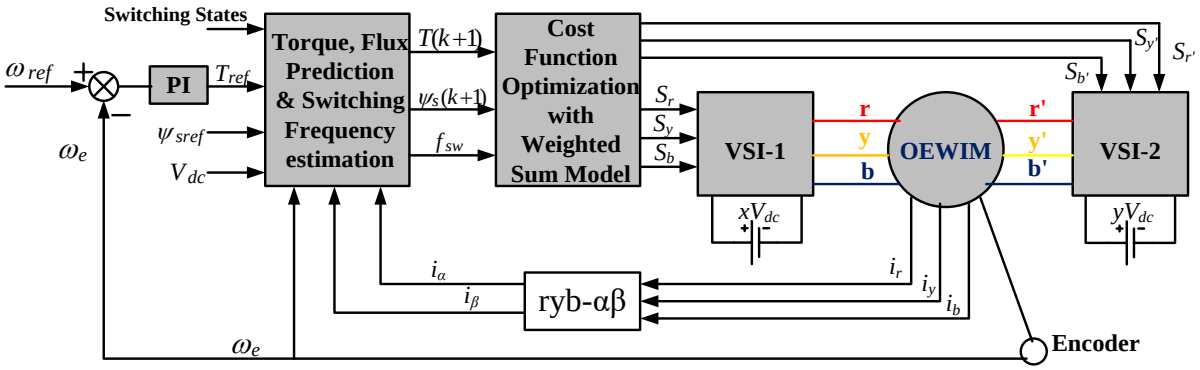

Figure 5.2 Block diagram of proposed PTC of OEWIM using normalized WSM

5.3.1 Implementation of Normalised WSM

The selection of weighting factor affects the performance of OEWIM drive. If the cost function comprises more than two control variables, then the selection of weighting factors is complicated. In the proposed PTC algorithm, the cost function comprises of three control objectives. The steps involved to implement proposed PTC are given below:

- Generate decision matrix using control objectives.
- Normalize the decision matrix.
- Obtain weighted normalized decision matrix.
- Determine the optimum voltage vector to meet control objective.

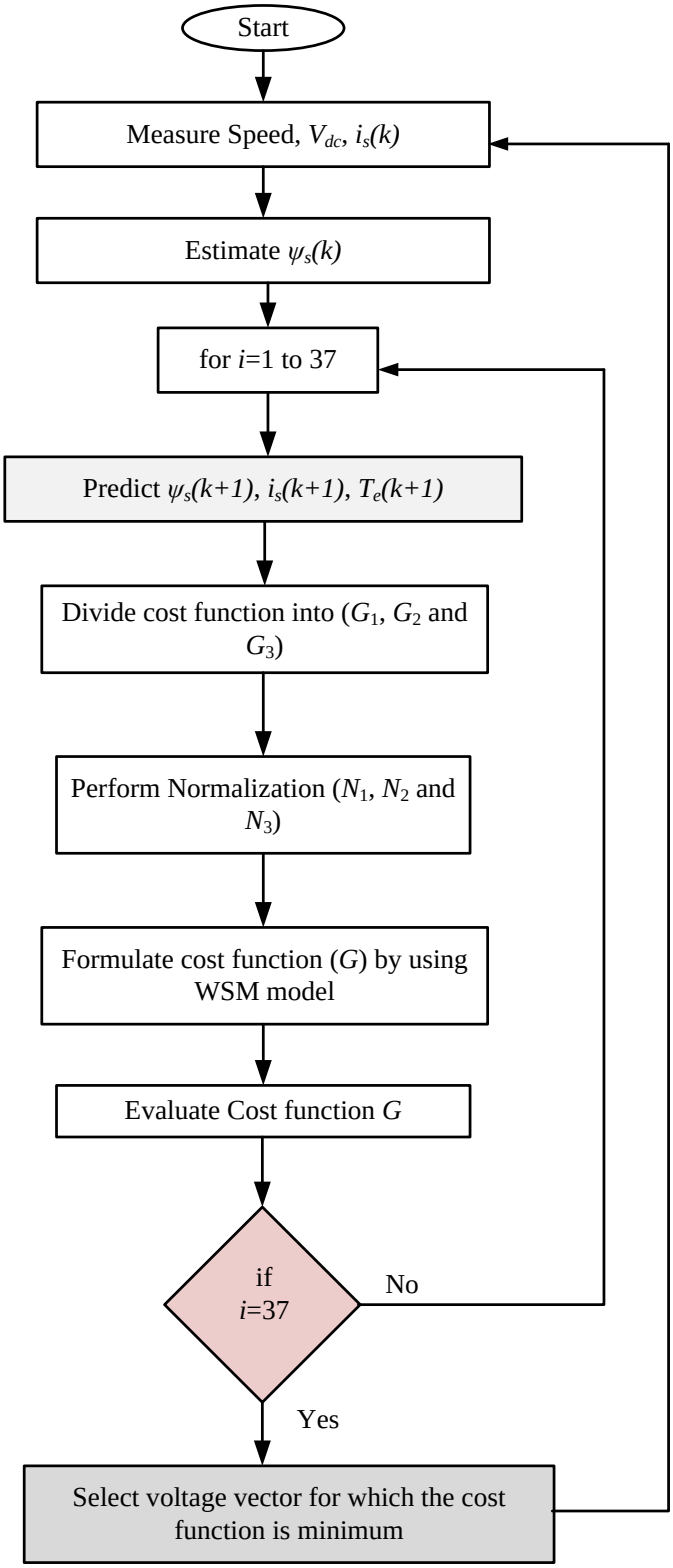

Figure 5.3 Flowchart of proposed NWSM model based PTC of OEWIM drive with four-level inversion

In classical PTC, single cost function is used, whereas in the proposed PTC multi-objective cost function is developed by separating it into individual cost functions. The control objectives used in the proposed PTC algorithm are given by (5.10) - (5.12).

$$\left[G_1\right]_m = \left|\left(T_{ref} - T_e\left(k+1\right)_m\right)\right| \tag{5.10}$$

$$\left[G_2\right]_m = \frac{T_{nom}}{\psi_{nom}}\left|\left(\psi_{sref} - \psi_s\left(k+1\right)_m\right)\right| \tag{5.11}$$

$$\text{and } \left[G_3\right]_m = \frac{1}{V_{dc}}\left|\left(v_s\left(k\right)_m - v_s\left(k+1\right)_m\right)\right| \tag{5.12}$$

Four-level inverter fed OEWIM drive has 37 possible space vector locations (switching states). The decision matrix is developed to reduce torque ripple (5.10), flux ripple (5.11) and switching frequency reduction (5.12). The decision matrix is shown below. The switching frequency of an inverter depends on the control effort involved to optimize the cost function. By reducing the control effort, it is possible to reduce the switching frequency. In general, the control effort is associated with voltage variations, current variations or switching losses.

In this chapter, the switching frequency of dual inverter configuration is controlled by reducing the number of voltage transitions.

$$\left[D\right]_m = \left[G_1 \quad G_2 \quad G_3\right]_m \tag{5.13}$$

Normalized decision matrices are obtained from (5.13) and it is given by

$$\left[N_1\right]_m = \frac{\left[G_1\right]_m - min\left[D\right]_m}{max\left[D\right]_m - min\left[D\right]_m} \tag{5.14}$$

$$\left[N_2\right]_m = \frac{\left[G_2\right]_m - min\left[D\right]_m}{max\left[D\right]_m - min\left[D\right]_m} \tag{5.15}$$

$$\left[N_3\right]_m = \frac{\left[G_3\right]_m - min\left[D\right]_m}{max\left[D\right]_m - min\left[D\right]_m} \tag{5.16}$$

By normalizing the control objectives (5.10) to (5.12), their range is converted to exist in the range of 0 to1.

With the help of normalized decision matrix, the cost function can be formulated by using weighted sum model (WSM) and is given by

$$G = w_1\left[N_1\right]_m + w_2\left[N_2\right]_m + w_3\left[N_3\right]_m = \sum_{i=1}^{3} w_i\left(N_i\right)_m \tag{5.17}$$

where, $w_1=w_2=w_3= 1/3$. The weighting factors used in proposed PTC are fixed quantities; hence the tedious tuning process is eliminated. Evaluation of cost function by using normalized weighted sum model for one sample period is shown in Table 5.1. In Table 5.1, v_s is voltage space vector, G_1 is torque control law, G_2 is flux control law and G_3 is control law to reduce switching frequency.

Table 5.1 Optimal voltage vector selection in one sample period from online simulation

Voltage Space Vector (v_s)	**G_1**	**G_2**	**G_3**	**N_1**	**N_2**	**N_3**	**G**
v_0	3.4256	0.4774	0.5879	0.4485	0.0625	0.077	0.196
v_1	4.3741	0.1618	0.7698	0.5727	0.0212	0.1008	0.231567
v_2	2.9703	0.3067	0.5879	0.3889	0.0402	0.077	0.1687
v_3	2.0218	0.3266	0.3849	0.2647	0.0428	0.0504	0.1193
v_4	2.4771	1.1128	0.444	0.3243	0.1457	0.0582	0.176067
v_5	3.8809	1.2605	0.6667	0.5082	0.1651	0.0873	0.253533
v_6	4.8294	0.6192	0.8012	0.6324	0.0811	0.1049	0.2728
v_7	5.3229	0.8048	0.9686	0.6969	0.1054	0.1268	0.3097
v_8	3.9188	0.9439	0.8012	0.5131	0.1236	0.1049	0.2472
v_9	2.5149	1.092	0.6667	0.3293	0.143	0.0873	0.186533
v_{10}	1.5664	0.4606	0.4444	0.2051	0.0603	0.0582	0.107867
v_{11}	**0.6179**	**0.1668**	**0.2222**	**0.0809**	**0.0218**	**0.0291**	**0.043933**
v_{12}	1.0732	0.956	0.2222	0.1405	0.1252	0.0291	0.098267
v_{13}	1.5286	1.7442	0.3849	0.2002	0.2284	0.0504	0.159667
v_{14}	2.9324	1.8979	0.5879	0.384	0.2485	0.077	0.2365
v_{15}	4.3363	2.0425	0.8012	0.5678	0.2674	0.1049	0.313367
v_{16}	5.2848	1.3991	0.8889	0.692	0.1832	0.1164	0.330533
v_{17}	6.2333	0.752	1.0184	0.8162	0.0985	0.1333	0.349333
v_{18}	5.7779	0.0258	0.9686	0.7566	0.0034	0.1268	0.2956
v_{19}	6.2711	1.4515	1.1759	0.8211	0.1901	0.154	0.3884
v_{20}	4.8673	1.5849	1.0184	0.6373	0.2075	0.1333	0.326033
v_{21}	3.4634	1.7272	0.8889	0.4535	0.2262	0.1164	0.265367
v_{22}	2.0596	1.8782	0.8012	0.2697	0.2459	0.1049	0.206833
v_{23}	1.1111	1.2488	0.5879	0.1455	0.1635	0.077	0.128667
v_{24}	0.1626	0.6233	0.3849	0.0213	0.0816	0.0504	0.0511
v_{25}	0.7859	0.0019	0.2222	0.1029	0.0003	0.0291	0.0441
v_{26}	0.3306	0.7901	0	0.0433	0.1035	0	0.048933
v_{27}	0.1247	1.5813	0.2222	0.0163	0.2071	0.0291	0.084167
v_{28}	0.5801	2.3715	0.4444	0.076	0.3105	0.0582	0.148233
v_{29}	1.9839	2.5314	0.5879	0.2598	0.3315	0.077	0.222767
v_{30}	3.3877	2.682	0.7698	0.4436	0.3512	0.1008	0.298533
v_{31}	4.7916	2.8233	0.9686	0.6274	0.3697	0.1268	0.374633
v_{32}	5.7401	2.1778	1.0184	0.7516	0.2852	0.1333	0.390033
v_{33}	6.6886	1.5285	1.1111	0.8758	0.2001	0.1455	0.407133
v_{34}	7.6371	0.8755	1.2373	1	0.1146	0.162	0.425533
v_{35}	7.1818	0.1011	1.1759	0.9404	0.0132	0.154	0.3692
v_{36}	6.7265	0.6746	1.1547	0.8808	0.0883	0.1512	0.373433

Table 5.1 is an example of individual cost function evaluated for all 37 possible combinations. Out of these switching combinations, the switching state which provides minimum value of cost function is selected as optimal voltage vector. The selected voltage vector is applied to dual inverter fed OEWIM drive configuration.

The cost function (5.17) uses multi-objective function, so the proposed PTC strategy can reduce ripples in torque, flux and also switching frequency. Number of switching state transitions in a fixed time period is called as average switching frequency. The switching frequency of OEWIM drive can be reduced by the number of voltage vector transitions.

5.4 Simulation and Experimental Results of PTC using NWSM

After implementing dynamic models of VSI and OEWIM, the proposed PTC algorithm is tested by implementing it in MATLAB/SIMULINK. The parameters used to implement the proposed algorithms are given in Table A.1 (Appendix). Figures 5.4 to Figure 5.10 demonstrate simulation and experimental results of classical and proposed PTC algorithms.

The four-level inversion is obtained by operating the two VSIs with unequal DC voltages (2:1 ratio). The two VSI's are operated with the voltages of 360 V and 180 V. Hence, the effective DC voltage is 540 V. The proposed PTC algorithm was tested at various operating conditions. The results of classical and proposed PTC algorithms are described for 100 rad/s, 200 rad/s and 250 rad/s. The simulation and experimental results are shown for forward and reverse motoring modes with no-load and load conditions.

Figure 5.4 describes speed, torque and flux of OEWIM drive for step changes at speeds of 100 rad/s, 200 rad/s and 250 rad/s in forward motoring mode. Figures 5.4(a) and 5.4(b) present simulated and experimental results of classical PTC for step changes in speed (forward motoring). Figures 5.4(c) and 5.4(d) present simulated and experimental results of the proposed PTC for step change in speed (forward motoring). From Figure 5.4 it is evident that the proposed PTC reduces torque and flux ripples.

Figure 5.5 describes speed, torque and flux of OEWIM drive for step changes in speed of -100 rad/s, -200 rad/s and -250 rad/s in reverse motoring mode. Figures 5.5(a) and 5.5(b) present simulated and experimental results of classical PTC for step changes in speed (reverse

motoring). Figures 5.5(c) and 5.5(d) present simulated and experimental results of the proposed PTC for step change in speed (reverse motoring). From Figure 5.5 it is evident that the proposed PTC gives low torque and flux ripples.

Figure 5.6 describes speed, torque and flux of OEWIM drive when a step change in speed applied from 250 rad/s to -250 rad/s (forward motoring to reverse motoring). Figures 5.6(a) and 5.6(b) present simulated and experimental results of classical PTC for step change in speed from forward motoring to reverse motoring. Figures 5.6(c) and 5.6(d) present simulated and experimental results of the proposed PTC for step change in speed from forward motoring to reverse motoring. From Figure 5.6 it is evident that the proposed PTC gives all the features of classical PTC. In addition it reduces some amount of torque and flux ripples. Figure 5.7 demonstrates speed, current and voltage of OEWIM drive at a steady speed of 250 rad/s.

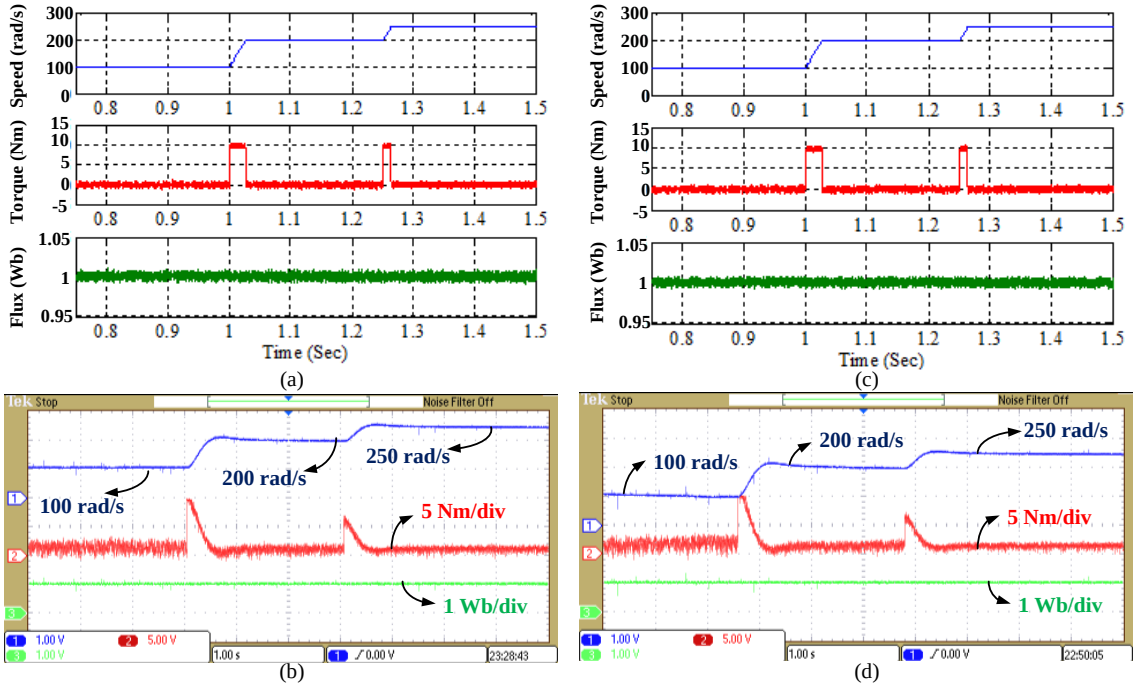

Figure 5.4 Forward motoring of dual inverter fed OEWIM: (a) Simulated response of classical PTC. (b) Experimental response of classical PTC. (c) Simulated response of proposed PTC and (d) Experimental response of proposed PTC

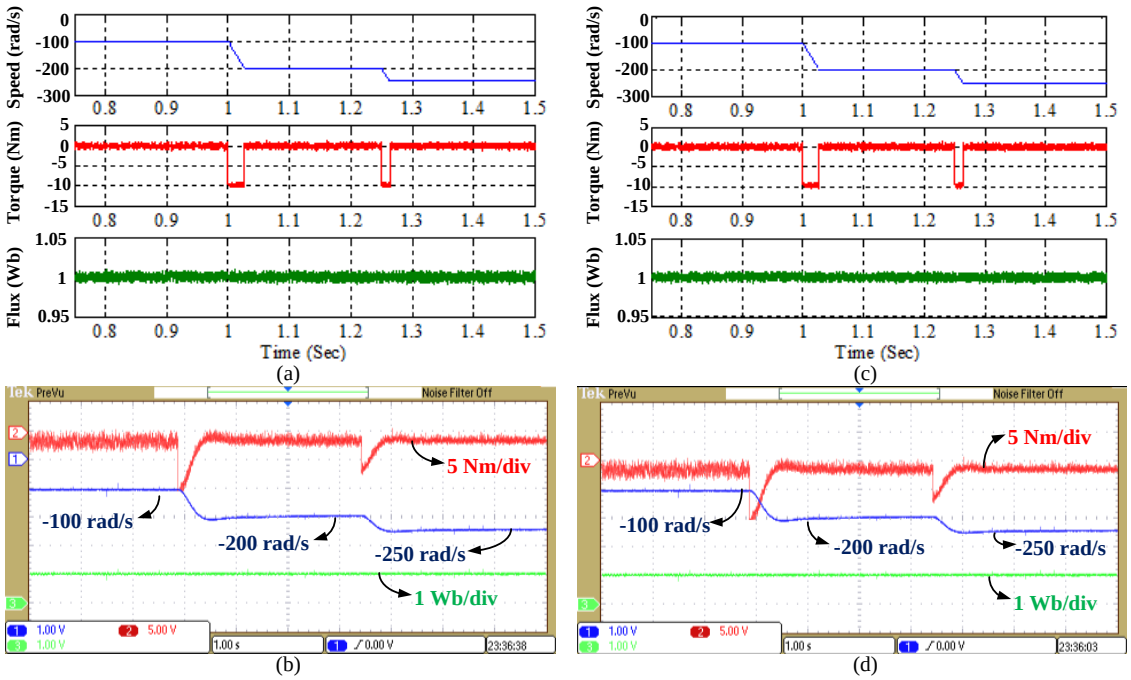

Figure 5.5 Reverse motoring of dual inverter fed OEWIM: (a) Simulated response of classical PTC. (b) Experimental response of classical PTC. (c) Simulated response of proposed PTC and (d) Experimental response of proposed PTC

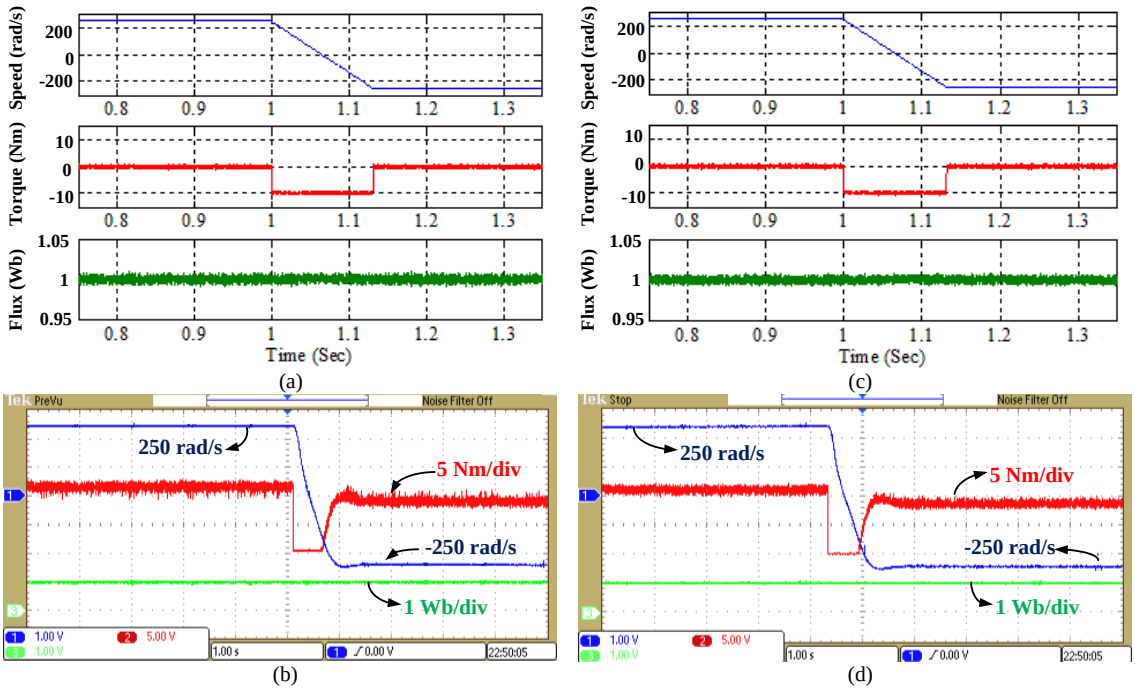

Figure 5.6 Forward and reverse motoring of dual inverter fed OEWIM: (a) Simulated response of classical PTC. (b) Experimental response of classical PTC. (c) Simulated response of proposed PTC and (d) Experimental response of proposed PTC

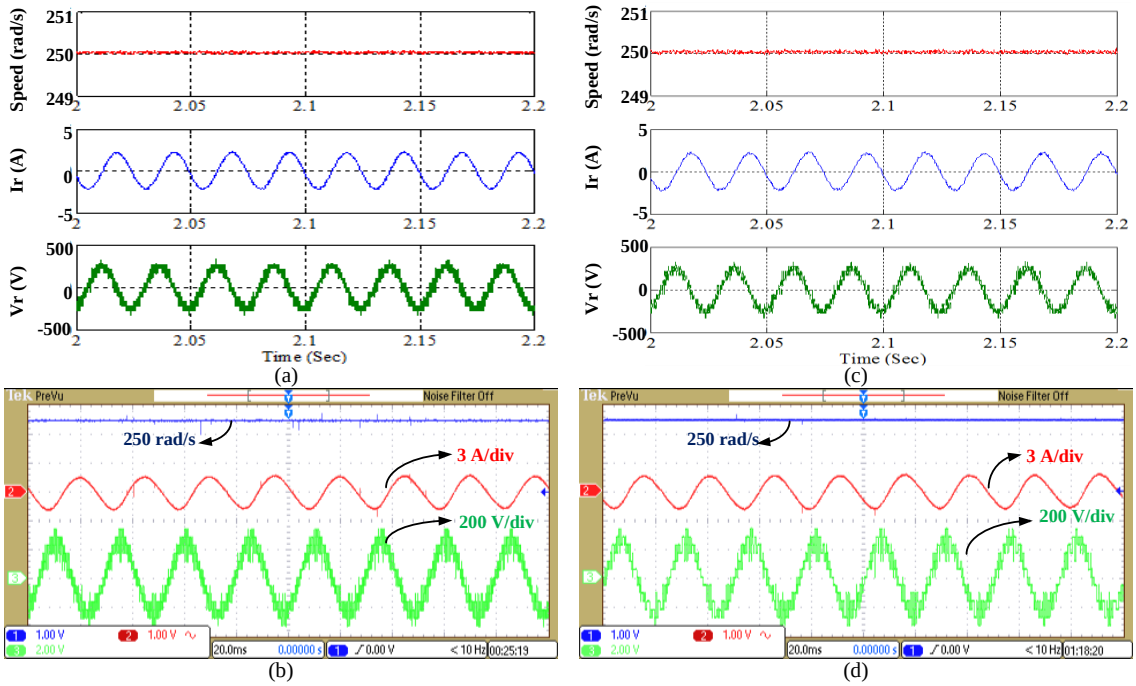

Figure 5.7 Steady-state speed, current and voltage of dual inverter fed OEWIM: (a) Simulated response of classical PTC. (b) Experimental response of classical PTC. (c) Simulated response of proposed PTC and (d) Experimental response of proposed PTC

Figures 5.7(a) and 5.7(b) present simulated and experimental results of classical PTC whereas Figures 5.7(c) and 5.7(d) presents simulated and experimental results of the proposed PTC. From Figure 5.7, it is observed that the proposed PTC can reduce switching frequency.

Figure 5.8 describes speed, torque and r-phase current of OEWIM drive in forward motoring at a steady speed of 200 rad/s and a load torque of 6 Nm. Figures 5.8(a) and 5.8(b) present simulated and experimental results of classical PTC for forward motoring. Figures 5.8(c) and 5.8(d) represent simulated and experimental results of the proposed PTC in forward motoring. Figure 5.9 describes speed, r-phase pulse and selection of optimum voltage vector at a steady-speed of 200 rad/s. Figures 5.9(a) and 5.9(b) presents simulated and experimental results of classical PTC, whereas 5.9(c) and 5.9(d) represents simulated and experimental results of proposed PTC. From Figure 5.9 it is clear that the proposed PTC operates with lower switching frequencies. Switching frequency (Hz) involved in classical and proposed PTC algorithms are shown in Figure 5.10. From Figure 5.7 and 5.9 it is notified that the proposed PTC operates at low switching frequencies. Hence, the switching frequency is reduced. Table 5.2 represents experimental steady-state torque and flux ripple of OEWIM

drive. Torque and flux ripples are obtained by considering the sum of the difference between the measured and reference over 125000 samples.

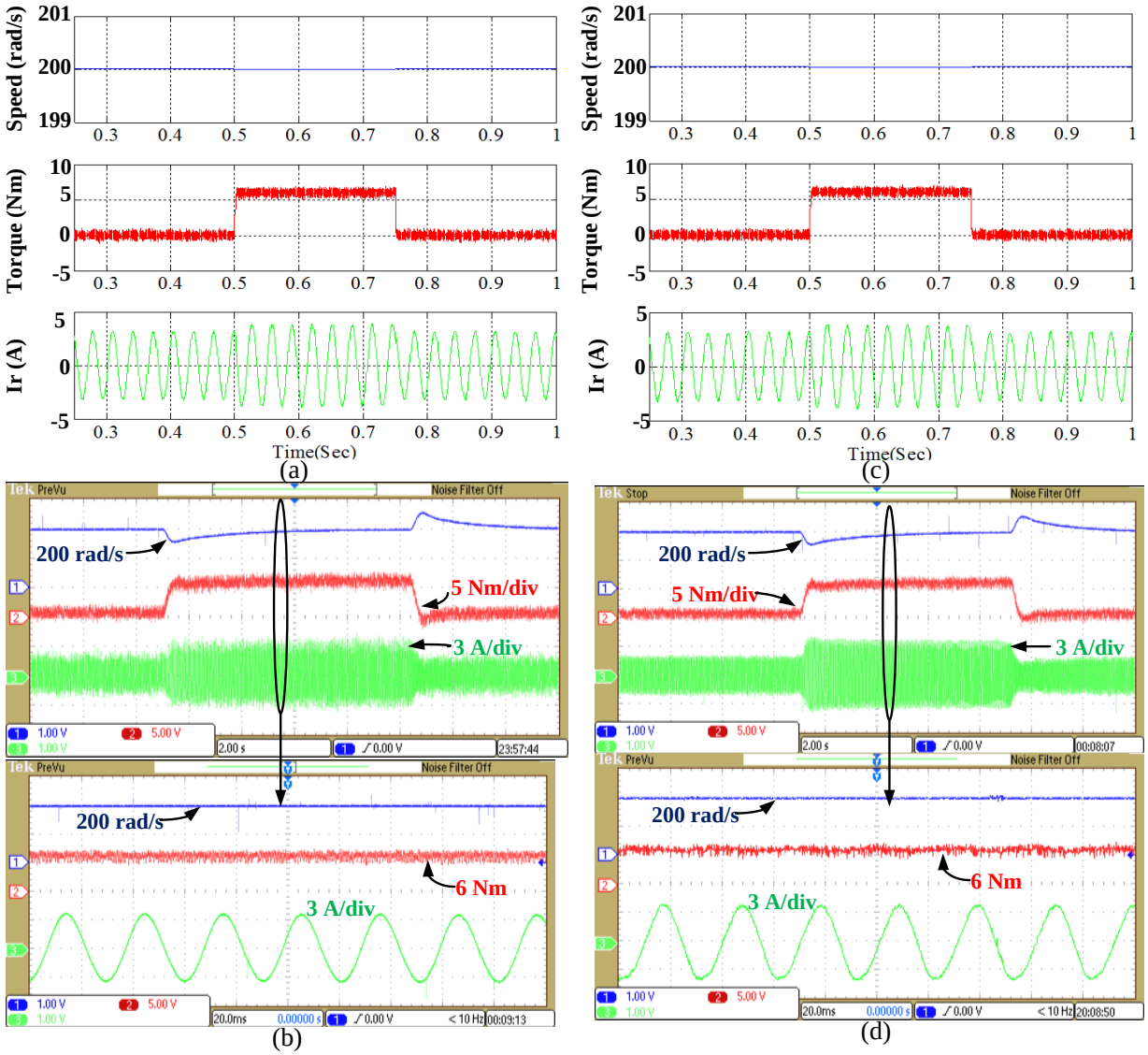

Figure 5.8 Forward motoring of OEWIM for a load torque of 6 Nm at 100 rad/s: (a) Simulated response of classical PTC. (b) Experimental response of classical PTC (top-dynamic variation of load, bottom-zoomed portion). (c) Simulated response of proposed PTC and (d) Experimental response of proposed PTC (top-dynamic variation of load, bottom-zoomed portion).

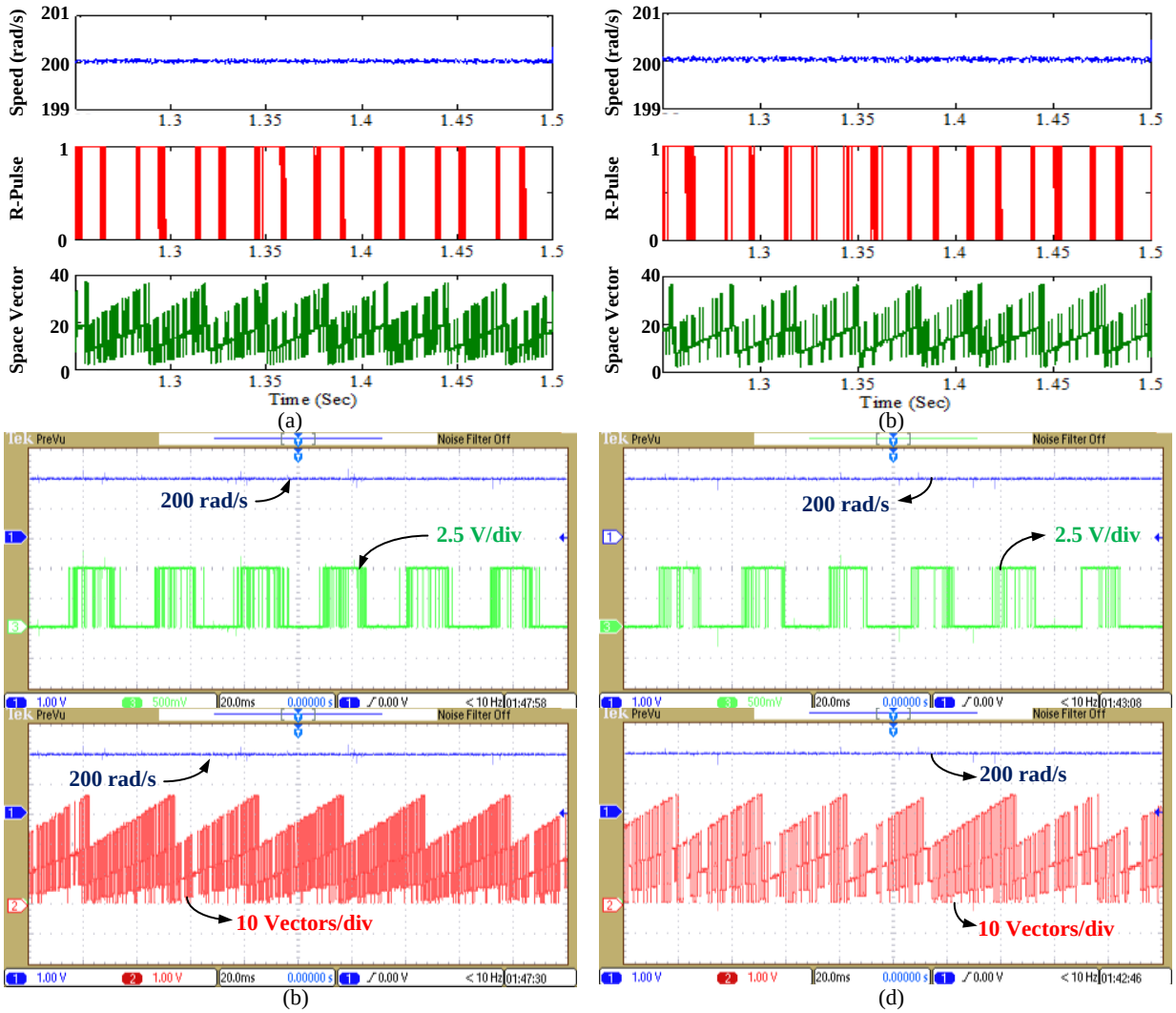

Figure 5.9 Steady-state speed, switching pulse of r-phase and selected voltage vector of four-level inverter fed OEWIM drive: (a) Simulated response of classical PTC. (b) Experimental response of classical PTC. (c) Simulated response of proposed PTC and (d) Experimental response of proposed PTC.

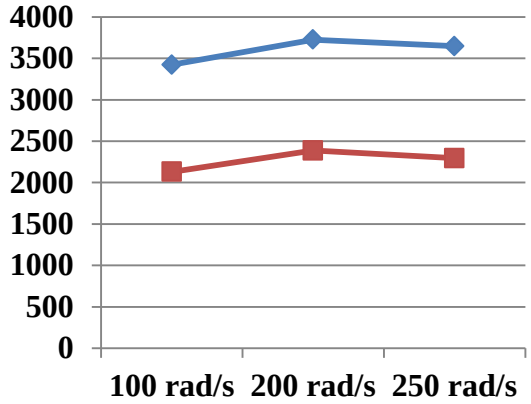

Figure 5.10 Switching frequency involved in classical (blue) and proposed PTC (red).

Table 5.2 Steady-state torque, flux ripple and switching frequency of OEWIM drive for various speeds of operation

Control Scheme	Speed (rad/s)	Torque ripple		Flux Ripple		Switching Frequency (Hz)
		Nm	%	Wb	%	
Classical PTC	100 rad/s	2.8	11.43	0.025	2.5	3423
Proposed PTC		2.5	10.21	0.022	2.2	2131
Classical PTC	200 rad/s	2.2	8.98	0.016	1.6	3727
Proposed PTC		2.0	8.16	0.015	1.5	2388
Classical PTC	250 rad/s	1.4	5.71	0.012	1.2	3648
Proposed PTC		1.25	5.10	0.01	1	2285

5.5 Weighting Factor Eliminated PTC of OEWIM Drive

The block diagram of proposed weighting factor elimination based PTC strategy to an OEWIM drive is shown in Figure 5.11. The algorithm used to implement this strategy is as follows:

Step 1: Estimate flux at k^{th} instant for all 37 voltage space vector combinations of dual inverter configuration by using current measurement and realization of voltage space vectors.

Step 2: Predict the flux at (k+1) instant by using (5.4) for 37 voltage space vector locations.

Step 3: Formulate cost function g_1 by using $\psi_s(k+1)$, ψ_{sref}.

Step 4: Evaluate the cost function g_1 and arrange the first 20 minimum values of cost function with their switching state combinations.

$$g_1 = \left|\psi_{sref} - \psi_s(k+1)\right| \tag{5.18}$$

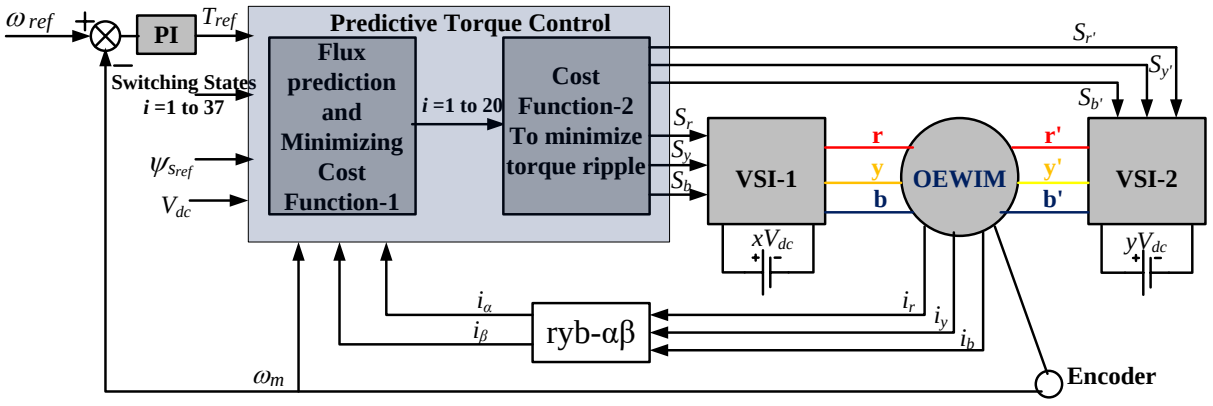

Figure 5.11 Block diagram of proposed weighting factor eliminated PTC strategy to an OEWIM drive

Step 5: Store these first 20 optimum voltage space vector combinations and $\psi_s(k+1)$ for those switching combinations.

Step 6: Predict current at $(k+1)$ instant by using (5.6) for the switching combinations obtained in step 4.

Step 7: By using predicted current and predicted flux obtained in Step 5 and Step 6 and predict torque at $(k+1)$ instant by (5.7).

Step 8: Formulate the cost function g_2, with the help of $T(k+1)$ and T_{ref}.

$$g_2 = \left| T_{ref} - T(k+1) \right| \tag{5.19}$$

Step 9: Minimize the cost function g_2 and the voltage vector which gives less torque ripple is chosen as optimum voltage vector and applied in the sequential control cycle.

The proposed algorithm has several advantages, when compared with classical PTC these are as follows:

(i) The cost function is divided into g_1 and g_2, therefore it eliminates weighting factors, and hence the effect of weighting factors is eliminated.

(ii) Cost function g_1, gives the voltage vectors which produce minimum flux ripple and the cost function g_2 delivers an optimal voltage vector which gives minimum torque ripple, therefore the obtained voltage vector can reduce flux ripple as well as torque ripple.

(iii) The cost function g_1 is evaluated for 37 combinations, whereas g_2 is evaluated and optimized only for 20 switching combinations. Therefore, the computational burden on controller reduces, since the prediction of flux is easy whereas the prediction of torque involves more number of steps.

(iv) In step 4, on arranging the ascending order of voltage vectors which gives minimum flux ripple provides another advantage i.e, the voltage vectors near to another gives minimum flux ripples, thereby the number of switching transitions between one voltage space vector to other voltage space vector is less, therefore switching frequency gets reduces. It does not involve additional terms into cost function to reduce switching frequency.

(v) As switching frequency reduces the common-mode voltage also gets decreases.

Figure 5.12 demonstrates the effect of voltage space vectors on flux ripple. The dark portioned voltage vectors shown in Figure 5.12 give minimum flux ripple, if the flux space

vector is in sector-1. Another advantage of this method is, it does not need sector information, whereas the recent PTC strategies [74] requires sector information therefore the complexity gets increases.

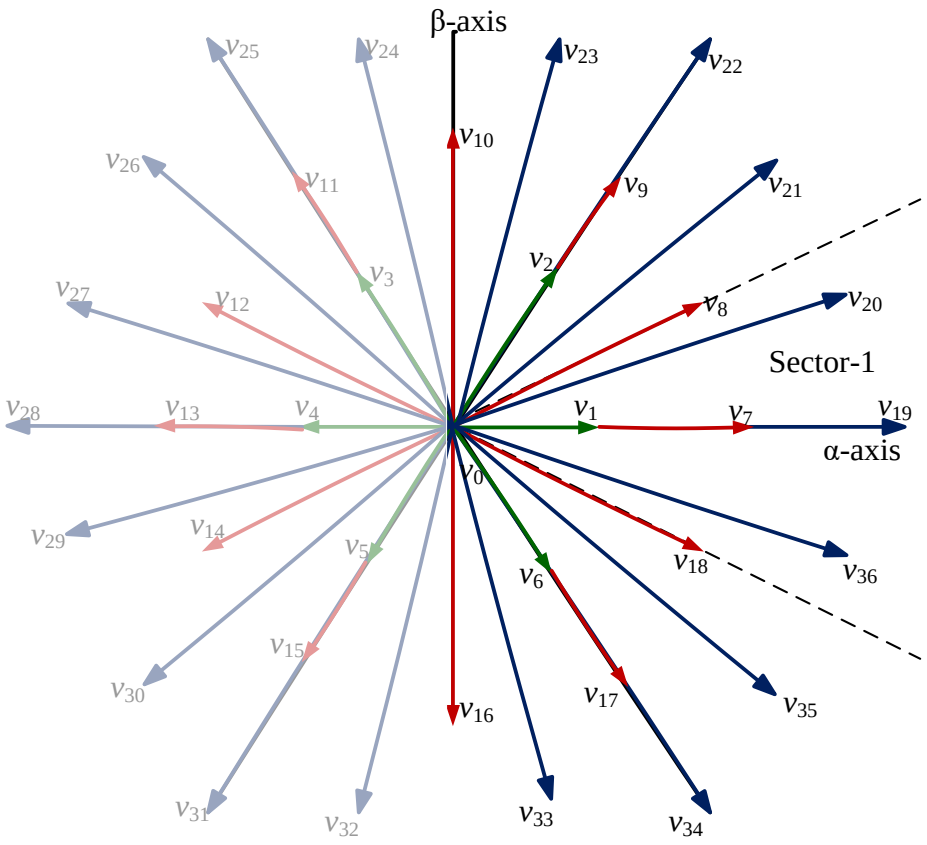

Figure 5.12 Voltage space vectors used to increase or decrease flux ripple by assuming flux space vector in sector1

Figure 5.13 represents flow chart of proposed PTC strategy. To develop the proposed PTC strategy, g_1 is used to minimize flux error whereas g_2 is used to minimize torque error. If the cost function g_1 is used to minimize the torque error, then g_1 should be evaluated for 37 space vector locations, out of these 37 space vectors to reduce torque ripple there exist 22 voltage vectors. Then g_2 should be evaluated for the 22 optimum switching combinations obtained from the minimization of g_1. The torque error based PTC strategy is shown in [74], as per this article if torque ripple is considered in function g_1 then it increases computational complexity and minimization of cost function g_2 has to be performed for 22 space vector locations rather than 20 space vector locations.

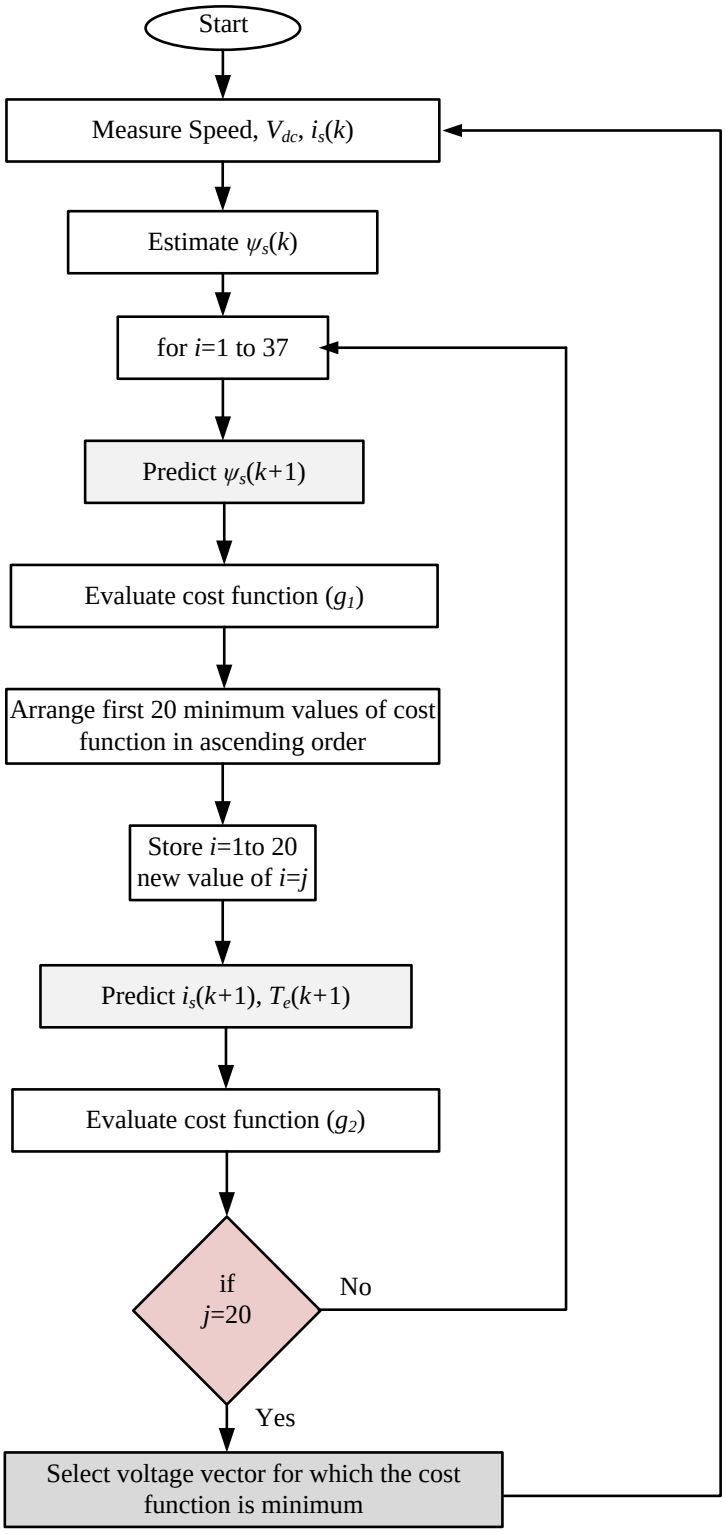

Figure 5.13 Flow chart of proposed weighting factor eliminated PTC strategy

5.6 Results and Discussions of Weighting Factor Eliminated PTC Strategy

In order to verify the effectiveness of developed PTC strategy, simulation and experimental studies are carried on OEWIM drive. After implementing the proposed PTC strategy, the obtained experimental results are compared with classical PTC strategy. The simulated response of OEWIM drive with classical and proposed PTC strategy is shown in Figure 5.14. Figure 5.15 demonstrates torque and flux of OEWIM drive at a steady speed of 150 rad/s and 200 rad/s. Figure 5.16 presents phase voltage, phase currents and switching transitions of OEWIM drive at a speed of 250 rad/s. Figure 5.17 demonstrates CMV of OEWIM drive at a speed of 250 rad/s. To verify the dynamic response of proposed PTC, the OEWIM drive is subjected to a sudden load torque and it is shown in Figure 5.18. Figure 5.14(a) represents simulated response of classical PTC whereas Figure 5.14(b) represents proposed PTC. Figure 5.14 shows speed, torque, flux, r-phase current, r-phase voltage and CMV of OEWIM drive for forward motoring to reverse motoring. Figure 5.14 is to describe the dynamic variation of speed from forward motoring (200 rad/s) to reverse motoring (-200 rad/s). From Figure 5.14, it is evident that torque ripple of proposed PTC is less. From Figure 5.14(a) and 5.14(b) it is also observable that the proposed PTC provides all characteristics as that of classical PTC in addition it gives less switching frequency and CMV.

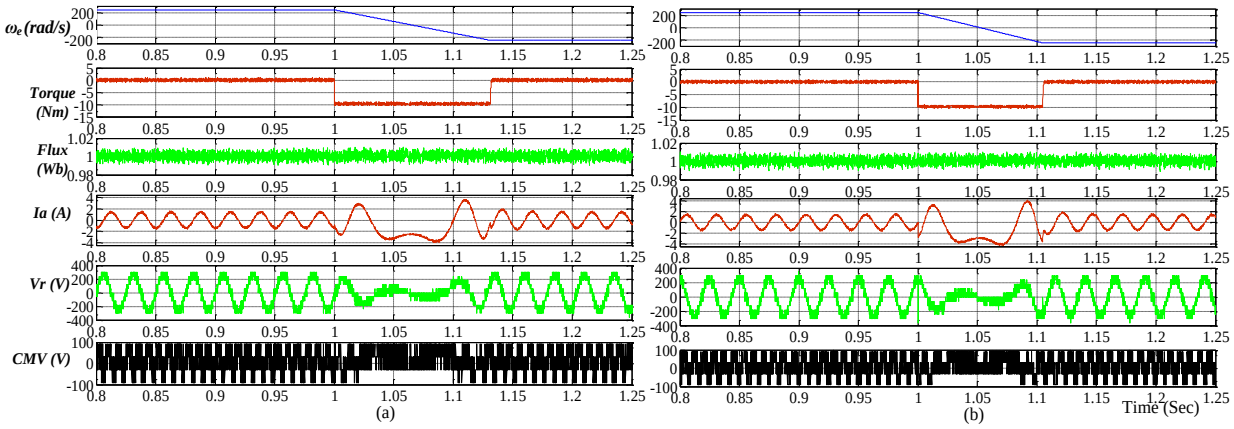

Figure 5.14 Simulated response of OEWIM drive: (a) Classical PTC and (b) Proposed PTC

The experimental studies are performed by implementing with dSPACE-1104 controller. Speed, DC-link voltage and phase currents are sensed with transducers and these are fed back to control algorithm by using analog to digital converters of dSPACE. From the

control algorithm, switching pulses are obtained and these are provided to inverter with the help of digital I/O pins. The experimental studies are performed for various speeds and different loading conditions, in the interest of brevity the response of OEWIM drive is shown for 150 rad/s, 200 rad/s and 250 rad/s during loaded and no-load conditions. From the experimental results also the proposed PTC algorithm provides all the features of classical PTC.

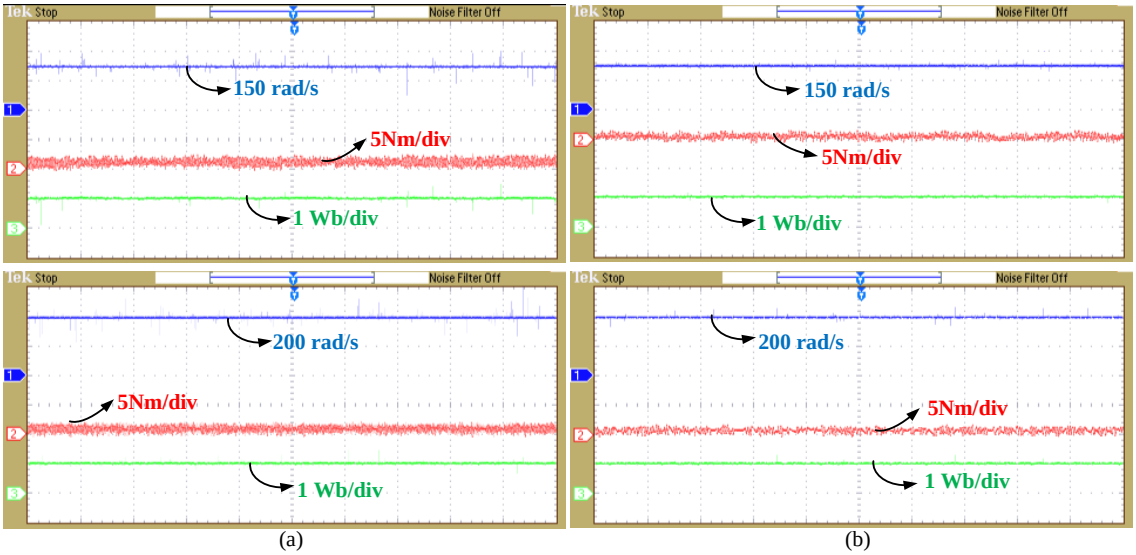

Figure 5.15 Experimental steady-state torque and flux ripple of OEWIM drive: (a) Classical PTC and (b) Proposed weighting factor eliminated PTC.

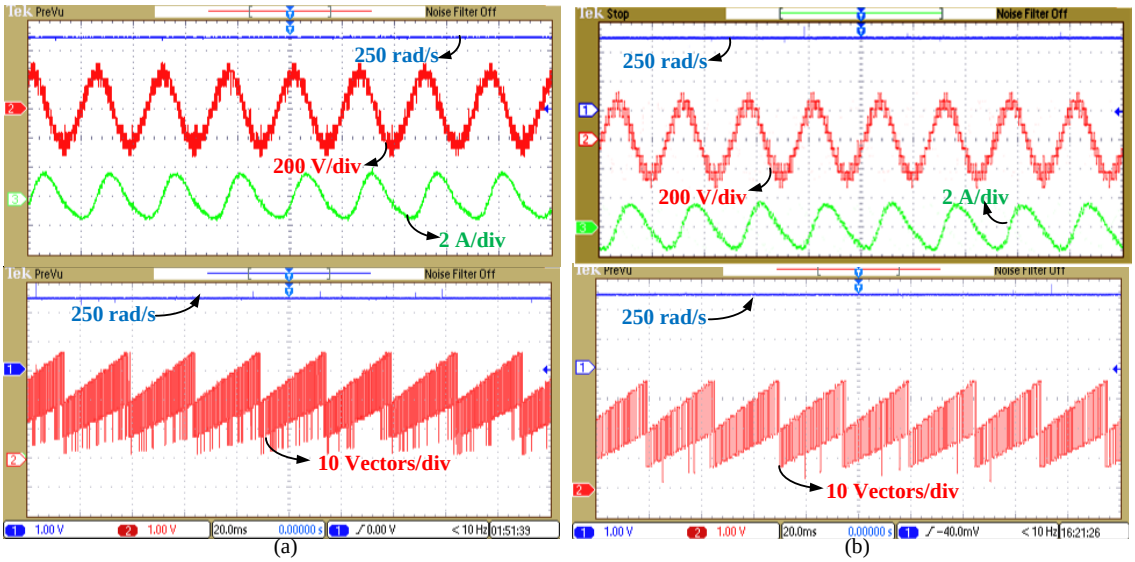

Figure 5.16 Experimental response of phase-voltage, phase-current and space vector transitions of OEWIM drive at a speed of 250 rad/s: (a) Classical PTC and (b) Proposed weighting factor eliminated PTC.

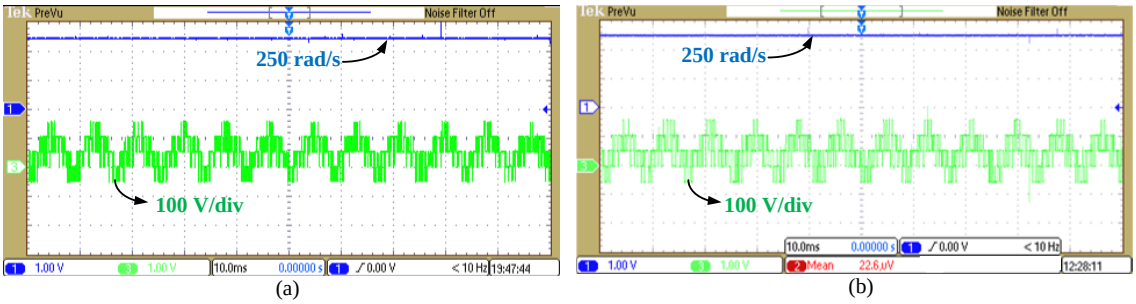

Figure 5.17 CMV of OEWIM drive at a steady speed of 250 rad/s: (a) Classical PTC and (b) Proposed PTC.

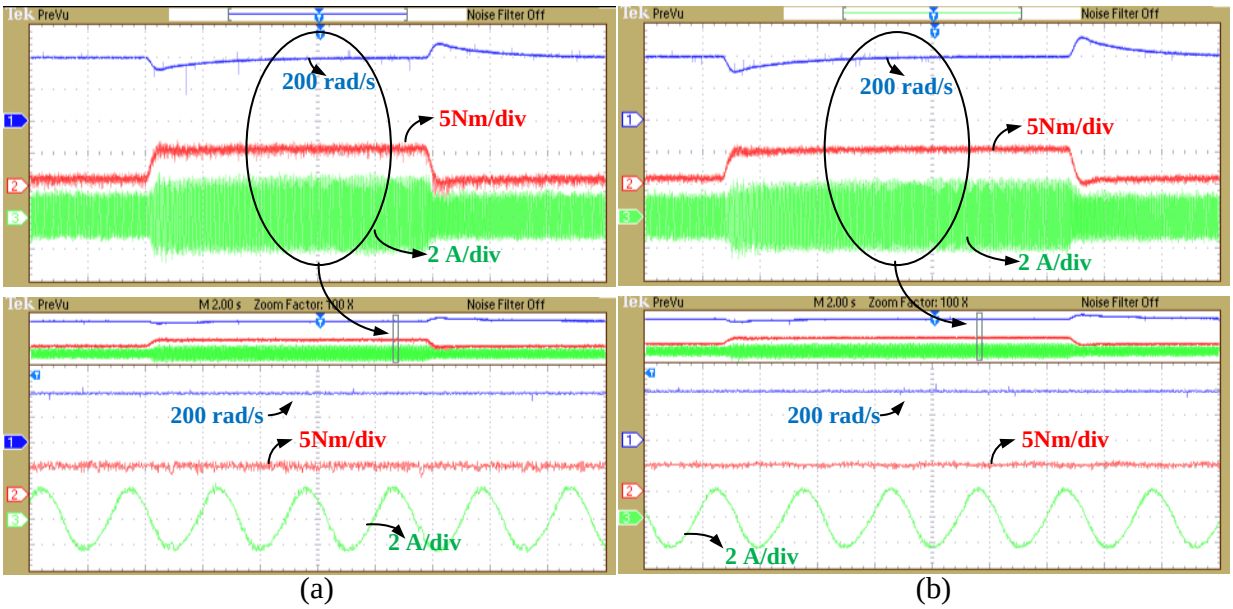

Figure 5.18 Phase current of OEWIM drive at a load torque of 6 Nm and steady speed of 250 rad/s: (a) Classical PTC and (b) Proposed weighting factor eliminated PTC.

From Figure 5.15(a) and 5.15(b), it is obvious that the proposed weighting factor eliminated PTC gives lesser ripples in torque and flux. Figure 5.16(a) presents phase voltage, phase current and voltage space vector transitions during no-load condition. From Figure 5.16(a) and 5.16(b) the proposed PTC operates with less switching frequency as compared to classical PTC. The switching frequency of classical PTC is 3.23 kHz, whereas proposed PTC operates with 2.87 kHz at 250 rad/s, hence from Figure 5.16 it is evident that proposed PTC operates with low switching frequencies. The CMV in proposed PTC is less when compared to classical PTC shown in Figure 5.17(a). CMV obtained in classical PTC is 84.2 V (RMS) and CMV with proposed PTC is 75.4 V (RMS) at 250 rad/s. Therefore proposed PTC gives less CMV. In Figure 5.18, dynamic load torque (top figure) is applied and the zoomed portion represents phase current and load torque at 200 rad/s (bottom figure). From Figure 5.18, it is

clearly observed that the proposed PTC gives less torque ripples and less current distortions. Experimental studies are performed for various speeds of operation, for simplicity only some of the results are presented.

Table 5.3, represents steady-state numerical values of peak to peak torque ripple and flux ripple. Computation of percentage torque and flux ripples is given in Appendix-B, (B.3) and (B.4). The proposed PTC is compared with classical PTC and recent PTC [74] form Table 5.3, it is identified that the proposed gives better performance. After implementing proposed PTC strategy and recent PTC strategies [74], it is evident that the proposed PTC is simple and easy. The complexities of [74] are: estimation of flux space phasor angles of both stator and rotor, identification of flux space phasor position, sector information of flux space phasor and an additional PI controller. The above problems are addressed by developed enhanced weighting factor eliminated PTC strategy.

Table 5.3 Quantified values of peak to peak steady-state torque and flux ripple

Speed (rad/s)	**Classical PTC**				**PTC [74]**				**Proposed PTC**			
	Torque ripple		**Flux ripple**		**Torque ripple**		**Flux ripple**		**Torque Ripple**		**Flux ripple**	
	Nm	**%**	**Wb**	**%**	**Nm**	**%**	**Wb**	**%**	**Nm**	**%**	**Wb**	**%**
100	3.65	14.91	0.035	3.5	3.45	14.09	0.033	3.3	2.82	11.51	0.028	2.8
200	3.24	13.23	0.024	2.4	2.86	11.68	0.023	2.3	2.32	9.47	0.017	1.7
250	2.58	10.53	0.016	1.6	2.35	9.59	0.016	1.6	1.86	7.59	0.013	1.3

5.7 Comparison of proposed DTC and PTC strategies

This thesis emphasizes application of various DTC and PTC strategies for the OEWIM drive. This section, describes various performance indices of OEWIM drive for the proposed DTC and PTC strategies. The performance indices such as average torque ripple, average flux ripple, rms value of CMV, average switching frequency, computational burden on the controller and response time of the OEWIM drive for a load torque has been considered.

Table 5.4, presents average torque ripple and flux ripple of OEWIM drive with two-level and multi-level inversion fed DTC and PTC strategies. The computation of % average torque and flux ripples are shown in Appendix-B, (B.1) and (B.2). Table 5.5, exhibits average torque and flux ripples of OEWIM drive for the classical and proposed PTC strategies. Table 5.6 and 5.7 represents the switching frequency of various DTC and PTC strategies. Table 5.8 and 5.9 presents the RMS value of CMV of various DTC and PTC strategies. Table 5.10 shows

the computational burden and response time of the various DTC and PTC strategies for the OEWIM drive.

Table 5.4 Steady-state average torque, flux ripple of OEWIM drive for various inversion schemes (in percentage)

Control Algorithm	Speed (rad/s)	Two-level Inversion		Three-level Inversion		Four-level Inversion	
		% Torque ripple	% Flux ripple	% Torque ripple	% Flux ripple	% Torque ripple	% Flux ripple
DTC	100	14.29	5.7	10.21	4.5	9.59	4.9
PTC		12.25	2.9	10.08	2.65	8.78	2.2
DTC	200	13.27	4.2	9.47	3.8	8.98	3.2
PTC		10.01	1.74	8.78	1.6	7.55	1.45
DTC	250	12.25	3.6	8.98	3.6	8.16	2.9
PTC		7.96	1.3	6.2	1.12	5.51	0.92

Table 5.5 Steady-state average torque, flux ripple of OEWIM drive for various PTC schemes (in percentage)

Speed (rad/s)	Classical PTC		NWSM PTC		WFE PTC	
	% Torque ripple	% Flux ripple	% Torque ripple	% Flux ripple	% Torque ripple	% Flux ripple
100	11.43	2.5	10.21	2.2	9.15	2.12
200	8.98	1.6	8.16	1.5	7.25	1.35
250	5.71	1.2	5.1	1	5.1	1

Table 5.6 RMS values of CMV for various multi-level inversion schemes

Speed (rad/s)	Two-level DTC	Three-level DTC	Four-level DTC	Two-level PTC	Three-Level PTC	Four-Level PTC
	CMV (V)	CMV (V)	CMV (V)	CMV (V)	CMV (V)	CMV (V)
100 rad/s	155.62	102.85	78.35	169.65	112.27	91.26
200 rad/s	141.82	97.25	72.46	158.5	102.85	86.54
250 rad/s	131	89.24	65.48	144.8	79.25	84.2

Table 5.7 RMS values of CMV for various multi-level inversion schemes

Speed (rad/s)	Classical PTC	NWSM PTC	WFE PTC
	CMV (V)	CMV (V)	CMV (V)
100 rad/s	91.26	87.25	88.28
200 rad/s	86.54	80.34	82.45
250 rad/s	84.2	71.45	75.4

Table 5.8 Average switching frequency of dual inverter fed OEWIM drive for various multi-level inversion schemes

Speed (rad/s)	Two-level DTC	Three-level DTC	Four-level DTC	Two-level PTC	Three-Level PTC	Four-Level PTC
	Switching Frequency (Hz)	Switching Frequency (Hz)	Switching Frequency (Hz)	Switching Frequency (Hz)	Switching Frequency (Hz)	Switching Frequency (Hz)
100 rad/s	2396	2418	2561	3028	3395	3684
200 rad/s	2460	2551	2628	3235	3487	3824
250 rad/s	2318	2485	2495	3146	3282	3726

Table 5.9 Average switching frequency of dual inverter fed OEWIM drive for NWSM PTC and WFE PTC

Speed (rad/s)	Classical PTC	NWSM PTC	WFE PTC
	Switching Frequency (Hz)	Switching Frequency (Hz)	Switching Frequency (Hz)
100 rad/s	3423	2131	2712
200 rad/s	3727	2388	2934
250 rad/s	3648	2285	2874

From the proposed DTC and PTC strategies, four-level inversion fed PTC, NWSM PTC and WFE PTC are found to be effective solutions to reduce torque ripple, flux ripples etc. From 5.4 to 5.5, it is evident that the NWSM PTC maintains less torque and flux ripples with low switching frequencies. The proposed WFE PTC needs high switching frequencies, but it maintains less torque ripple and flux ripple compared to NWSM PTC.

Table 5.10 Computational burden and response time of the proposed DTC and PTC strategies for the OEWIM drive

DTC/PTC Strategy	Computational Time	Response Time
2-level DTC	38.6 µs	0.4 s
3-level DTC	42.14 µs	0.38 s
4-level DTC	50.26 µs	0.38 s
2-level PTC	52.5 µs	0.36 s
3-level PTC	59.25 µs	0.36 s
4-level PTC	65.5 µs	0.36 s
NWSM PTC	68.5 µs	0.36 s
WFE PTC	58.4 µs	0.36 s

5.8 Summary

This chapter, provides basic idea to implement classical PTC to an OEWIM drive with all possible space vectors of dual inverter configuration. Improved PTC strategies for an OEWIM drive using normalized WSM PTC and weighting factor eliminated PTC are developed. In classical PTC, selection of weighting factor plays a vital role on the performance of OEWIM drive. This chapter suggests a method to enhance the selection of weighting factors. The switching frequency involved in multi-level inversion fed OEWIM drives is too high. To address this problem, multi-objective cost function is formulated with the help of WSM to reduce switching frequency, torque and flux ripples. Classical PTC can reduce torque and flux ripples with high switching frequencies. The proposed PTC strategies can reduce torque, flux ripples and also enable significant reduction in switching frequency. Simulation and experimental results shows the effectiveness of the proposed PTC algorithm.

Chapter 6

Conclusions and Scope for Future Work

Chapter 6

Conclusions and Scope for Future Work

This thesis investigated the performance of OEWIM drive with DTC and PTC strategies. This thesis addresses the problems involved in the implementation of DTC scheme for multi-level inversion fed induction motor drives. The outcomes of this thesis are summarized in section 6.1.

6.1 Conclusions

This thesis laid emphasis on the implementation of DTC strategies for an OEWIM drive. The advantages offered by OEWIM drive with other multi-level inversion topologies are presented. The configuration of OEWIM does not require complex control strategies and more number of switches. OEWIM configuration can provide four-level output voltage with less number of switches. The other multi-level inversion topologies require more number of switches to deliver four-level output voltage (chapter-3). The proposed DTC and PTC algorithms utilize two two-level inverters for its operation; however this configuration provides four-level output voltage.

The OEWIM drive has been operated with equal and unequal DC-link voltages. In chapter-2 the dual inverter configuration operated with equal DC sources, hence this configuration provides two-level and three-level inversion. The voltage vectors are classified into two categories in order to simplify the look-up tables. The three-level inversion fed DTC of OEWIM utilizes three-level torque hysteresis controller and a two-level flux hysteresis controller similar in classical DTC of induction motor. By using three-level inversion scheme, torque and flux ripples are reduced. The voltage vectors used in three-level inversion will always give minimum CMV, so the proposed three-level inversion fed DTC scheme gives less CMV when compared with classical two-level DTC.

In chapter-3 an effective voltage switching state algorithm is proposed to a direct torque controlled OEWIM drive with four-level inversion. The voltage vectors used in this scheme are divided into three categories based on rotor speed. By dividing the voltage vectors into various

categories, the switching frequency, torque and flux ripples are reduced and also the selection of voltage vector becomes easy. The four-level inversion uses only 37 voltage vectors. These 37 voltage vectors give minimum CMV out of 64 switching combinations. The improvisations of four-level inversion scheme are as follows:

- The effective DTC strategies developed in this study use three-level torque hysteresis and two-level flux hysteresis controllers whereas the other MLI fed DTC strategies use multi-level torque and flux hysteresis controllers [24]-[26], hence the strategies designed in this study are simple.
- MLI fed DTC strategies require complex look-up table, whereas the proposed four-level inversion uses simple look-up tables.
- The voltage vectors are classified accordingly to rotor speed.
- The four-level inverter configuration provides low CMV and fewer ripples in torque and flux when compared with two-level inversion scheme and classical DTC of induction motor.
- Finally simplified DTC strategies are implemented to an OEWIM drive for symmetrical and unsymmetrical configurations.

The limitations observed in chapter-2 and chapter-3 are: necessity of look-up tables, identification of flux space vector location, identification sector of flux space phasor, complex use of trigonometric calculations and the use of hysteresis controllers. In discrete platform, the hysteresis controllers cause higher ripples and variable switching frequency. To abate these limitations model predictive based DTC strategies are implemented in chapter-4 and chapter-5.

Chapter-4 focused on discrete realization of power converter and OEWIM configuration. The discrete modelling of power converter and load is necessary in model predictive control. The discrete models of power circuit and OEWIM are used to estimate flux at k^{th} instant. Flux and currents at k^{th} instant are used to predict the future behaviour of OEWIM drive.

The flux and currents at k^{th} instant are used to estimate flux and torque at $(k+1)$ instant. The obtained torque and flux at $(k+1)$ instant are compared with reference torque and flux with the help of cost function optimization. This thesis proposed modified cost functions to reduce

torque, flux ripples, CMV and also switching frequencies. In chapter-4, the PTC of OEWIM drive with two, three and four-level inversion schemes was introduced with modified cost function. Another limitation of PTC is computational burden on the controller, to reduce the computational burden voltage vectors were categorised into various groups based on rotor speed. The effectiveness of the proposed PTC is demonstrated by testing the OEWIM drive with all possible configurations.

In chapter-5, the PTC of OEWIM was introduced to simplify the selection of weighting factors using normalized weighted sum model. The limitation observed in chapter-4 is the cost function which comprises dissimilar terms; the evaluation of cost function with dissimilar terms needs weighting factor. In real time implementation the tuning of weighting factors is quite cumbersome and there exist 37 active voltage vectors in four-level inversion, so the switching frequency may increase. In order to address the problem of weighting factors and also to reduce switching frequency, a multi-criterion decision making algorithm (normalized WSM) is used. In general the switching frequency control is quite cumbersome. To control switching frequency, the proposed PTC utilizes the changes in voltage space vectors applied to OEWIM drive hence it reduces computational complexity. The proposed normalized WSM based PTC strategy gives the same performance as that of classical PTC with reduced switching frequencies. A novel weighting factor eliminated PTC strategy for an OEWIM drive has been introduced. The developed weighting factor eliminated PTC utilizes two individual cost functions to reduce flux and toque ripples. The cost function used in chapter-5 comprises of torque error control, flux error control and the third term is switching frequency control. In general, the switching frequency control is quite cumbersome. To control switching frequency instead of using switch transitions, the proposed DTC utilizes the changes in voltage space vectors which reduce computational complexity. Finally, simplified DTC and PTC strategies are developed to OEWIM drive.

6.2 Scope for Future Work

Any research never ends without leaving open window for further research, hence the findings from this thesis present rich possibilities:

- The proposed DTC and PTC are applicable for special machines like PMSM (Permanent Magnet Synchronous Machine).
- The Proposed DTC and PTC strategies can be extended for more than four-level inversion by replacing two two-level inverters with three-level inverters.
- The proposed DTC and PTC strategies operate with variable switching frequency; in order to obtain constant switching frequency modulation techniques are unavoidable.
- PTC is highly parameter dependent; the implementation of PTC with parameter insensitive may be taken up for research in future.
- The proposed DTC and PTC strategies utilize encoders and transducers. Sensor-less control with sliding mode control or MRAS (model reference adaptive systems) or EKF or full order observer based DTC/PTC schemes are possibilities for research in future.
- The proposed PTC algorithms use modified cost function. However, in the modified cost function tuning of weighting factors is unavoidable.
- The eliminations of tuning factors by replacing the terms in the cost function is another area of research problem.
- One of the example to replace the cost function is; torque of OEWIM drive is proportional to q-axis current or q-axis flux, whereas flux error is proportional to d-axis flux. The cost function can be replaced with β-axis and α-axis flux terms.

Appendix-A
Experimental Test-Rig

The experimental setup used to verify the proposed DTC and PTC schemes of OEWIM drive are developed using dSPACE DS-1104 and it is presented in detail in this section. The block diagram of the experimental setup for investigating all the proposed schemes is shown in Figure. A.1. This block diagram consists of a 5 HP, 4-pole, 50 Hz, 3-phase OEWIM coupled with a 5 HP, dc generator on one side and an incremental shaft encoder on the other side, IGBT based voltage source inverters, dSPACE DS-1104, two Hall-effect current sensors for measurement of stator currents, one Hall-effect voltage sensor for measurement of dc-link voltage and a front end 3-phase diode rectifier. The outputs of the Hall-effect voltage and current sensors are used to estimate the stator flux and torque. The photograph of experimetal setup is shown in Figure. A.2.

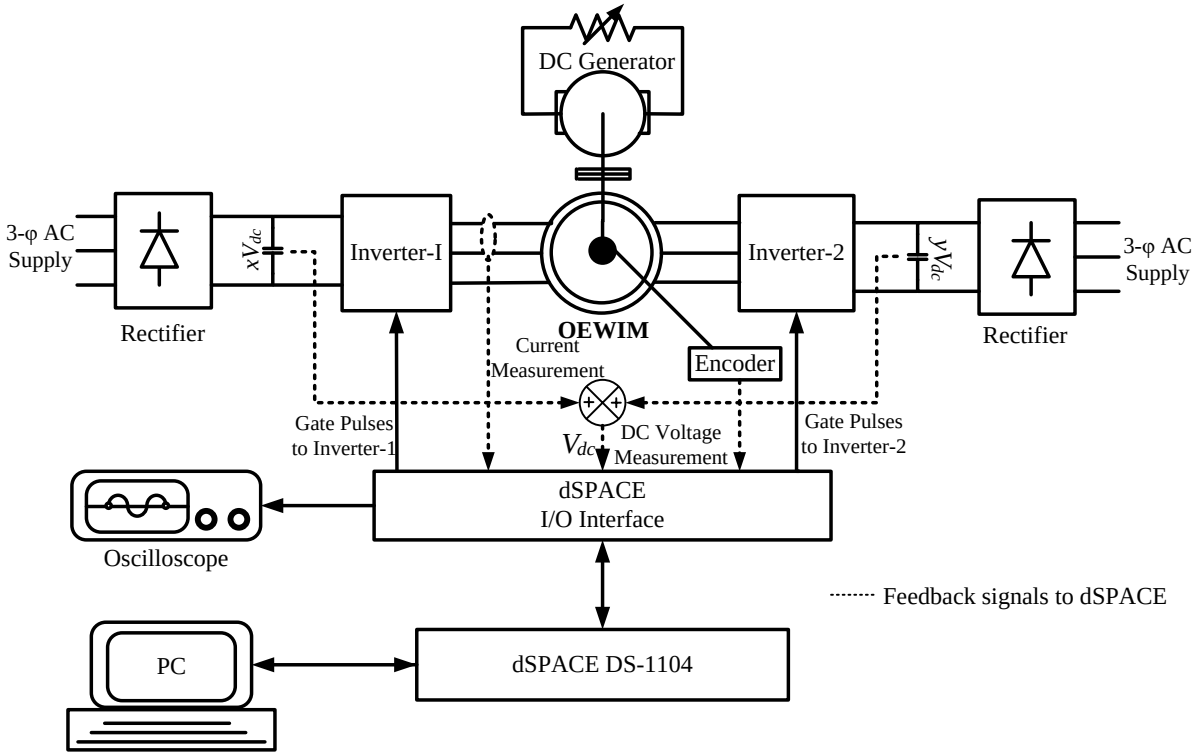

Figure A.1 Block diagram of experimental setup

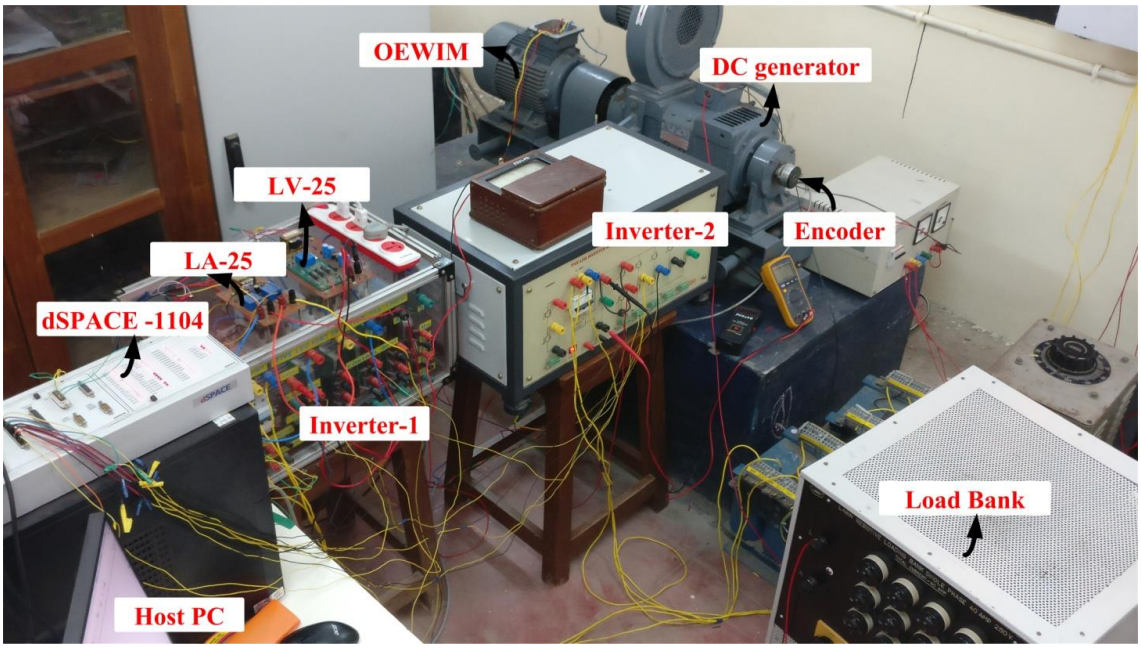

Figure A.2 Experimental test-rig used to verify proposed DTC and PTC strategies.

Photographs of various apparatus of the experimental setup such as current sensor and voltage sensor are shown in Figures. A.3 and A.4. The data sheets for the above are given in [89], [90].

Table A.1 Rating and specifications of OEWIM drive used for simulation and experimental verification

Name of the Parameter	**Symbol**	**Quantity**
Stator Resistance	R_s	4.2 Ω
Rotor Resistance	R_r	2.67 Ω
Stator Inductance	L_s	0.54 H
Rotor Inductance	L_r	0.54 H
Mutual Inductance	L_m	0.512 H
Poles	P	4
Moment of Inertia	J	0.031 kg-m2
Line-Line Voltage	V_{rms} (L-L)	400 V
Rated Power	P_{nom}	3.7 kW
Rated Torque	T_{nom}	24.48 Nm
Nominal (or) Reference Flux	ψ_{ref} (or) ψ_{nom}	1 Wb
Nominal Speed	N_r	1440 RPM
Synchronous Speed	N_s	1500 RPM
Nominal Angular Speed	ω_m (Mechanical Systems)	150.8 rad/s
Nominal Angular Speed	ω_r (or) ω_e (electrical Systems)	301.6 rad/s

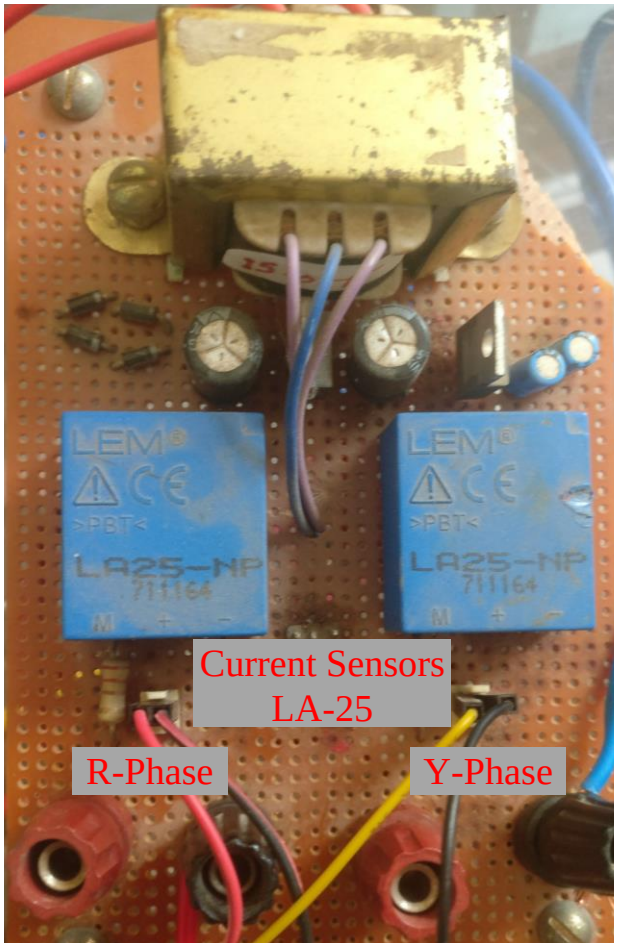

Figure A.3 Current sensors used for experimental verification

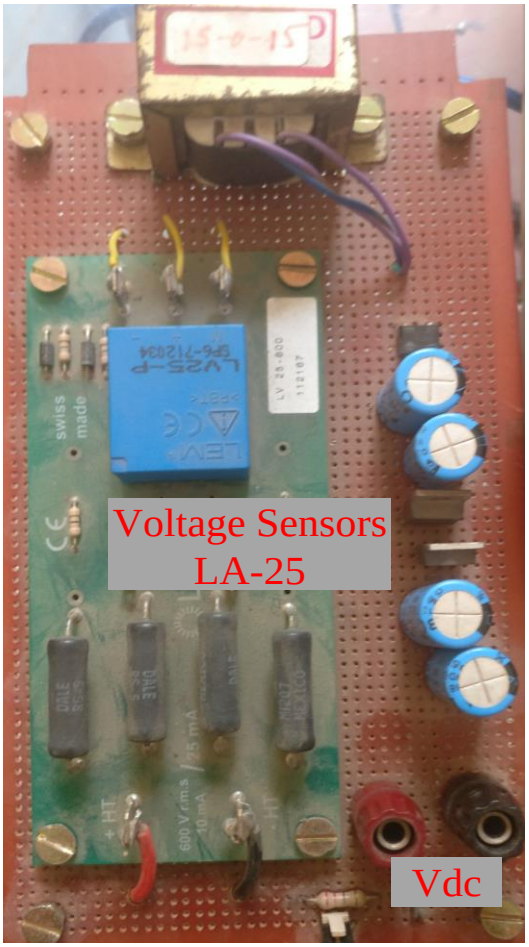

Figure A.4 Voltage sensors used for experimental verification

In order to implement the proposed DTC and PTC control schemes of OEWIM drive in real-time dSPACE DS1104 R & D control board is used as an interface between MATLAB/ SIMULINK/RTI model and OEWIM drive. This control board is placed in the PCI slot of the personal computer (PC), then the PC becomes a power PC. Software related to dSPACE control board has to be installed in the PC. The dSPACE control board software requires MATLAB/ SIMULINK/RTW as prerequisite. Simulink models for all the proposed control schemes are developed. To connect a simulink model to the induction motor drive, it is necessary to introduce I/O interfaces into the model using dSPACE RTI blocks. This will allow the simulation to interface with hardware connected. A model will be created with Simulink and RTI blocks using the Simulink® CoderTM (formerly Real-Time Workshop®). This generates C code. The RTI build process compiles the generated C code and links the object files and

libraries into an executable application and downloads the application to the real-time hardware directly after the compilation (build). The build status is displayed in the MATLAB Command Window and generates the four files namely

PPC : The real-time application to be downloaded to a PowerPC board

MAP : Map file with address information of variables

TRC : Variable description files to be used by Control Desk.

SDF : System description files with references to the PPC, MAP, and TRC file

Using the information from the SDF file the Control Desk can read and write the variables in real-time. Control Desk provides numerous instruments with their control knobs to measure the variables, to control the variables, to view the output and to change the scale of the output parameter displayed. The values of various parameters can be changed in real-time to observe their effect in real-time and also for fine tuning of parameters in real-time. Experimental results in steady-state and transient operation for all the four proposed control schemes are obtained by executing the appropriate MATLAB/SIMULINK files and models. Experimental results of conventional DTC and SVM-DTC are presented in next section and also all the proposed schemes are presented in chapters 4, 5, 6 and 7. The induction motor parameters are presented in Table. A.1.

Appendix-B

Methods to find Torque ripple and Flux ripple

In this thesis, average values of torque, flux ripples and peak to peak torque, flux ripple are used. The average torque and flux ripples are defined as follows.

The average torque and flux ripples are obtained by considering sum of difference between actual value and reference value over N samples. The percentage torque and flux ripples are obtained by using the following formulae (B.1) and (B.2).

$$\%\,\text{Torque ripple} = \left(\frac{\text{Average Torque ripple}}{\text{Rated Torque}}\right)*100 \tag{B.1}$$

$$\%\,\text{Flux ripple} = \left(\frac{\text{Average Flux ripple}}{\text{Rated Flux}}\right)*100 \tag{B.2}$$

The peak to peak values of torque and flux ripples are obtained by considering the variation of torque and flux values as shown below. In Figure B.1 shown below, torque ripple is 2.4 Nm and the flux ripple is 0.03 Wb.

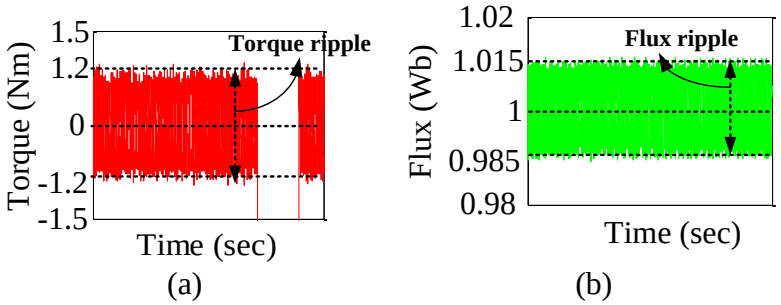

Figure B.1 Calculation of peak to peak ripples of OEWIM drive: (a) Torque ripple and (b) Flux ripple

$$\%\text{Torque ripple} = \left(\frac{\text{Peak to Peak Torque Variation}}{\text{Rated Torque}}\right)*100 \tag{B.3}$$

$$\%\text{Flux ripple} = \left(\frac{\text{Peak to Peak Flux Variation}}{\text{Rated Flux}}\right)*100 \tag{B.4}$$

References

[1] D. W. Novotny and T. A. Lipo, *Vector control and dynamics of AC drives*. Oxford University Press, Madison, USA, 1996.

[2] H. W. Beaty and J. J. L. Kirtley, *Electric Motor Handbook.* McGraw-Hill Book Company, New York, USA, 1998.

[3] P. C. Krause, O. Wasynczuk and S. D. Sudhoff, *Analysis of electric machinery and drive systems*. IEEE Press Power Engineering Series and Wiley- Interscience, Piscastaway, NJ, USA, 2002.

[4] Peter Vas, *Sensorless vector and direct torque control*, Oxford University Press, USA, 1998.

[5] F. Blaschke, "The principle of field-orientation as applied to the transvector closed-loop control system for rotating-field machines," in *Siemens Review*, vol. 34, no. 3, pp. 217-220, 1972.

[6] S. Sathikumar and J. Vithayathil, "Digital simulation of field-oriented control of induction motor," in *IEEE Transactions on Industrial Electronics*, vol. IE-31, no. 2, pp. 141-148, May 1984.

[7] R. Marino, S. Peresada and P. Valigi, "Adaptive input-output linearizing control of induction motors," in *IEEE Transactions on Automatic Control*, vol. 38, no. 2, pp.208-221, Feb. 1993.

[8] I. Takahashi and T. Noguchi, "A new quick-response and high-efficiency control strategy of an induction motor," in *IEEE Transactions on Industry Applications*, vol. IA-22, no. 5, pp. 820-827, Sept. 1986.

[9] M. Depenbrock, "Direct self-control (DSC) of inverter-fed induction machine," in *IEEE Transactions on Power Electronics*, vol. 3, no. 4, pp. 420-429, Oct. 1988.

[10] G. S. Buja and M. P. Kazmierkowski, "Direct torque control of PWM inverter-fed AC motors-a survey," in *IEEE Transactions on Industrial Electronics*, vol. 51, no. 4, pp. 744-757, Aug. 2004.

[11] B. V. Reddy, V. T. Somasekhar, "A dual inverter fed four-level open end winding induction motor with a nested rectifier-inverter," in *IEEE Transactions on Industrial Electronics*, vol. 9, no. 2, pp. 938-946, May 2013.

[12] S. Lakhimsetty, N. Surulivel and V. T. Somasekhar, “Improvised SVPWM strategies for an enhanced performance for a four-level open-end winding induction motor drive,” in *IEEE Transactions on Industrial Electronics*, vol. 64, no. 4, pp. 2750-2759, Apr. 2017.

[13] A. D. Kiadehi, K. E. K. Drissi and C. Pasquier, “Angular modulation of dual-inverter fed open-end motor for electrical vehicle applications,” in *IEEE Transactions on Power Electronics*, vol. 31, no. 4, pp. 2980-2990, Apr. 2016.

[14] S. Lu and K. Corzine, “Multilevel multi-phase propulsion drives,” in proceedings: *IEEE Electric Ship Technologies Symposium*, Philadelphia, PA, pp. 363-370, Oct. 2005.

[15] Y. Kawabata, M. Nasu, T. Nomoto, E. C. Ejiogu, and T. Kawabata, “High-efficiency and low acoustic noise drive system using open winding AC motor and two space-vector modulated inverters,” in *IEEE Transactions on Industrial Electronics*, vol. 49, no. 4, pp. 783- 789, Aug. 2002.

[16] V. Fernao Pires, J. F. Martins, C. Hao “Dual-inverter for grid connected photovoltaic system: modeling and sliding mode control,” in *Solar Energy*, vol. 86, no. 7, pp. 2106-2115, May 2012.

[17] I. Subotic, N. Bodo, E. Levi, and M. Jones, “On-board integrated battery charger for EVs using an asymmetrical nine-phase machine,” in *IEEE Transactions on Industrial Electronics*, vol. 62, no. 5, pp. 3285-3295, May 2015.

[18] D. Telford, M. W. Dunnigan and B. W. Williams, “A comparison of vector control and direct torque control of an induction machine,” *in Conference Proceedings: IEEE PESC’00*, Galway, pp. 421-426, Jun. 2000.

[19] D. Casadei, F. Profumo, G. Serra and A. Tani, “FOC and DTC: Two viable schemes for induction motors torque control,” in *IEEE Transactions Power Electronics*, vol. 17, no.5, pp. 779-787, Nov. 2002.

[20] T. Sutikno, N. R. N. Idris and A. Jidin, “A review of direct torque control of induction motors for sustainable reliability and energy efficient drives,” in Elsevier publications, *Renewable and Sustainable Energy Reviews*, vol. 32, pp. 548-558, Apr. 2014.

[21] L. Zhong, Md. F. Rahman, W. Y. Hu and K. W. Lim, “Analysis of direct torque control in permanent magnet synchronous motor drives,” in *IEEE Transactions on Power Electronics*, vol. 12, no. 3, pp. 528-536, May 1997.

[22] R. Ramchand, K. Gopakumar, C. Patel, K. Sivakumar, A. Das, and H. A. Rub, "Online computation of hysteresis boundary for constant switching frequency current-error space-vector-based hysteresis controller for VSI fed IM drives," in *IEEE Transactions on Power Electronics*, vol. 27, no. 3, pp. 1521-1529, Mar. 2012.

[23] V. Ambrozic, G. S. Buja and R. Menis, "Band-constrained technique for direct torque control of induction motor," in *IEEE Transactions Industry Applications*, vol. 51, no. 4, pp. 776-784, Aug. 2004.

[24] M. Cirrincione, M. Pucci and G. Vitale, "A DTC algorithm for induction motor drives with 3-level diode-clamped inverters," in *Journal of Electrical Systems*, vol. 1, no. 4, pp. 17-32, Dec. 2005.

[25] A. S. Kosmodamianskii, V. I. Vorobev, and A. A. Pugachev, "Direct torque control of induction motors fed by a single frequency converter," in *Russian Electrical Engineering*, vol. 86, no. 9, pp. 527–533, Sep. 2015.

[26] M. K. Rahim, F. Patkar, A. Jidin, M. Z. R. Z. Ahmadi, R. N. Firdaus, W. A. Halim and A. Razi, "Reduced torque ripple and switching frequency using optimal DTC switching strategy for an open-end winding of induction machines," in conference proceedings: *IEEE PEDS 2015*, Sydney, Australia, pp. 767-772, Jun. 2015.

[27] T. Noguchi, M. Yamamoto, S. Kondo, and I. Takahashi, "Enlarging switching frequency in direct torque-controlled inverter by means of dithering," in *IEEE Transactions on Industry Applications*, vol. 35, no. 6, pp. 1358-1366, Nov. 1999.

[28] N. R. N. Idris and A. H. M. Yatim, "Direct torque control of induction machines with constant switching frequency and reduced torque ripple," in *IEEE Transactions on Industrial Electronics*, vol. 51, no. 4, pp. 758-767, Aug. 2004.

[29] T. G. Habetler, F. Profumo, M. Pastorelli and L. M. Tolbert, "Direct torque control of induction machines using space vector modulation," in *IEEE Transactions on Industry Applications*, vol. 28, no. 5, pp. 1045-1053, Sep. 1992.

[30] J. K. Kang and S. K. Sul, "New direct torque control of induction motor for minimum torque ripple and constant switching frequency," in *IEEE Transactions on Industry Applications*, vol. 35, no. 5, pp. 1076-1082, Sep. 1999.

[31] K. K. Shyu, J. K. Lin, V. T. Pham, M. J. Yang, and T. W. Wang, "Global minimum torque ripple design for direct torque control of induction motor drives," in *IEEE Transactions on Industrial Electronics*, vol. 57, no. 9, pp. 3148-3156, Sep. 2010.

[32] G. Adamidis, Z. Koutsogiannis and P. Vagdatis, "Investigation of the performance of a variable-speed drive using direct torque control with space vector modulation," in *Electric Power Components and Systems*, vol. 39, no. 12, pp. 1227-1243, Aug. 2011.

[33] T. Vinay Kumar and S. S. Rao, "Modified direct torque control of three phase induction motor drives with low ripple in flux and torque," in *Leonardo Journal of Sciences (LJS)*, vol. 10, no. 18, pp. 27-44, Jun. 2011.

[34] T. Vinay Kumar and S. S. Rao, "Hardware implementation of direct load angle controlled induction motor drive," in *Electric Power Components and Systems*, vol. 42, no. 14, pp.1505-1516, Sep. 2014.

[35] X. Zhang and G. H. B. Foo, "A constant switching frequency-based direct torque control method for interior permanent-magnet synchronous motor drives," in *IEEE/ASME Transactions on Mechatronics*, vol. 21, no. 3, pp. 1445-1456, Jun. 2016.

[36] F. B. Salem and N. Derbel, "Direct torque control of induction motors based on discrete space vector modulation using adaptive sliding mode control," in *Electric Power Components and Systems*, vol. 42, no. 14, pp. 1598-1610, Sep. 2014.

[37] B. Kirankumar, Y. V. Siva Reddy and M. Vijayakumar, "Multilevel inverter with space vector modulation: intelligence direct torque control of induction motor," in *IET Power Electronics*, vol. 10, no. 10, pp. 1129-1137, Aug. 2017.

[38] T. Vinay Kumar and S. S. Rao, "Direct torque controlled induction motor drive based on cascaded three two-level inverters," in *International Journal of Modelling and Simulation*, vol. 34, no. 2, pp. 70-82, Jan. 2014.

[39] K. I. Nirsha and P. P. Rajeevan, "A direct torque control scheme for dual inverter fed induction motor drive with a common DC voltage source," in conference proceedings: *IECON 2017-43rd annual conference of IEEE industrial electronics society*, Bejing, pp. 1674-1679, 2017.

[40] A. Kumar, B. G. Fernandes and K. Chatterjee, "DTC of open-end winding induction motor drive using space vector modulation with reduced switching frequency," in

conference proceedings: *2004 IEEE 35th Annual Power Electronics Specialists Conference*, vol. 2, pp. 1214-1219, Nov. 2004.

[41] Arbind Kumar, B. G. Fernandes and K. Chatterjee, "Direct torque control of open-end winding induction motor drive using the concept of imaginary switching times for marine propulsion systems," in conference proceedings: *31st Annual Conference of IEEE Industrial Electronics Society*, pp. 1-6, Nov. 2005.

[42] B. R. Vinod and M. R. Baiju, "Direct torque control implemented on a three-level open-end winding induction motor drive," in conference proceedings: *2016 IEEE International Conference on Power Electronics, Drives and Energy Systems (PEDES)*, Trivandrum, pp. 1-6, Dec. 2016.

[43] C. Patel, P. P. Rajeevan, A. dey, R. Ramchand, K. Gopa kumar and M. P. Kazmeirkowski, "Fast direct torque control of open end induction motor drive using 12-sided polygonal voltage space vectors," in *IEEE Transactions on Power Electronics*, vol. 27, no. 1, pp. 400-410, Jan. 2012.

[44] M. Hajian, J. Soltani, G. A. Markadeh and S. Hosseinnia, "Adaptive nonlinear direct torque control of sensorless im drives with efficiency optimization," in *IEEE Transactions on Industrial Electronics*, vol. 57, no. 3, pp. 975-985, Mar. 2010.

[45] N. V. R. Naik and S. P. Singh, "Improved torque and flux performance of type-2 fuzzy-based direct torque control induction motor using space vector pulse width modulation," in *Electric power components and systems*, vol. 42, no. 6, pp. 658-669, Mar. 2014.

[46] M. Hafeez, M. N. Uddin, N. A. Rahim and H. W. Ping, "Self-tuned NFC and adaptive torque hysteresis-based DTC Scheme for IM drive," in *IEEE Transactions on Industry Applications*, vol. 50, no. 2, pp. 1410-1420, Mar. 2014.

[47] B. Metidji, N. Taib, L. Baghli, T. Rekioua and S. Bacha, "Low-cost direct torque control algorithm for induction motor without AC phase current sensors," in *IEEE Transactions on Power Electronics*, vol. 27, no. 9, pp. 4132-4139, Sep. 2012.

[48] M. Cirrincione, M. Pucci, G. Vitale and G. Cirrincione, "A new direct torque control strategy for the minimization of common-mode emissions," in *IEEE Transactions on Industry Applications*, vol. 42, no. 2, pp. 504-517, Mar. 2006.

[49] J. Rodriguez and P. Cortes, *Predictive control of power converters and electrical drives.* John Wiley & Sons, Ltd., USA, Publication, 2012.

[50] J. Maciejowski, *Predictive control with constraints*. New York, Prentice-Hall, 2002.

[51] E. Camacho and C. Bordons, *Model predictive control*. Berlin, Germany, Springer-Verlag, 2007.

[52] J. Rawlings and D. Q. Mayne, *Model predictive control, theory and design*. Madison, Nob Hill Publications, 2009.

[53] J. Rodriguez, M. P. Kazmierkowski, J. R. Espinoza, P. Zanchetta, H. A. Rub, H. A. Young and C. A. Rojas, "State of the art of finite control set model predictive control in power electronics," in *IEEE Transactions on Industrial Electronics*, vol. 9, no. 2, pp. 1003-1016, May 2013.

[54] S. Kouro, P. Cortes, R. Vargas, U. Ammann and J. Rodriguez, "Model predictive control-a simple and powerful method to control power converters," in *IEEE Transactions on Industrial Electronics*, vol. 56, no. 6, pp. 1826-1838, Jun. 2009.

[55] J. Rodriguez, R. M. Kennel, J. R. Espinoza, M. Trincado, C. A. Silva and C. A. Rojas, "High-performance control strategies for electrical drives: an experimental assessment," in *IEEE Transactions on Industrial Electronics*, vol. 59, no. 2, pp. 812–820, Feb. 2012.

[56] Md. Habibullah and D. D. C. Lu, "A speed-sensorless FS-PTC of induction motors using extended kalman filters," in *IEEE Transactions on Industrial Electronics*, vol. 62, no. 11, pp. 6765-6778, Nov. 2015.

[57] F. Wang, Z. Zhang, X. Mei, J. Rodriguez and R. Kennel, "Advanced control strategies of induction machine: field oriented control, direct torque control and model predictive control," in energies, vol. 11, no. 1, pp. 1-13, Jan. 2018.

[58] P. Correa, M. Pacas and J. Rodriguez, "Predictive torque control for inverter-fed induction machines," in *IEEE Transactions on Industrial Electronics*, vol. 54, no. 2, pp. 1073-1079, April 2007.

[59] M. Nemec, D. Nedeljkovic and V. Ambrozic, "Predictive torque control of induction machines using immediate flux control," in *IEEE Transactions on Industrial Electronics*, vol. 54, no. 4, pp. 2009-2017, Aug. 2007.

[60] H. Miranda, P. Cortes, J. I. Yuz and J. Rodriguez, "Predictive torque control of induction machines based on state-space models," in *IEEE Transactions on Industrial Electronics*, vol. 56, no. 6, pp. 1916-1924, Jun. 2009.

[61] T. Geyer, G. Papafotiou and M. Morari, “Model predictive direct torque control-part I: concept, algorithm, and analysis,” in *IEEE Transactions on Industrial Electronics*, vol. 56, no. 6, pp. 1894-1905, Jun. 2009.

[62] G. Papafotiou, J. Kley, K. G. Papadopoulos, P. Bohren and M. Morari, “Model predictive direct torque control-part II: implementation and experimental evaluation,” in *IEEE Transactions on Industrial Electronics*, vol. 56, no. 6, pp. 1906-1915, June 2009.

[63] J. Scotock, T. Geyer and U. K. Madawala, “A comparison of model predictive control schemes for MV induction motor drives,” in *IEEE Transactions on Industrial Informatics*, vol. 9, no. 2, pp. 909-919, May 2013.

[64] J. Beerten¸ J. Verveckken and J. Driesen, “Predictive direct torque control for flux and torque ripple reduction,” in *IEEE Transactions on Industrial Electronics,* vol. 57, no. 1, pp. 404-412, Jan. 2010.

[65] P. Karamanakos, P. Stolze, R. M. Kennel, S. Manias and H. D. T. Mouton, “Variable switching point predictive torque control of induction machines,” in *IEEE Journal of Emerging and Selected Topics in Power Electronics*, vol. 2, no. 2, pp. 285-295, June 2014.

[66] Y. Zhang and H. Yang, “Model predictive torque control of induction motor drives with optimal duty cycle control,” in *IEEE Transactions on Power Electronics*, vol. 29, no. 12, pp. 6593-6603, Dec. 2014.

[67] Y. Zhang and H. Yang, “Two-vector-based model predictive torque control without weighting factors for induction motor drives,” in *IEEE Transactions on Power Electronics*, vol. 31, no. 2, pp. 1381-1390, Feb. 2016.

[68] C. Xia, X. Qiu, Z. Wang and T. Shi, “Predictive torque control for voltage source inverter-permanent magnet synchronous motor based on equal torque effect,” in *IET Electric Power Applications*, vol. 10, no. 3, pp. 208-216, Mar. 2016.

[69] Y. Zhang, H. Yang and B. Xia, “Model-predictive control of induction motor drives: torque control versus flux control,” in *IEEE Transactions on Industry Applications*, vol. 52, no. 5, pp. 4050-4060, Sep. 2016.

[70] Y. Zhang and H. Yang, “Generalized two-vector-based model-predictive torque control of induction motor drives,” in *IEEE Transactions on Power Electronics*, vol. 30, no. 7, pp. 3818-3829, Jul. 2015.

[71] Y. Zhang, H. Yang and B. Xia, "Model predictive torque control of induction motor drives with reduced torque ripple," in *IET Electric Power Applications*, vol. 9, no. 9, pp. 595-604, Nov. 2015.

[72] S. A. Davari, "Predictive direct angle control of induction motor," in *IEEE Transactions on Industrial Electronics*, vol. 63, no. 8, pp. 5276-5284, Aug. 2016.

[73] C. A. Rojas, J. Rodriguez, F. Villarroel, J. R. Espinoza, C. A. Silva and M. Trincado, "Predictive torque and flux control without weighting factors," in *IEEE Transactions on Industrial Electronics*, vol. 60, no. 2, pp. 681-690, Feb. 2013.

[74] Md. Habibullah, D. D. C. Lu, D. Xiao, J. E. Fletcher and Md. F. Rahman, "Low complexity predictive torque control strategies for a three-level inverter driven induction motor," in *IET Electric Power Applications*, vol. 11, no. 5, pp. 776-783, May 2017.

[75] J. Rodriguez, J. Pontt, C. Silva, P. Cortes, U. Ammann and S. Rees, "Predictive direct torque control of an induction machine," in conference proceedings: *European Power Electronics-Power Electronics and Motion Control (PEMC)*, Riga, Lativa, pp. 1-6, Sep. 2004.

[76] P. Cortes, S. Kouro, B. L. Rocca, R. Vargas, J. Rodriguez, J. I. Leon, S. Vazquez and L. G. Franquelo "Guidelines for weighting factors design in model predictive control of power converters and drives," in Proceedings: *IEEE International Conference on Industrial Technology*, Australia, pp. 1-7, May 2009.

[77] S. A. Davari, D. A. Khaburi, F. Wang and R. M. Kennel, "Using full order and reduced order observers for robust sensorless predictive torque control of induction motors," in *IEEE Transactions on Power Electronics*, vol. 27, no. 7, pp. 3424-3433, Jul. 2012.

[78] Md. Habibullah, D. D. C. Lu, D. Xiao, J. E. Fletcher and Md. F. Rahman, "Predictive torque control of induction motor sensor-less drive fed by a 3L-NPC inverter," in *IEEE Transactions on Industrial Informatics*, vol. 13, no. 1, pp. 60-70, Feb. 2017.

[79] C. A. Rojas, S. Kouro, M. Perez and F. A. C. Villarroel, "Multiobjective fuzzy predictive torque control of an induction machine fed by a 3L-NPC inverter," in conference proceedings: *IEEE International Symposium on Predictive Control of Electrical Drives and Power Electronics*, pp. 21-26, Oct. 2015.

[80] V. Yaramasu, M. Rivera, M. Narimani, B. Wu and J. Rodriguez, “Finite state model based predictive current control with two-step horizon for four-leg NPC converters,” in *Journal of Power Electronics*, vol. 14, no. 6, pp. 1178-1188, Nov. 2014.

[81] A. Linder and R. Kennel, “Model predictive control for electrical drives,” in proceedings: *Power Electronics Specialists Conference*, Recife, Brazil, pp. 1793-1799, Jun. 2005.

[82] P. Zanchetta, “Heuristic multi-objective optimization for cost function weights selection in finite states model predictive control,” in *Workshop on Predictive Control of Electrical Drives and Power Electronics*, pp. 70-75, Oct. 2011.

[83] R. Vargas, U. Ammann, B. Hudoffsky, J. Rodriguez and P. Wheeler, “Predictive torque control of an induction machine fed by a matrix converter with reactive input power control,” in *IEEE Transactions on Power Electronics*, vol. 25, no. 6, pp. 1426-1438, Jun. 2010.

[84] M. B. Shadmand, R. S. Balog and H. A. Rub, “Auto-tuning the cost function weight factors in a model predictive controller for a matrix converter VAR compensator,” in proceedings: *2015 IEEE Energy Conversion Congress and Exposition (ECCE)*, Montreal, QC, pp. 3807-3814, Sep. 2015.

[85] Md. Habibullah, D. D. C. Lu, D. Xiao and Md. F. Rahman, “A simplified finite-state predictive direct torque control for induction motor drive,” in *IEEE Transactions on Industrial Electronics*, vol. 63, no. 6, pp. 3964-3975, Jun. 2016.

[86] B. Zhu, K. Rajashekara and H. Kubo, “Comparison between current-based and flux/torque-based model predictive control methods for open-end winding induction motor drives,” in *IET Electric Power Applications*, vol. 11, no. 8, pp. 1397-1406, Sep. 2017.

[87] P. C. Fishburn, *Additive Utilities with Incomplete Product Set: Applications to Priorities and Assignments*. Operations Research Society of America, Baltimore, MD, USA, 1967.

[88] E. Triantaphyllou, *Multi-Criteria Decision Making: A Comparative Study*. Kluwer Academic Publishers (now springer), The Netherlands, Dordrecht, pp. 320. ISBN 0-7923-6607-7, 2000.

[89] https://www.lem.com/sites/default/files/products_datasheets/lv_25-p.pdf

[90] https://www.lem.com/sites/default/files/products_datasheets/la_25-p.pdf

Publications

Journals

1. Kunisetti V. Praveen Kumar and Thippiripati Vinay Kumar, “An effective four-level voltage switching state algorithm for direct torque controlled open end winding induction motor drive by using two two-level inversion,” in *Electric Power Components and Systems,* vol. 45, no. 19, pp. 2175-2187, 2017.

2. Kunisetti V. Praveen Kumar and Thippiripati Vinay Kumar, “An enhanced three-level voltage switching state algorithm for direct torque controlled open end winding induction motor,” in *Journal of Institution of Engineers, (India), Series B,* vol. 99, no. 3, pp. 235-243, 2018.

3. Kunisetti V. Praveen Kumar and Thippiripati Vinay Kumar, “Predictive torque control of open end winding induction motor drive fed with multilevel inversion using two two-level inverters,” in *IET-Electric Power Applications,* vol. 12, no. 1, pp. 54-62, 2018.

4. Kunisetti Venkata Praveen Kumar, Kodumur Meesala Ravi Eswar and Thippiripati Vinay Kumar, “Improvised predictive torque control strategy for an open end winding induction motor drive fed with four-level inversion using normalised weighted sum model,” in *IET-Power Electronics,* vol. 11, no. 5, pp. 808-813, 2018.

Conference Proceedings

1. K. V. Praveen Kumar and T. Vinay Kumar, “Experimental implementation of direct torque control of Open end winding induction motor,” in conference proceedings: *2016 IEEE Region 10 Conference (TENCON),* Singapore, pp. 3318-3323, Nov. 2016.

2. K. V. Praveen Kumar and T. Vinay Kumar, “Predictive torque control strategy of an open end winding induction motor with less common-mode voltage,” in conference proceedings: *Proc. International Conference on Industrial Technology-2018,* University of Lyon, France, Lyon, pp. 498-503, Feb. 2018.

Curriculum-Vitae

Name	:	Kunisetti V Praveen Kumar
Date of Birth	:	20th August 1990
Gender	:	Male
Contact Number	:	+91-9160919516
Email Id	:	kvpraveenkumar15@gmail.com

Academic Qualifications

Program	University	%/CGPA	Year of completion
M. Tech (Power Electronics)	JNTU Kakinada	84.2	2014
B. Tech (Electrical and Electronics Engineering)	JNTU Kakinada	76.2	2011